

ADA106033

LEVEL

(12)

AD

CONTRACT REPORT ARBRL-CR-00467

AFATL-TR-71-81

HULL/EPIC3 LINKED EULERIAN/LAGRANGIAN  
CALCULATION IN THREE DIMENSION

Prepared by

Orlando Technology, Incorporated  
P. O. Box 855  
Shalimar, FL 32579

JUL 28 1981

A

September 1981



US ARMY ARMAMENT RESEARCH AND DEVELOPMENT COMMAND  
BALLISTIC RESEARCH LABORATORY  
ABERDEEN PROVING GROUND, MARYLAND

Approved for public release; distribution unlimited.

DRAFT FILE COPY

81 10 22

Destroy this report when it is no longer needed.  
Do not return it to the originator.

Secondary distribution of this report by originating  
or sponsoring activity is prohibited.

Additional copies of this report may be obtained  
from the National Technical Information Service,  
U.S. Department of Commerce, Springfield, Virginia  
22151.

The findings in this report are not to be construed as  
an official Department of the Army position, unless  
so designated by other authorized documents.

*The use of trade names or manufacturers' names in this report  
does not constitute endorsement of any commercial product.*

UNCLASSIFIED  
SECURITY CLASSIFICATION OF THIS PAGE (When Data Entered)

REPORT DOCUMENTATION PAGE		READ INSTRUCTIONS BEFORE COMPLETING FORM	
1. REPORT NUMBER  CONTRACT REPORT ARBRL-CR-00467	2. GOVT ACCESSION NO  AD-A106	33 TYPE OF REPORT & PERIOD COVERED	
4. TITLE (and subtitle)  HULL/EPIC3 LINKED EULERIAN/LAGRANGIAN CALCULATION IN THREE DIMENSION	5. SPONSORING ORG. REPORT NUMBER		
6. AUTHOR(s)  Daniel A. Matuska John J. Osborn	CONT'D. GRANT NUMBER(s)  DAAK11-79-C-0106 ✓		
7. PERFORMING ORGANIZATION NAME AND ADDRESS  Orlando Technology, Incorporated P.O. Box 855 Shalimar, Florida 32579	10. PROGRAM ELEMENT, PROJECT, TASK AREA & WORK UNIT NUMBERS		
11. CONTROLLING OFFICE NAME AND ADDRESS  US Army Armament Research and Development Command US Army Ballistic Research Laboratory ATTN: DRDAR-BL Aberdeen Proving Ground, MD 21005	12. REPORT DATE  11 SEPTEMBER 1981		
13. MONITORING AGENCY NAME & ADDRESS (if different from Controlling Office)  AFATL	14. NUMBER OF PAGES 94		
15. SECURITY CLASS. (of this report)  UNCLASSIFIED			
16. DECLASSIFICATION/DOWNGRADING SCHEDULE			
17. DISTRIBUTION STATEMENT (of this Report)  Approved for public release; distribution unlimited.			
18. DISTRIBUTION STATEMENT (of the abstract entered in Block 20, if different from Report)  11 SEPTEMBER 1981			
19. SUPPLEMENTARY NOTES  AFATL-TR-81-71			
20. KEY WORDS (Continue on reverse side if necessary and identify by block number)  Eulerian Impact Lagrangian Wave Propagation Hydrocode High Strain Rate Testing Continuum Mechanics Material Failure Penetration			
21. ABSTRACT (Continue on reverse side if necessary and identify by block number)  This report documents a demonstration calculation performed to evaluate the three-dimensional Eulerian/Lagrangian linked hydrocode developed under this contract. The calculation consists of a staballoy rod impacting an armor plate at obliquity 65 degrees and velocity 1 km/sec. Calculational results compared favorably with experimental data. The linked calculation was completed with the use of about nine total CDC 7600 computer hours as compared to the estimated 35 hours if the calculation had been run with only the Eulerian code.			

DD FORM 1 JAN 73 1473 EDITION OF 1 NOV 65 IS OBSOLETE

UNCLASSIFIED

SECURITY CLASSIFICATION OF THIS PAGE (When Data Entered)

SECURITY CLASSIFICATION OF THIS PAGE(When Data Entered)

SECURITY CLASSIFICATION OF THIS PAGE(When Data Entered)

**FORWARD**

This report documents the results of a calculation performed to demonstrate the capability of the linked HULL/kPIC3 Eulerian/Lagrangian system developed under BRL contract DAAK11-79-C-0106. This work was performed by Daniel A. Matuska and John J. Osborn during the period July 1979 through October 1980. The calculational results are compared with experimental data with favorable results. The BRL Project Manager was Dr. John Zukas. The authors are indebted to Dr. Zukas and his associate, Mr. Kent Kimsey, for their invaluable assistance during the completion of this effort.

## TABLE OF CONTENTS

Section	Title	Page
I	Introduction.....	1
II	Technical Approach.....	2
	A. Initial Impact - Transient Phase.....	2
	B. Steady Penetration.....	3
	C. Break-Through.....	3
	D. Penetrator Equilibration.....	3
III	Material Properties.....	7
IV	The Eulerian Calculation-HULL.....	15
	A. Plane Strain Approximation.....	15
	B. Three-Dimensional Calculation.....	17
V	EPIC Calculation and Comparison With Experiment.....	25
VI	Conclusions.....	31
	REFERENCES.....	32
Appendix		
	A. Taylor-Anvil Experiments.....	33
	B. Notched Tensile Experiments.....	39
	C. HULL Calculation Setup and Sample Output.....	57
	DISTRIBUTION LIST.....	87

## LIST OF FIGURES

Figure	Title	Page
1	Demonstration Oblique Penetration Calculation Geometry.....	6
2	RHA and Staballoy Cylinders After Impact.....	8
3	Comparisons of Calculated vs Experimental RHA Cylinder Impacts.....	9
4	RHA Yield Strength Comparison.....	10
5	Calculated Impacts With BRL MR 2703 Model (Top) and Non-Work Hardening Model (Bottom) at Final Deformation.....	11
6	Predicted RHA Strains.....	12
7	Failure Criterion.....	14
8	HULL Mesh Configuration in the Plane of the Penetrator/ Target Ensemble.....	16
9	Density Contours of Demonstration Calculation to Compare Coarse Zone Case (Top) and Fine Zone Case (Bottom) in Plane Strain.....	18
10	Density Contours of Coarse Zone Case in Plane Strain at 30 $\mu$ sec.....	19
11	Density Contours of Fine Zone Case in Plane Strain at 30 $\mu$ sec.....	20
12	HULL Mesh Configuration For Three-Dimensional Demonstration Calculation.....	21
13	Density Contours of Demonstration Calculation in Three Dimensions.....	23
14	Density Contours of Demonstration Calculation in Three-Dimensions at 30 $\mu$ sec.....	24
15	HULL and EPIC Rods at 20 Microseconds.....	26
16	HULL and EPIC Rods at 41.6 Microseconds.....	27
17	EPIC Velocity Plots to 200 Microseconds.....	28
18	Experimental Versus Calculational Results.....	29

## **SECTION I INTRODUCTION**

The Terminal Ballistics Division of the Army Ballistic Research Laboratory has the responsibility for developing techniques which will guide the design of both armored protective systems and ordnance which can defeat such armor. Long rod penetrators have demonstrated significant promise in defeating modern armored systems. This has led to efforts to develop an understanding of the physical processes of penetration with respect to the response of both the target and the penetrator. Both experimental and analytic means are used to support these efforts. The physical processes of dynamic penetration are dominated by non-linear, compressible effects which are hydrodynamic, plastic and elastic in nature. These processes interact with, and are often terminated by, material failure or fracture. All of these effects, except failure, can be described by solution of the non-linear partial differential equations of continuum mechanics. Unfortunately, the underlying system of equations do not have an analytic solution unless several, possibly devastating, simplifying assumptions are made. The only current alternative is to cast the partial differential equations as a system of finite difference analogs and solve these numerical relations with the aid of large scale computers. These calculations are time-consuming and costly in both man-power and computing machinery resources. Current machinery and computer programs (hydrocodes) are capable of describing most normal-incidence penetration problems for which the material properties are well-characterized. Normal incidence calculations permit the assumption of symmetry with respect to an axis of rotation. This allows the spatial description to be simplified to a two-dimensional axisymmetric system which reduces both computer storage and computational requirements. Oblique penetration events do not permit this simplification. Calculations to simplify oblique penetration through the use of plane strain approximations have reproduced the qualitative aspects of the phenomena, but fail to illustrate the correct temporal relationships, since surface relief processes are not correctly modeled. In addition, the magnitude of hydrodynamic waves and the geometric similarity of plastic and elastic waves are not preserved. In order to perform a realistic calculation of an oblique penetration event, it is necessary to include three spatial dimensions. A three-dimensional calculation will require on the order of  $N$  times as much computer time and storage, where  $N$  is the number of discretized elements in the added dimension; thus, two-dimensional calculations, which require an hour of computational central processor time and 100,000 storage elements, would require several ten's of hours and several millions of words of storage in three-dimensions. From a practical point of view, the ability to complete these calculations is dominated by the economics of computing, and by the amount of time required to complete a calculation and interpret the results.

The purpose of this effort was to devise a feasible computational methodology for performing calculations of long rod penetrators perforating spaced target arrays. Section II of this report describes the technical approach, Section III the source of material properties, and subsequent sections describe the computational techniques.

## SECTION II TECHNICAL APPROACH

The penetration or perforation of a spaced array of armor plates by a long rod can be characterized by describing the phenomenology in four phases.

### A. Initial Impact - Transient Phase

During the first or initial impact stage, the highest magnitude stresses are produced. The peak amplitude of these waves can be approximated by:

$$T = \left( \frac{\rho_p}{\rho_t} \right)^{1/3} V \rho_t C_t / 2 + \left( \frac{\rho_p}{\rho_t} \right)^{2/3} V^2 S_t \rho_t / 4$$

where:

T = peak stress amplitude

$\rho_t$  = target material density

$\rho_p$  = penetrator material density

$C_t$  = target material bulk sound speed

$S_t$  = target material shock velocity/particle velocity slope

V = impact velocity

This high initial stress is attenuated as the wave advances into the target and back along the length of the penetrator by free surface relief and by geometric divergence. By the time the wave front has advanced into the target a few penetrator diameters, it will have been reduced an order of magnitude in amplitude. It will be reduced to the elastic wave amplitude in the penetrator, when the wave front has reached a distance of about 3 diameters back from the impact point in the penetrator. These high initial stresses are largely hydrodynamic since their amplitudes are many times the plastic flow stress of the penetrator and target materials. For example, a steel penetrator impacting a steel target at normal incidence with a velocity of 1 km/sec will give rise to peak initial stresses in excess of 150 kilobars (kb). This is ten times the flow stress of 15 kb, which is about the maximum flow stress of the best hardened steel alloys.

### B. Steady Penetration

As the rod/target interface advances into the target, the flow approaches steady state. Material is displaced from the rod front at an almost constant rate. This second or steady penetration phase will continue until the rod is decelerated by rearward propagating elastic wave, the rod material is exhausted or the deformation front in the target encounters a discontinuity such as a free surface or a differing material impedance. During this phase of penetration, a plastic deforming region is induced in the rod. This region extends from the target/penetrator interface back into the rod to the distance at which radial free surface relief at the rod periphery reduces the amplitude of the wave to the elastic limit of the rod material. Thus, a velocity gradient exists in the rod with the highest velocity at the interface and a velocity characteristic of the rod material elastic wave velocity at some distance back from the interface. A corresponding hydrodynamic, plastic, and elastic wave profile exists in the target material. All of these waves are, of course, modified by relief and reflection of waves which have propagated into both rod and target, and have encountered discontinuities at the material interfaces.

### C. Break-Through

The third or break-through phase starts as the waves in the target begin to displace material upon relief at the target surface opposite the point of impact. If the target is thin compared to the initial penetrator contact area, and the impact velocity is high enough, the initial wave release in a tensile state may result in tensile tearing of the plate near surface material or spallation. If the impact is lower, petaling and tearing may result. As the plate thickness increases, the break-through phase will be characterized by the production of a plug which is adiabatically sheared from the surrounding target materials. As the impact velocity is increased, the stresses induced in the target will cause the plug to breakup or shatter upon release from the surrounding target material.

### D. Penetrator Equilibration

If the target is a single plate, the break-through phase essentially terminates interest in the penetration process. If subsequent plates of target material will be encountered, the behavior of the rod in the intervening region between plates may be of importance. This fourth, or penetrator equilibrating phase, is the response of the penetrator to the stresses induced during the initial impact and steady penetration phases. The velocity gradient in the nose of the rod is dissipated by rod deformation for some period of time after it has perforated the plate. This deformation results in rod shortening for normal incidence impacts, and in rod shortening and bending for oblique impacts. These deformations take place over several wave transits of the length of the penetrator. If the plastic flow exceeds the ability of the rod materials ability to respond, the flow processes will be terminated by the growth of failure initiation centers which will relieve the induced stresses.

If a sufficient number of these nucleation centers grow and connect up, the flow process terminates in macroscopic penetrator fracture. At the rod nose, this is exhibited by the shedding of material as it flows radially outward. At greater distances back in the rod, bending strains can cause the rod to be broken into separate, disconnected elements. The state of the rod elements after all stresses have been completely or partially relieved, describes the initial conditions for impact on subsequent target elements.

All of the hydrodynamic, plastic and elastic phenomena described in the preceding can be modeled by either laboratory reference (Eulerian) or mass reference (Lagrangian) hydrocode calculations. Each methodology has its advantages.

Eulerian calculations consider the continuous media (solids in this case) to be moving through a regular mesh which describes the computational region. Interfaces which move with respect to the computational coordinate system, must be preserved as they cross grid or mesh lines. During the course of a calculation which encompasses many time steps, these interfaces will be diffused since they do not exist on a clearly defined calculational mesh boundary and their definition within a mesh or cell is not as exact as the remainder of the calculation. This feature of an Eulerian code is also an advantage. The severe distortions which result from the penetration process are not restricted by the initial choice of the mesh configuration.

Lagrangian calculations are completed by subdividing the materials between material interfaces into arbitrary meshes as defined by the initial configuration of the problem. Thus for a penetration calculation, the target will be modeled by one computational region, and the penetrator by another. They will interact across slide lines or planes with assignments of one face as master and the other as a slave. This interaction across regions is not as precise as the other portions of the calculation, and can result in the accumulation of errors. In addition, as materials deform during the penetration event, the computational mesh, which is embedded in the material, is also deformed. This results in irregular mesh shapes, which though in principle are allowable, in practice result in a reduction in the order of accuracy. The accumulated errors may result in an invalid solution. In addition, and probably more important, the deformation of the mesh results in decreasing the size of the allowable time step, since the maximum time step for stability considerations is given by:

$$Dt = DX/\text{MAX } (C_s, U)$$

where

Dt = the time step

DX = minimum cell or mesh dimension

C<sub>s</sub> = material sound speed

U = material particle velocity

The time step,  $Dt$ , is chosen as the minimum over all computational regions and therefore, the most distorted element or mesh in the calculation, drives the speed with which the calculation can advance. On the positive side, Lagrangian codes are capable of preserving material interfaces with great fidelity. Small free surface motions can be predicted without extreme sensitivity to the number of mesh elements in the calculation.

From the foregoing, it would appear that both Eulerian and Lagrangian calculations have their advantages and disadvantages when they are applied in calculational regimes where each is most capable. Thus for a long rod penetration event, the initial impact through breakout phases, which are violent and characterized by large deformations, are best handled by an Eulerian hydrocode. The longer time equilibrating phase after target perforation is best handled by a Lagrangian code, since the Lagrangian code can concentrate on calculations with the rod, and ignore the surrounding medium. Also, the Lagrangian methodology is capable of more accurate representation of the slower bending and surface relief processes which follow target break-through.

The methodology employed in this work was to use the three-dimensional version of the HULL code (REF 1) to perform calculations during plate perforation. A sufficient portion of the penetrator and target must be included in the HULL calculation to preclude the arrival of spurious wave reflections back at the deformed rod nose before perforation is complete. During the course of the Eulerian calculation, material velocity data was recorded at a large number of data collection points or stations in the deforming rod nose whenever the velocity changed by more than 2 percent. These station data were collected as a function of time to allow a subsequent definition of the rod nose surface velocity during deformation.

The station data were then used as boundary conditions for a Lagrangian calculation performed by the EPIC3 (REF 2 and 3) code. The EPIC3 calculation modeled the entire rod, but ignored the target material. The station velocity data were applied to the surface nodes in EPIC3 as a function of time. These displacements produce stress fields in the penetrator that replicate those calculated during the course of the HULL calculation. After perforation, the station data are no longer used as boundary conditions, and the rod is allowed to equilibrate. During this portion of the calculation, only the EPIC3 code is run. The resulting linked calculation is more economical and more accurate than could be run with either of the component hydrocodes.

This methodology was demonstrated by calculating the oblique penetration of an armor plate by a stabilloy penetrator. The geometric configuration of this calculation is illustrated by Figure 1. The next sections of this report describe the material property definitions and the HULL and EPIC3 calculations.

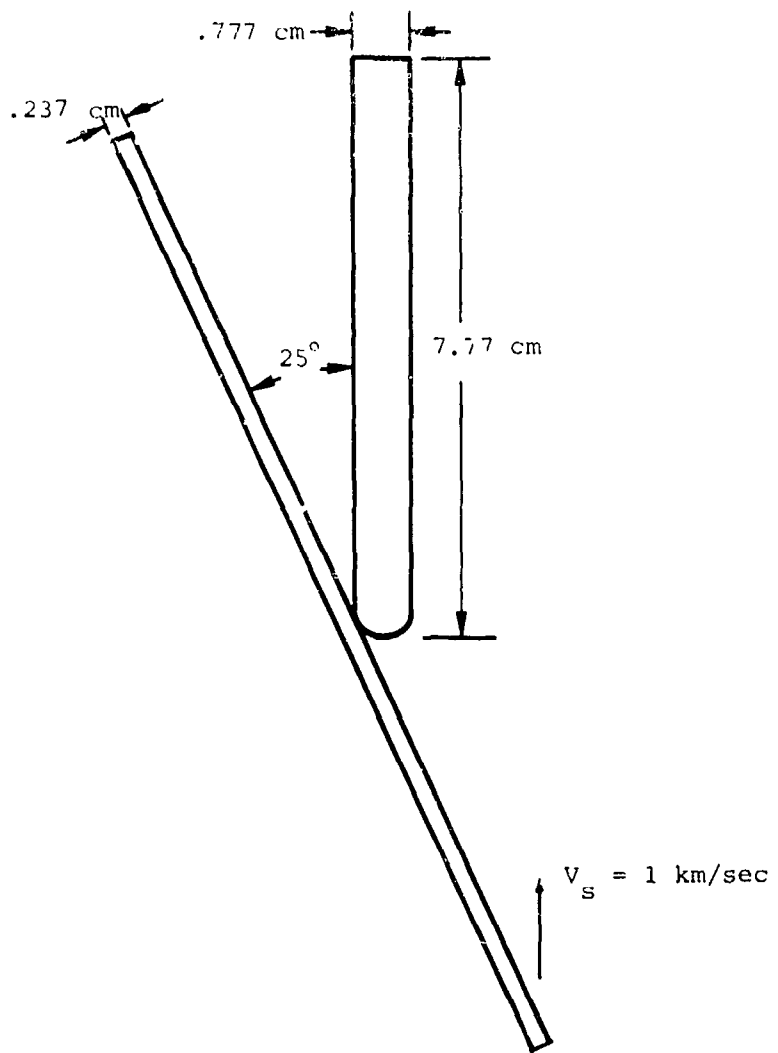


Figure 1. Demonstration Oblique Penetration Calculation Geometry.

### SECTION III MATERIAL PROPERTIES

The materials of interest for the demonstration calculation were a staballoy ( $U-0.75T_1$ ) and rolled homogeneous armor (RHA) from a thin plate. Samples of the staballoy were obtained from Nuclear Metals, Inc. and the RHA from the Ballistics Research Laboratory. Taylor anvil specimens were machined from the material samples and fired by the Denver Research Institute. The results of these tests are included in Appendix A. Figure 2 presents pictures of the deformed cylinders from two of the tests. In addition, the staballoy was subjected to notched tensile tests by the Southwest Research Institute. Their report is included as Appendix B.

The Taylor anvil specimens were analyzed by performing two-dimensional Lagrangian calculations of the impact. An OTI version of Sandia's TOODYIV (REF 4) code was used for these calculations. Figure 3 presents the results of several TOODY runs for RHA Test 5 (an impact at 0.33 km/sec) in terms of calculated final radius ( $R_f$ ) and final length ( $L_f$ ) vs the observed values. Points labelled A through K are the calculational values based on using several yield strength models. The models are identified by three numbers. The first number is the assumed initial yield stress in kilobars, the second number is the tangent modulus in kilobars and the third number is the saturation or maximum stress in kilobars. Models I, J and K all provide results which are very close to the observed data. All three models predict very little work hardening for this plate, at least in the rolling direction. This is consistent with the smooth (non-bulged) appearance of the impacted cylinders. The model developed from these tests is shown in Figure 4. Also shown is a thin plate RHA model previously developed by the Ballistics Research Laboratory (REF 5) in low-rate tensile tests. TOODY calculations indicate that the specimens would be quite bulged if this model were valid for the strain rates ( $> 20,000 \text{ sec}^{-1}$ ) seen in the anvil tests. Figure 5 shows final predicted cylinder shapes for the previous BRL model and model I for RHA Test 5. Only one-half of the cylinder is shown since the axis is an axis of rotational symmetry. The bulged area required by the low-rate model is clearly visible in the cylinder shapes.

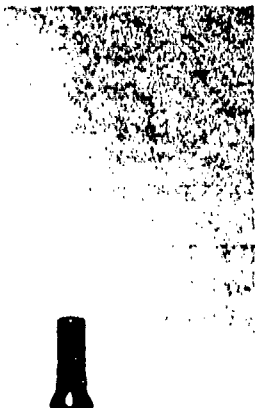
With the exception of the very high velocity RHA Test 4 (0.44 km/sec), none of the RHA samples exhibited any centerline fracturing. Figure 6 shows predicted final centerline radial tensile strain and axial compressive strain for Test 5. The material is seen to undergo over 70 percent tensile strain without fracturing. Measurement of the final Test 4 cylinder indicates that the RHA can be expected to fail at strains slightly over 100 percent.

The staballoy anvil tests were considerably less instructive because the cylinders fractured into many small pieces at velocities in excess of 0.11 km/sec. At these low velocities the cylinders really had not deformed sufficiently to allow a model fit. Even large changes in assumed yield strength resulted in changes in final shape which were considered to be within the bounds of expected measurement errors.

RHA

TEST 5

V = 1083 FPS



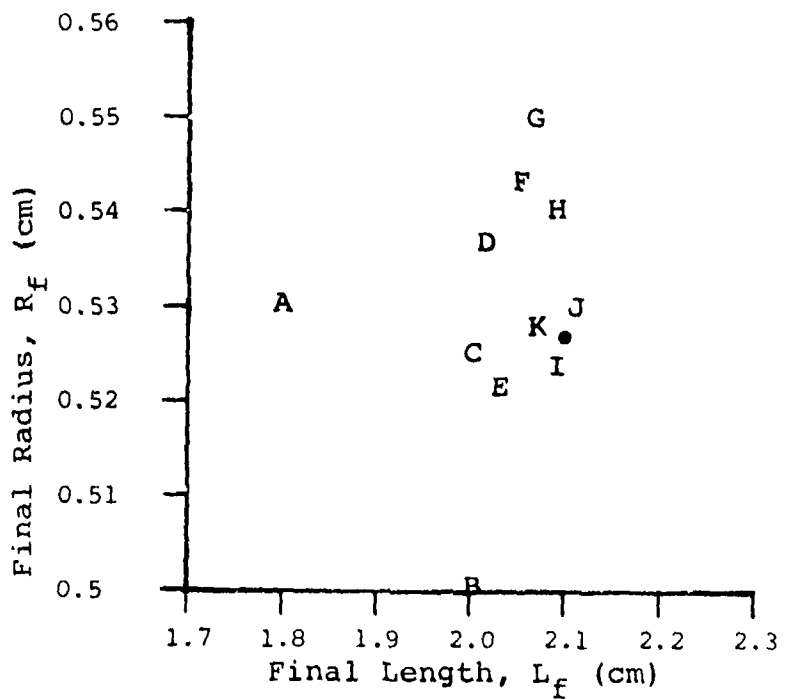
STABALLOY

TEST 10

V = 315 FPS



Figure 2. RHA and Staballoy Cylinders  
After Impact.



• RESULTS OF RHA TEST 5

<u>Point</u>	<u>Initial Yield Strength (kb)</u>	<u>Tangent Modulus (kb)</u>	<u>Final Yield Strength (kb)</u>
A	7	9	16
B	11	9	20
C	12	5	17
D	13	3	16
E	13	6	16
F	14	6	15
G	15	0	15
H	16	0	16
I	16	6	17
J	17	0	17
K	15	2	17

Figure 3. Comparisons of Calculated vs Experimental RHA Cylinder Impacts.

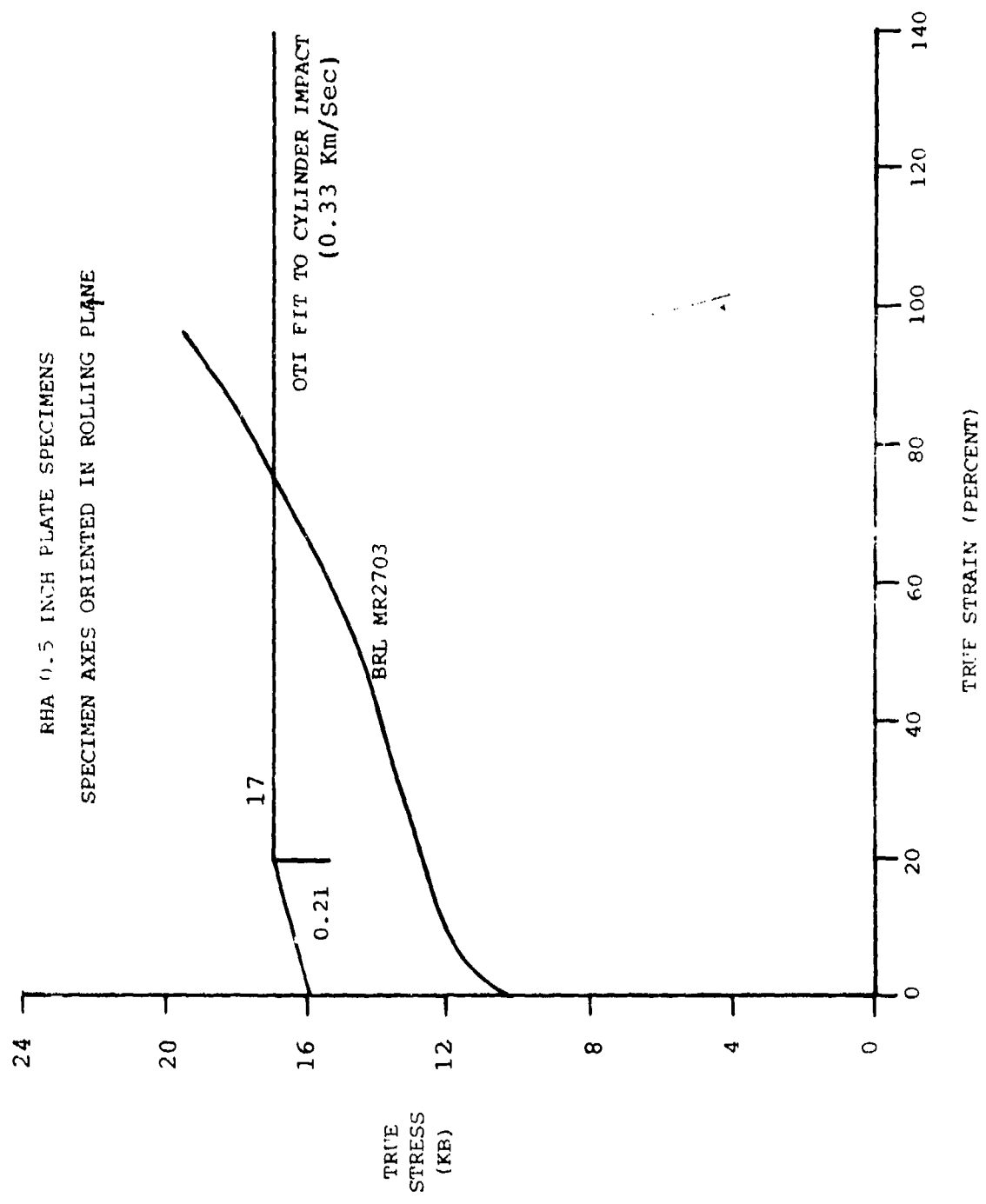
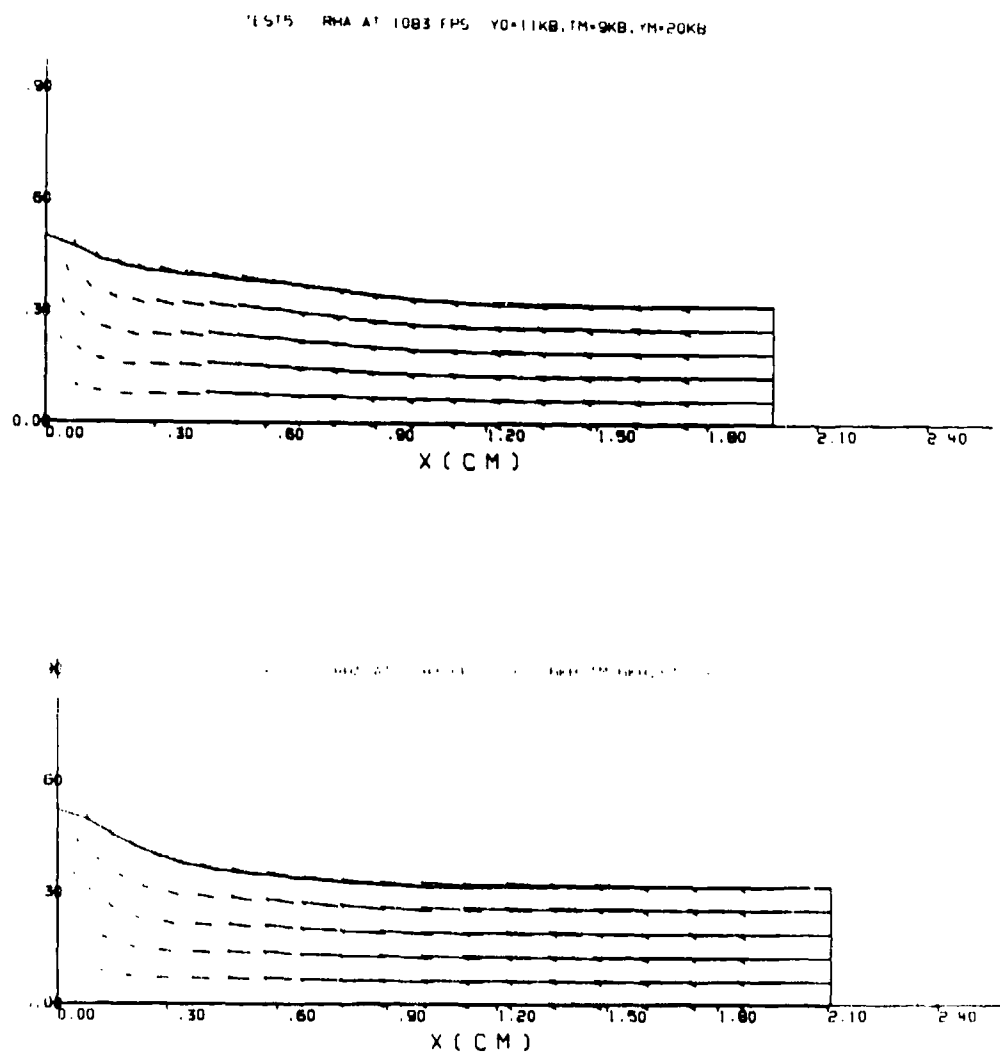


Figure 4. RHA Yield Strength Comparison.



**Figure 5.** Calculated Impacts With BRL MR 2703 Model (Top) and Non-Work Hardening Model (Bottom) at Final Deformation.

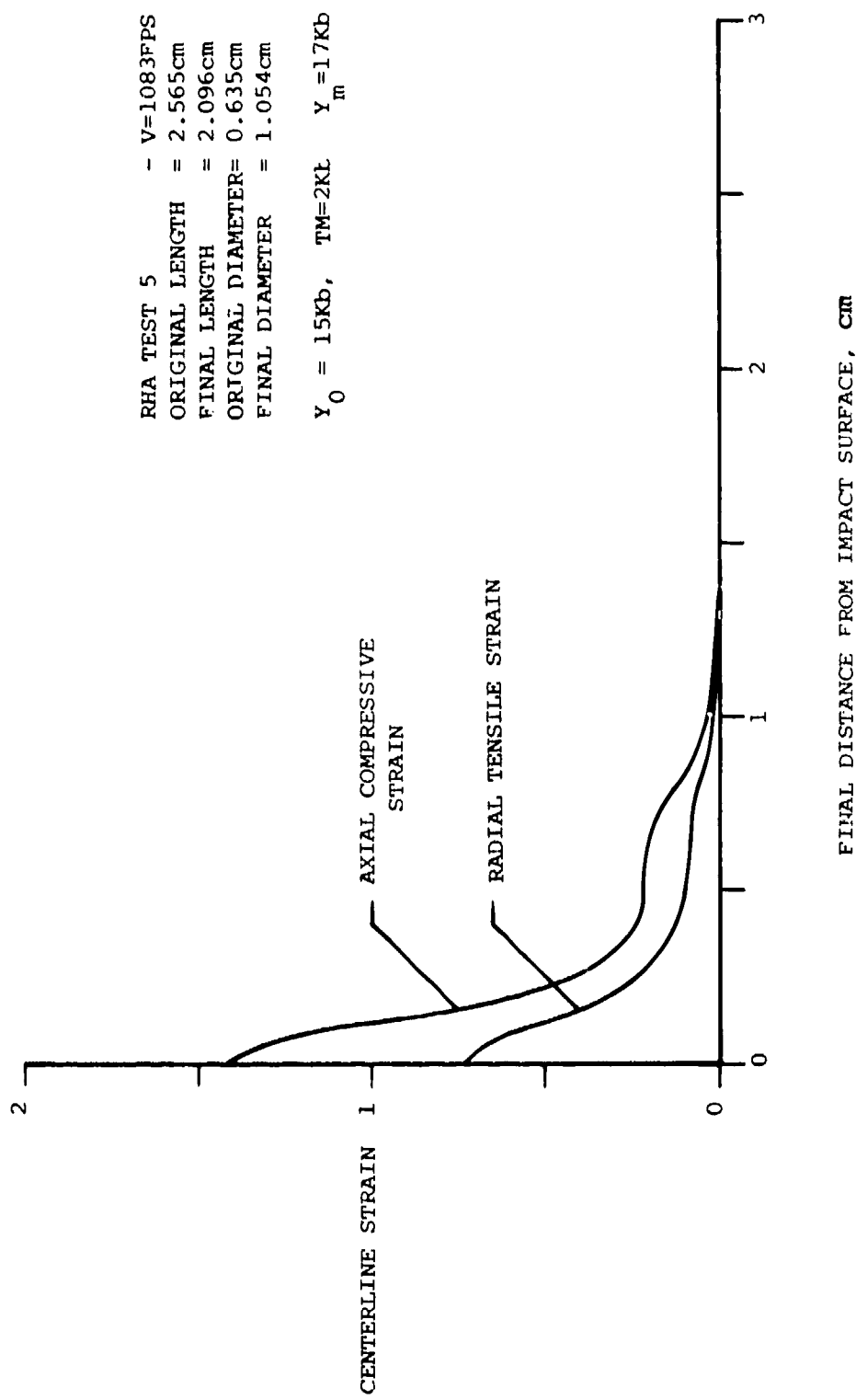


Figure 6. Predicted RHA Strains.

The Southwest Research Institute notched tensile tests were used to provide a yield strength and fracture model for the staballoy of interest. Figure 7 repeats the failure data described in Appendix B. Strain at failure is plotted versus mean stress,  $P$ , divided by the material's yield strength,  $Y$ . The ratio,  $P/Y$ , is controlled by notch size as discussed in Appendix B. As  $P/Y$  approaches unity, the stress state is approaching that for a plane strain situation (i.e., one expected in thin plate impact tests). At  $P/Y = 1/3$ , the stress state is one of uniaxial stress and represents an unconfined tensile test. At  $P/Y$  values less than  $1/3$ , the material is laterally confined. There was no data collected in this latter region.

The staballoy yield strength model selected from Appendix B is one in which the initial yield strength is 10 kilobars and reaches a saturation level of 15 kilobars at a strain of 50 percent.

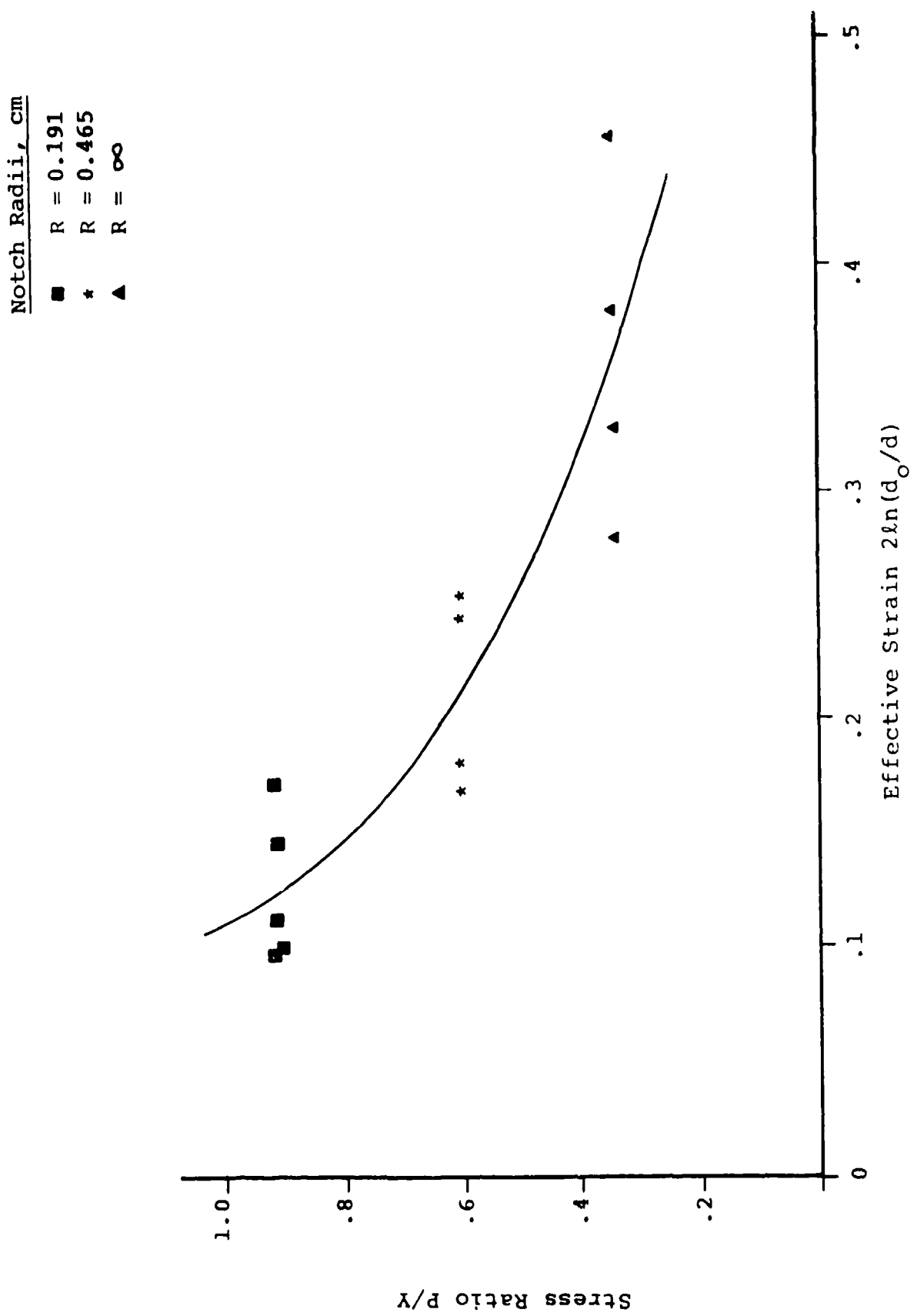


Figure 7. Staballoy Failure Criterion.

## SECTION IV THE EULERIAN CALCULATION - HULL

The demonstration calculation to evaluate the three-dimensional Eulerian/Lagrangian link concept with HULL and EPIC3 was run with the geometric configuration of Figure 1. The RHA and staballoy material properties used in the HULL calculation were as indicated in the following table.

### MATERIAL PROPERTIES USED BY HULL

	Density (gm/cc)	Sound Speed (km/sec)	$V_s/V_p$	Flow Stress (kb)
RHA	7.86	4.61	1.73	15
Staballoy	18.9	2.48	1.53	16

These properties were preliminary results from the work described in the preceding section. The differences are not significant and are probably representative of variations in the material properties encountered from different production runs.

#### A. Plane Strain Approximation

As a preliminary to the full scale three-dimensional HULL calculation, it was decided to run the calculation in two dimensions using the plane strain approximation. This is a reasonable practice before performing a large three-dimensional calculation. The cheaper two-dimensional calculation can be used to evaluate the choice of zoning and to illustrate the qualitative phenomenological features which will be present in the full-scale calculation.

The first two-dimensional plane strain calculation was done with ten zones across the diameter of the penetrator. A constant subgrid, in which uniform square zones were defined, was set up around those portions of the penetrator and target which were expected to suffer the most deformation. This mesh configuration is illustrated by Figure 8. The calculation was run with the penetrator initially at rest in the Eulerian mesh. The target was given a vertical velocity toward the penetrator of 1.036 km/sec. The choice of whether penetrator or target is moved through the mesh is arbitrary. In this calculation, penetrator response was of most interest. By fixing the penetrator in the mesh, Eulerian diffusion was minimized.

Data collection points or stations were also inserted in the mesh. The stations collect the state variables for the cell in which they reside as the calculation proceeds. These data are not collected every time step, but only

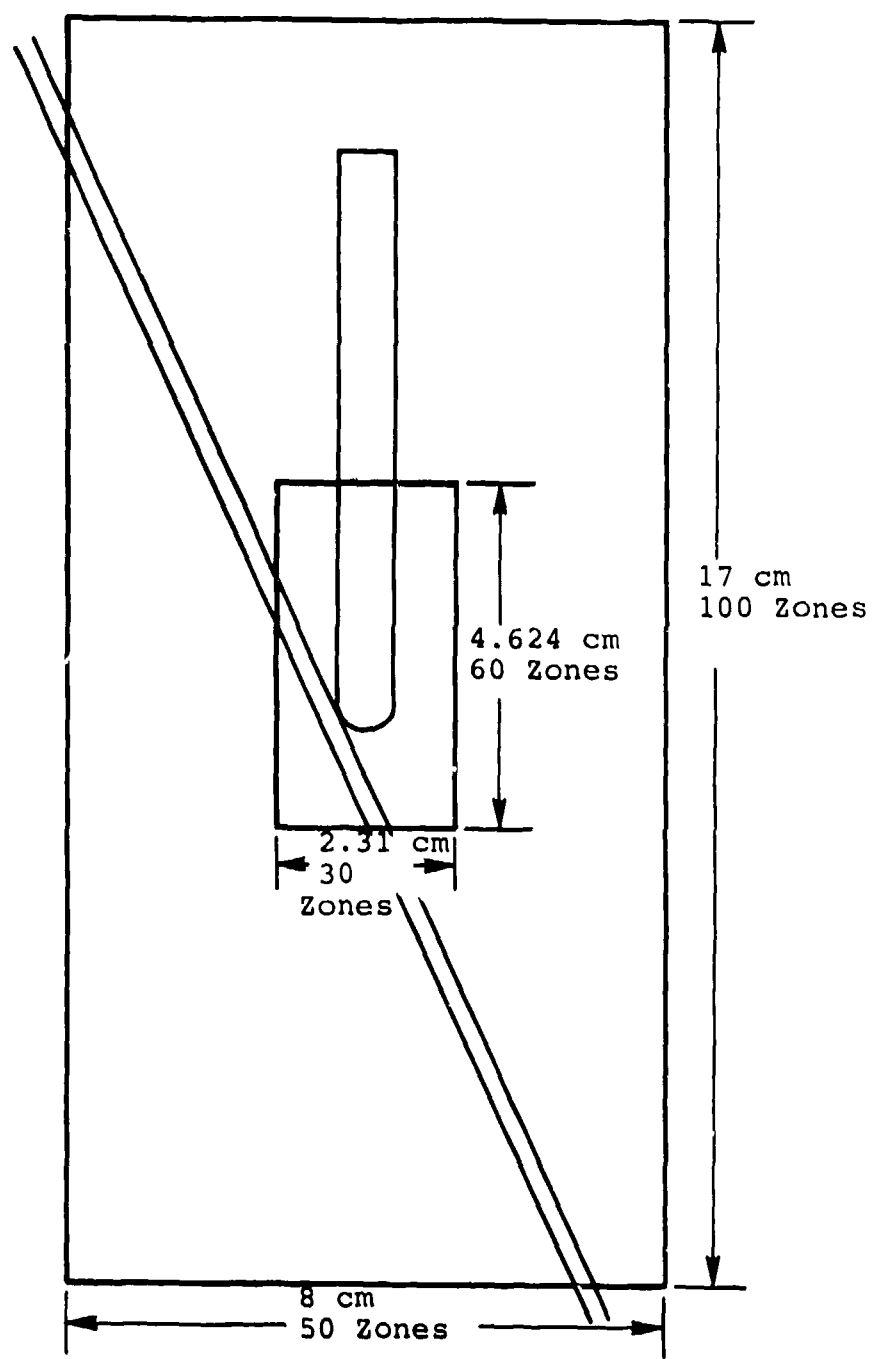


Figure 8. HULL Mesh Configuration in the Plane of the Penetrator/Target Ensemble.

when one of the state variables changes by a significant amount. In this calculation, time data was collected whenever the velocity varied from the previously collected value by more than 2 percent. HULL has the capability to run with either Eulerian stations, which remain fixed in the laboratory reference frame, or Lagrangian stations, which follow the flow of the material in the zone occupied by the station. In this calculation, the stations were Eulerian. The three-dimensional calculation was set up with stations that were Lagrangian in the vertical or target motion direction, and Eulerian in the radial direction in order to reduce the number of required stations. Thus stations in the penetrator nose would follow the rod deformation as the nose receded. The first station was placed at the tip of the rod penetrator. This station was used to furnish vertical velocity to the HULL continuous rezone option. This HULL option permits the user to cause arbitrary motion of any or all grid lines in any coordinate direction. During the course of this calculation, the entire mesh was translated vertically by the velocity determined at station 1. This in effect caused the rod nose to remain in the same Eulerian zone throughout the entire course of the calculation. Thus, the initial resolution defined by the constant subgrid was retained for the entire calculational time.

This first exploratory calculation was run to 45  $\mu$ sec in about 20 CDC 7600 central processor minutes. The second plane strain calculation was run to evaluate the sensitivity of the solution to discretization or zone size. Twice the number of zones was used in each dimension. Time snap-shots of the two calculations are included as Figure 9. Figure 10 is a density contour plot of the coarsely zoned calculation which illustrates the zone numbers in the upper and right margins. For comparison, Figure 11 is the equivalent plot from the fine zone calculations at the same time of 30  $\mu$ sec. The dots, in the region of the rod nose in these figures, indicate the position of stations or data collection points. The amount of penetrator and target deformation was similar for these two calculations. Accordingly, it was decided to run the three-dimensional calculation with the smaller number of zones.

### B. Three-Dimensional Calculation

The third dimension added was normal to the plane of the plots of the preceding figures. Since the rod is a right circular cylinder, it was possible to reduce the magnitude of the calculation by making the plane passing through the rod center a reflecting or symmetry plane. The HULL code permits any mesh boundary to be transmissive or reflective. Thus, the calculation consisted of half the number of planes in the added coordinate than was used in the transverse coordinate direction for the plane strain calculations. The resulting computer time estimate was therefore 25 times the 20 minutes required for the two-dimensional case, or about 8.3 hours.

The three-dimensional calculation was setup with the initial mesh configuration illustrated by Figure 12. The subgrid had 30 zones in the x coordinate direction extending from 1.155 cm to 1.155 cm. The y coordinate was zoned with a total of 25 zones with 15 zones in the subgrid extending from the image plane at  $y=0$  to 1.155 cm. The subgrid in the z coordinate direction was composed of 60 zones with the bottom at 1.386 cm and the top at 3.234 cm.

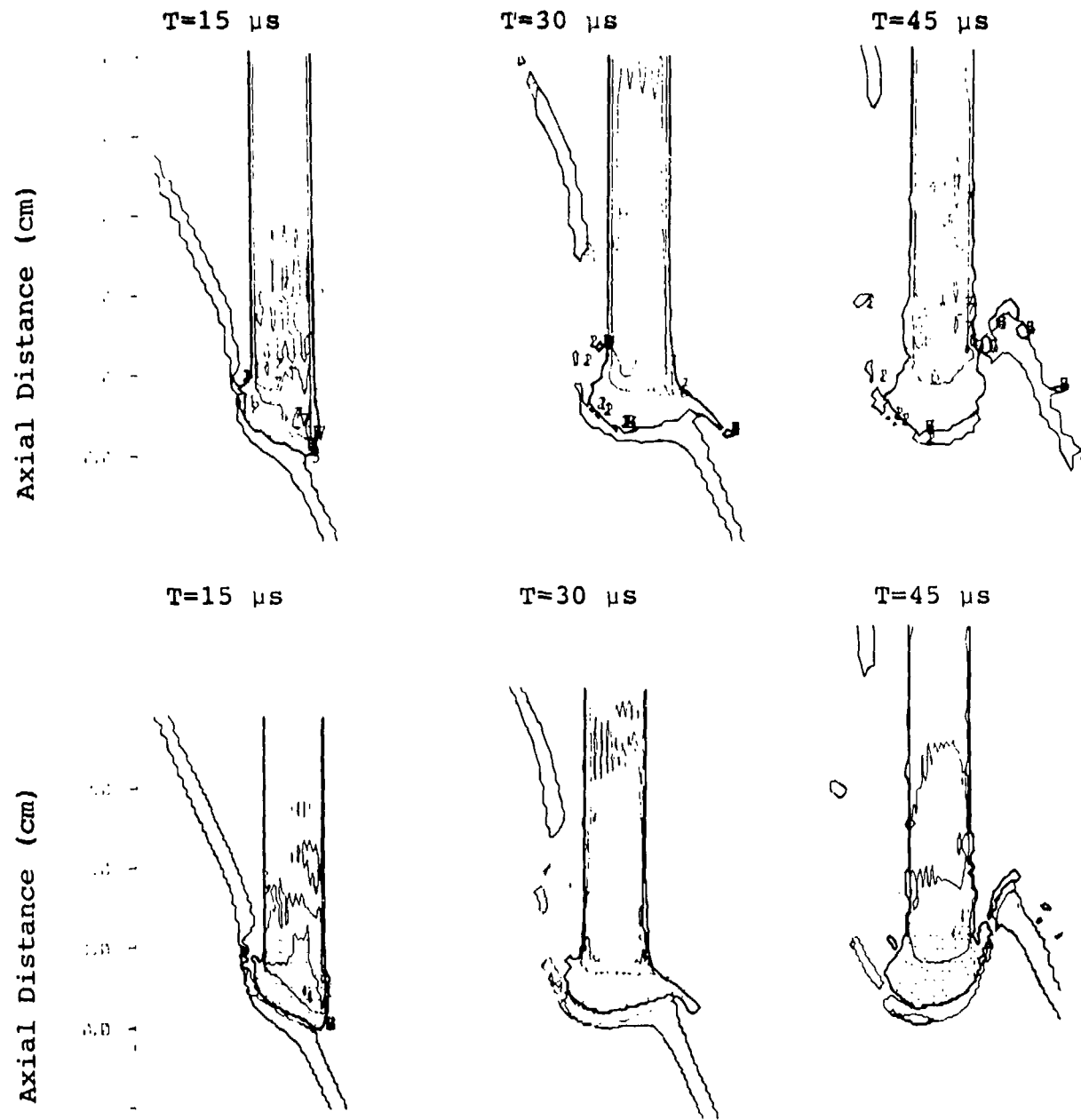


**Figure 9.** Density Contours of Demonstration Calculation to Compare Coarse Zone Case (Top) and Fine Zone Case (Bottom) in Plane Strain.

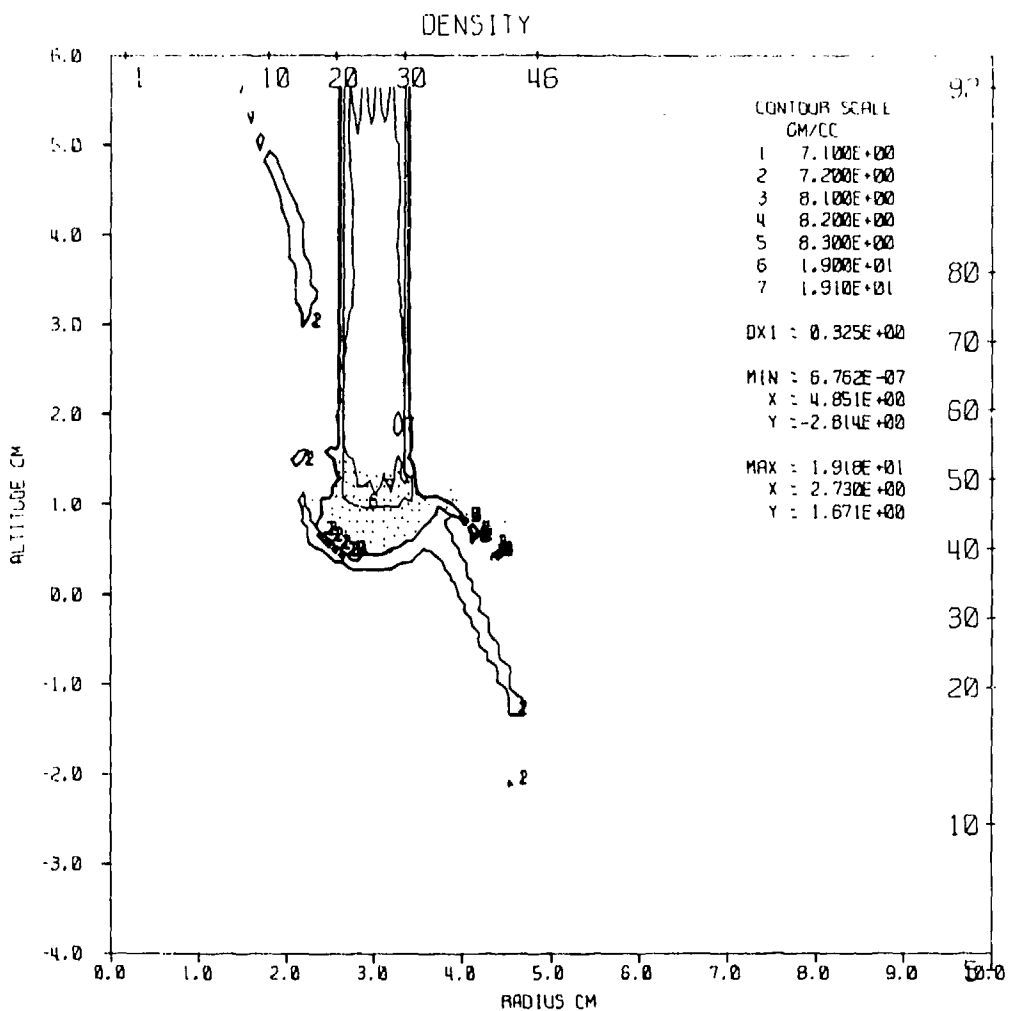


Figure 10. Density Contours of Coarse Zone Case in Plane Strain at 30  $\mu$ sec.

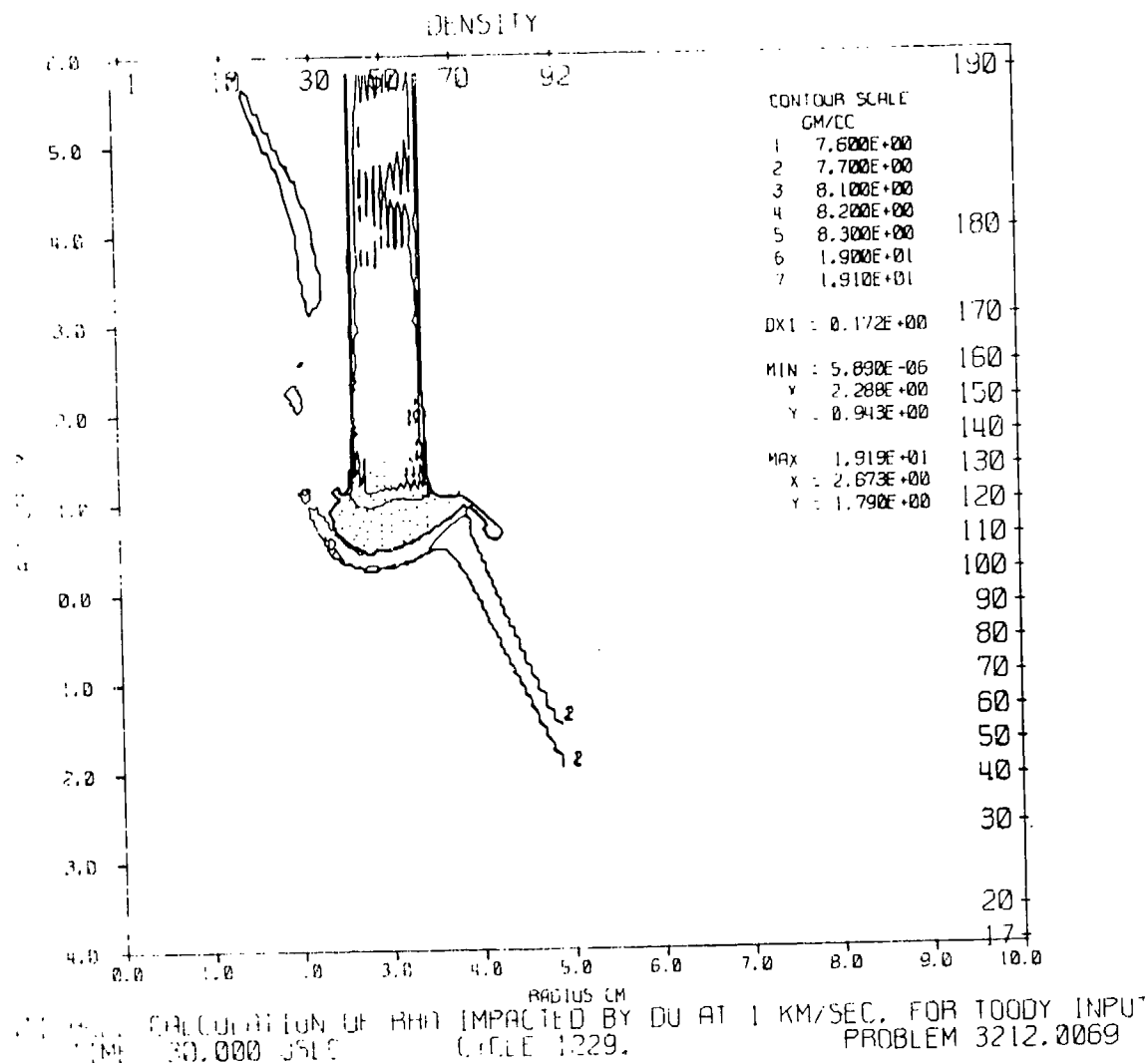


Figure 11. Density Contours of Fine Zone Case in Plane Strain at 30  $\mu$ sec.

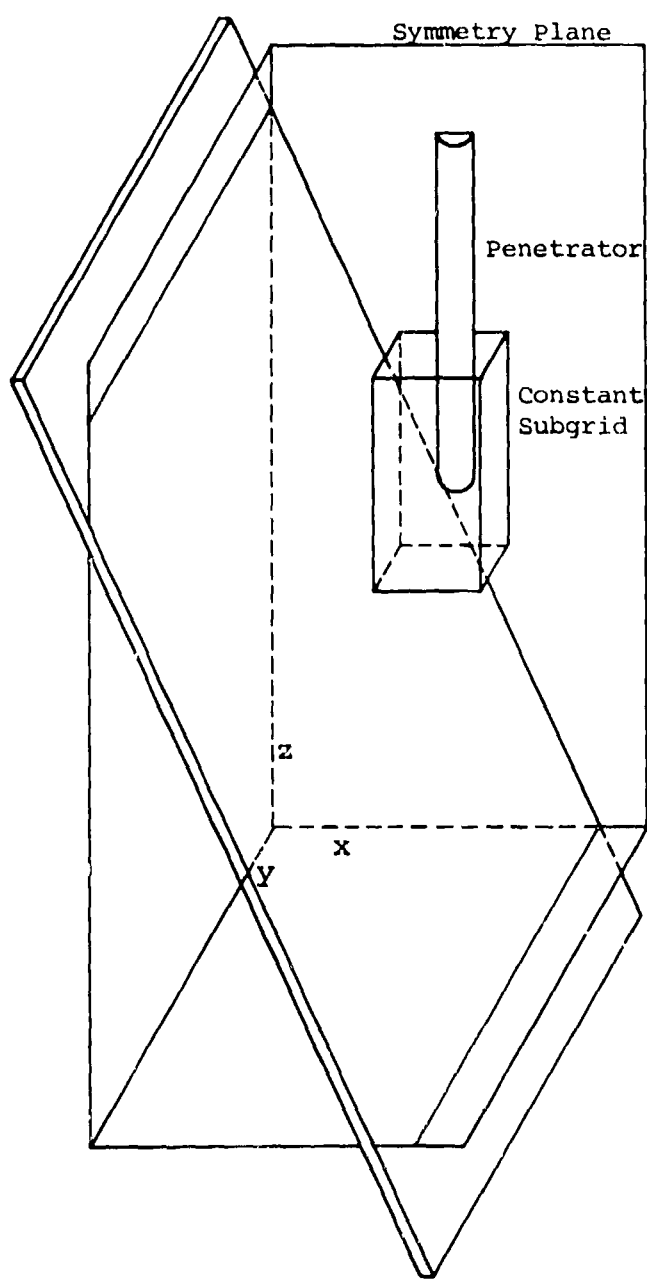


Figure 12. HULL Mesh Configuration For Three-Dimensional Demonstration Calculation.

The input data to construct this mesh and to insert target and penetrator is included with sample output in Appendix C.

The three-dimensional calculation was run with continuous rezoning on the BRL CDC 7600 computer. The mesh storage requirement for 50x100x25 cells with 20 variables per cell was 2.5 million words. The total code occupancy on the BRL machine was 70,067 words SCM and 125,192 words LCM for a total of 195,259 words of memory. HULL requires that only four planes (normal to the Z coordinate) be resident in random access memory. The remainder of the mesh was stored on high-speed disks and the data was transferred in and out of memory as the computations were completed on each plane of data. The entire calculation was run to 47  $\mu$ sec in 7.5 central processor hours. Figure 13 is a composite of density contour snap-shots illustrating the dominant features of the calculation. Figure 14 is included for comparison with the two-dimensional calculations of Figures 10 and 11. From the calculation it is evident that during the initial stage of impact the nose of the rod is rotated away from the target by the impact forces. As break-through starts, the rod nose is rotated back toward the normal as target material is deformed into the path of the penetrator. Thus, one would expect the time dependent transverse wave structure, induced by the initial impact stresses and the short quasi-steady penetration phase, to result in a bending moment. These effects are more prominent at later times in the Lagrangian portion of the calculation described in the next section.

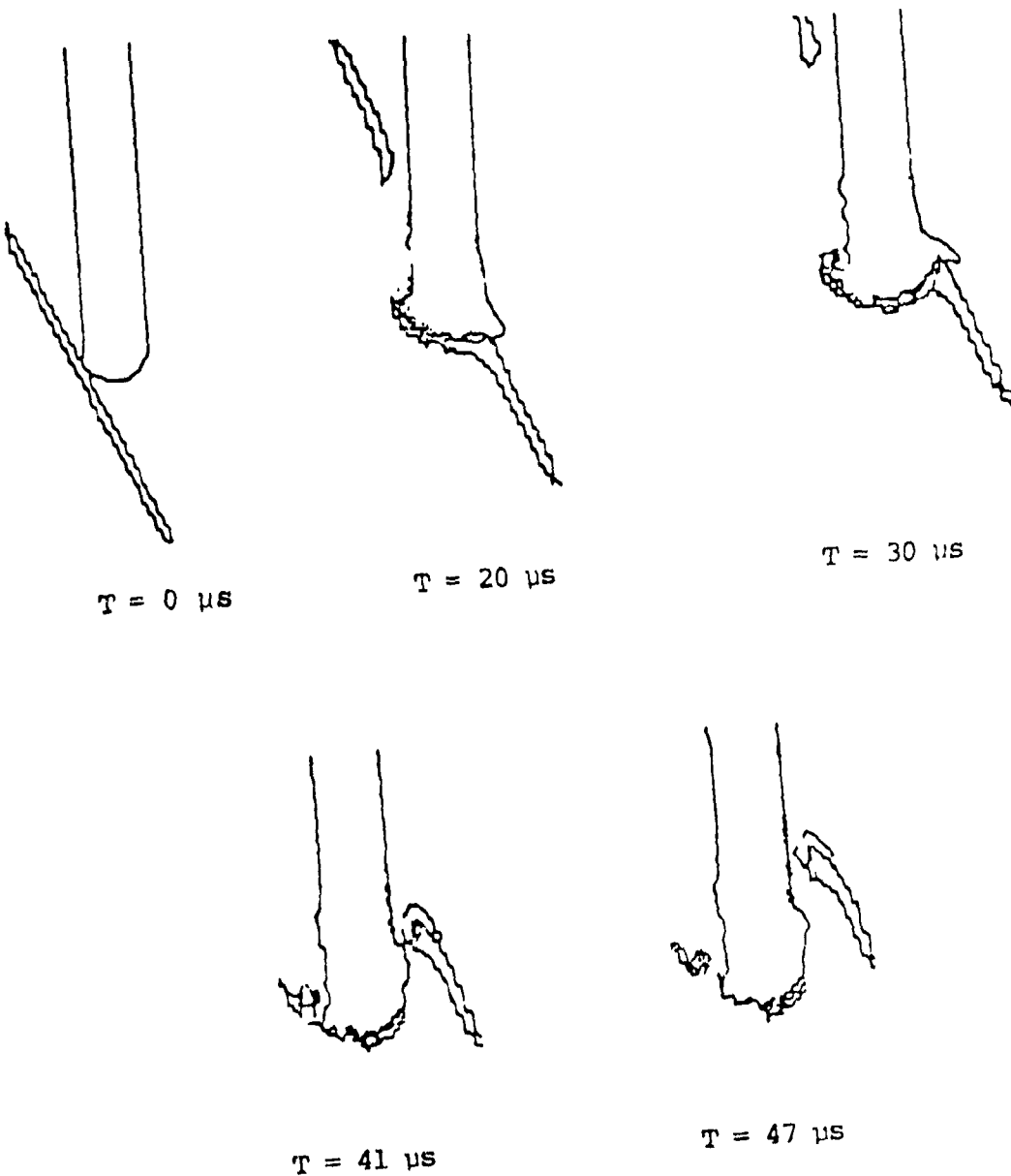


Figure 13. Density Contours of Demonstration Calculation in Three Dimensions.

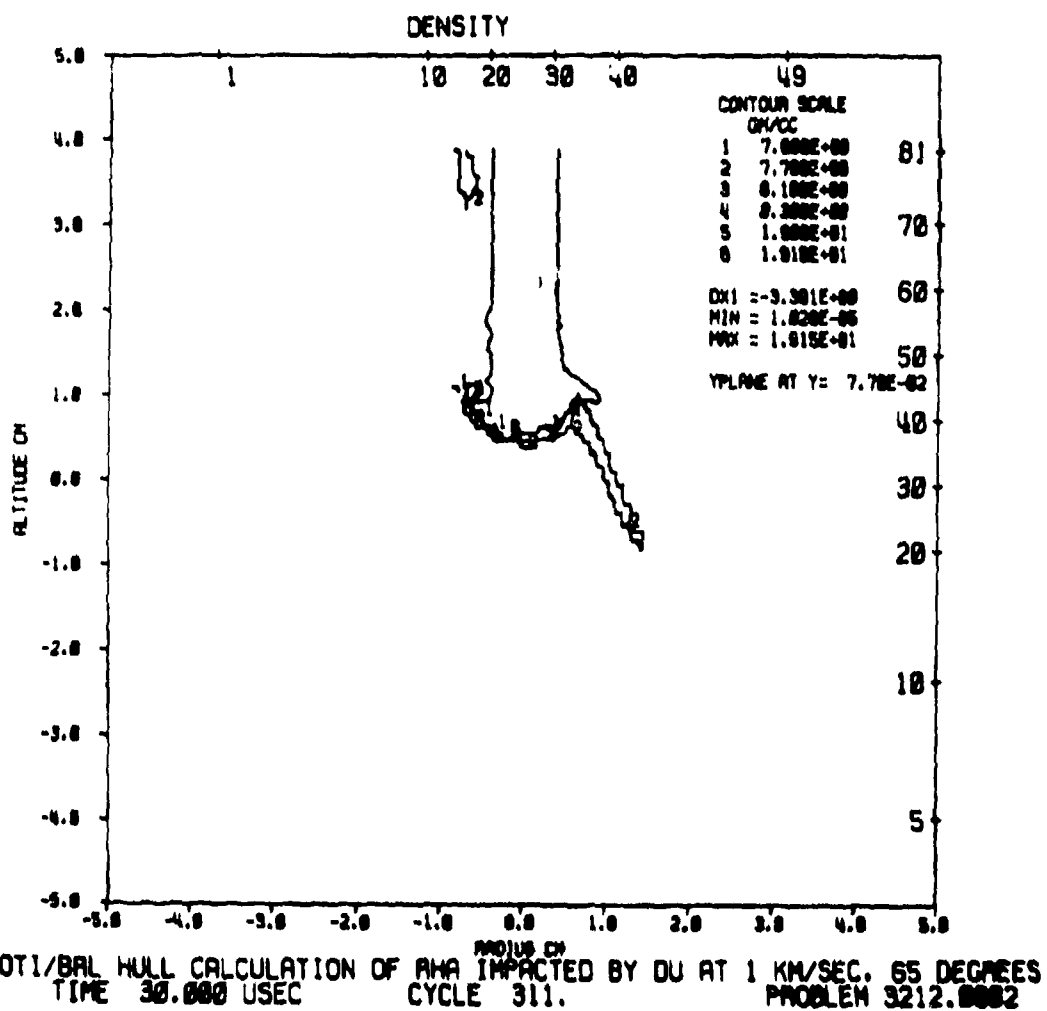


Figure 14. Density Contours of Demonstration Calculation in Three-Dimensions at 30  $\mu$ sec.

## SECTION V EPIC CALCULATION AND COMPARISON WITH EXPERIMENT

The rod of interest was modelled, less the hemispherical nose-cap, in the linked version of EPIC3 (REF 2 and 3). The hemispherical nose-cap was not included because it was obvious from the HULL calculations that the cap rapidly disappears from the rod in very high distortion flow. At the front of the rod, nodes were identified as being driven with HULL velocities. All other surface nodes were free. A detailed description of the link is contained in Reference 5. The reference also contains a list of input used for this problem.

Figure 15 is a plot of EPIC element geometry and velocity vectors at approximately 2.0 microseconds superimposed on a plot of the HULL density contours at the same time. The figure clearly illustrates that the velocity link produces correct flow in the penetrator. Figure 16 presents the same information at slightly over 41 microseconds. By this time one plane of elements had been dropped from the EPIC calculation at the front of the penetrator. This was required to maintain an adequate time step in the calculation. The elements had become too highly compressed and distorted. The newly exposed nodes were identified as being driven by HULL. EPIC was forced to drop one more plane of elements just before running out of HULL data at 49 microseconds.

From 49 microseconds to 200 microseconds EPIC ran without HULL input. A montage of velocity vector views of the rod in its plane of symmetry are shown in Figure 17 for this time period. The rod is oriented in the figure so as to properly demonstrate the rotation seen in the calculation.

Figure 18 is a comparison of calculational and experimental data at run termination. The experimental rods were traced from x-rays provided by the BRL. The scales in the x-rays and the calculation are identical. The comparison is considered very good. The calculated rod's extent of shortening and rotation are very close. Experimentally the rod weighed 57.99 gm and was travelling at 0.977 km/sec at 200 microseconds. In the calculation, the final rod weight was 56.51 gm and the final velocity was 0.997 km/sec. Small differences can be seen in the rod's nose section. These are attributed to possible differences in the yield strength, the rather crude zoning and the fact that element planes had to be dropped from the problem rather than rezoned to a more regular mesh. The yield strength model used in the EPIC calculation is the room temperature staballoy model discussed in Section III with the addition of a thermal softening curve. The thermal softening used assumed that the staballoy maintains 80 percent of its room temperature yield strength when heated to 50 percent of melt. The model uses this point and the theoretical points of no yield strength loss at room temperature and completely zero yield strength at melt. If the rod material is actually softer than this model indicates, the nose section curvature and rotation would be closer to the experimentally observed deformation. There was insufficient computer time available to conduct a zoning study for the EPIC portion of the calculation or to vary yield strength models. It is believed by the BRL that finer

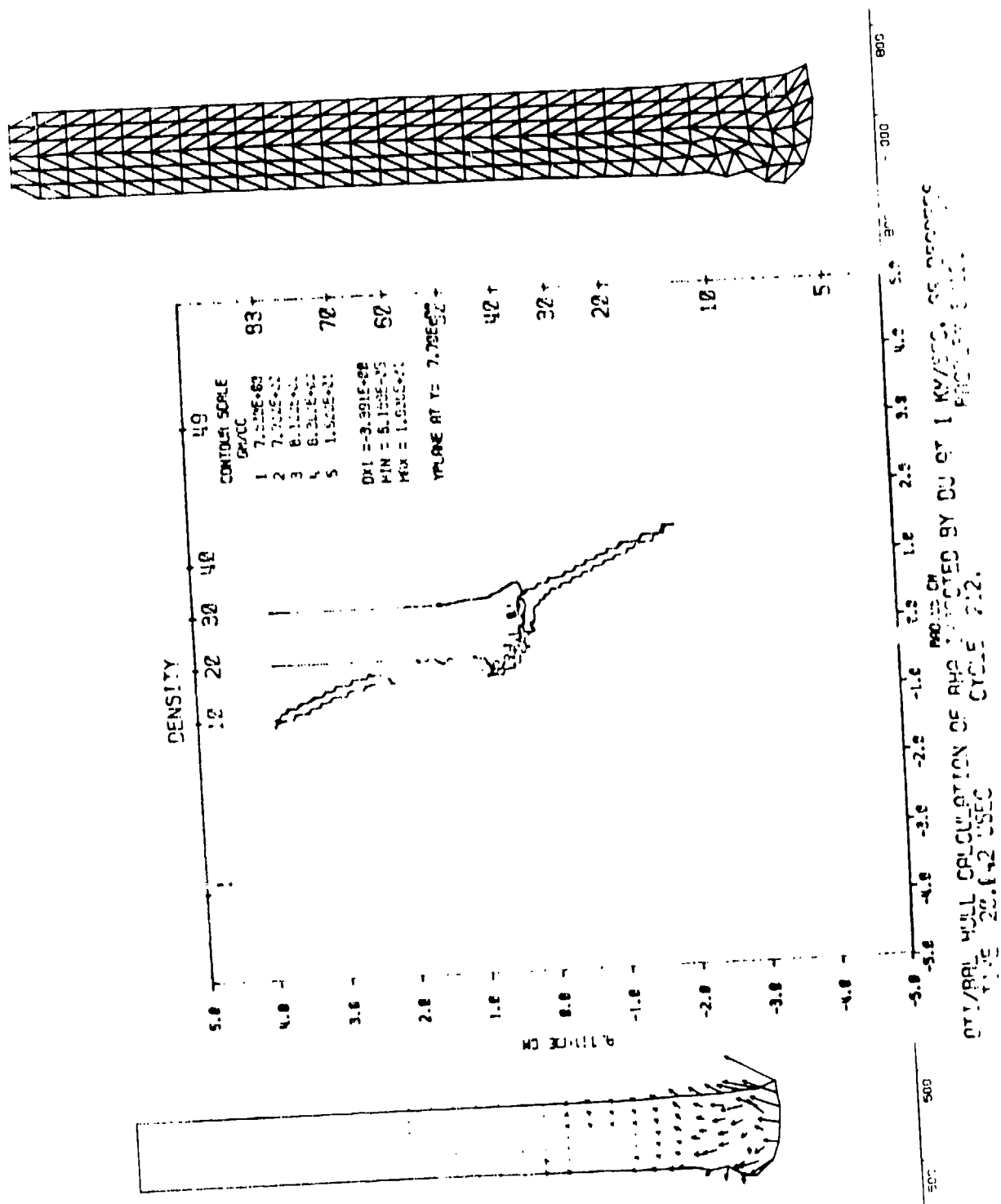


Figure 15. HULL and EPIC Rods at 20 Microseconds.

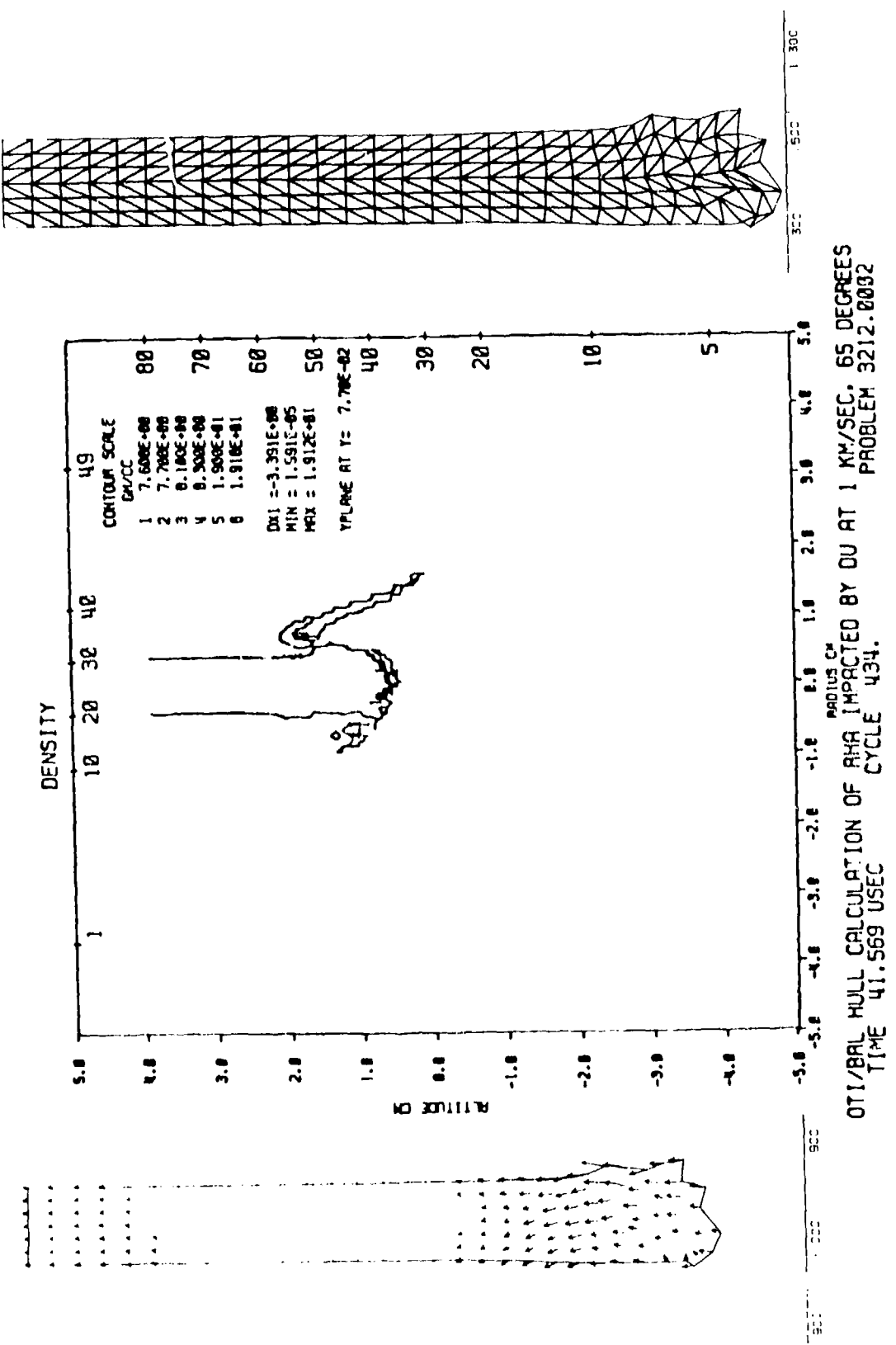


Figure 16. HULL and EPIC Rods at 41.6 Microseconds.

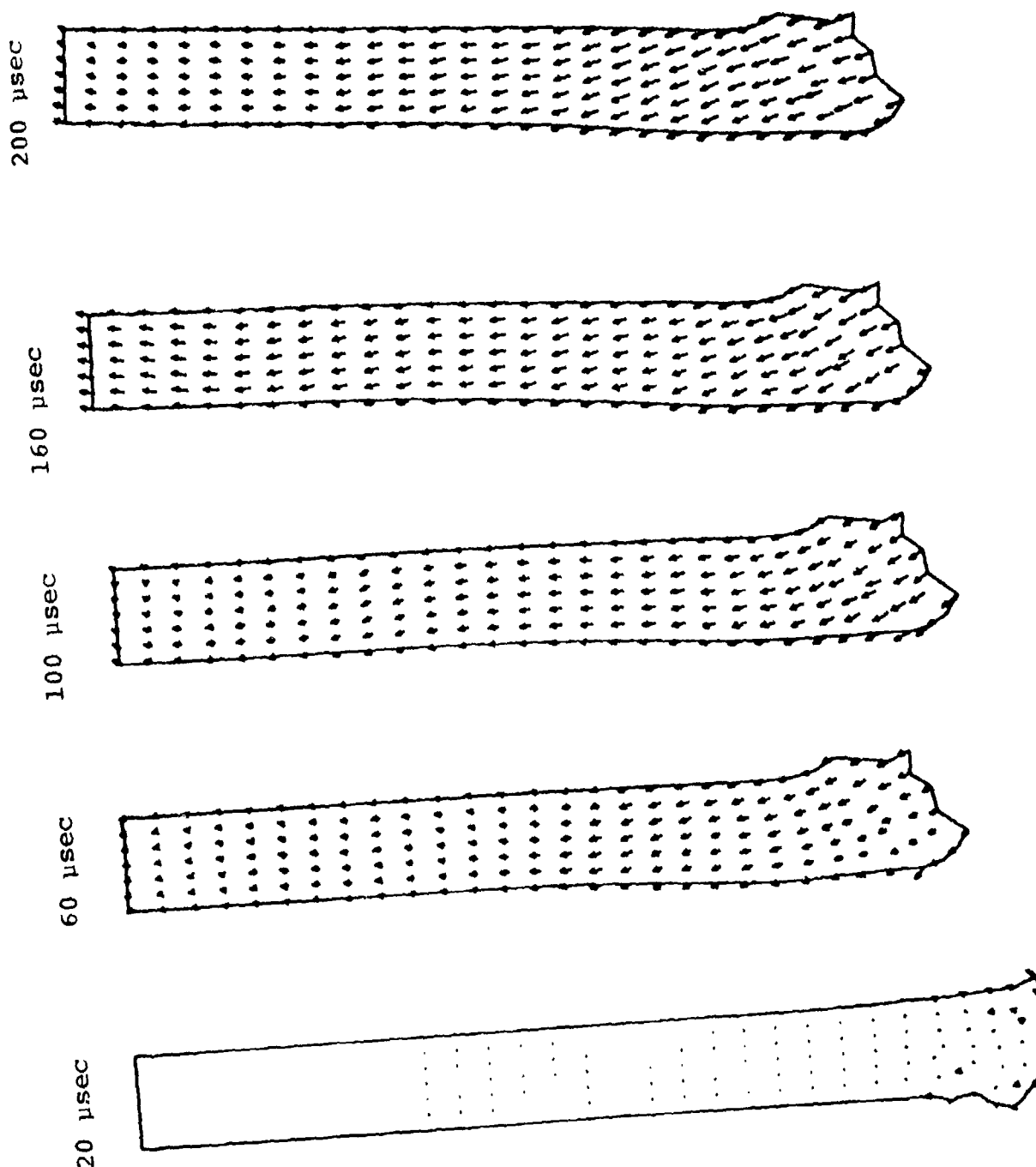


Figure 17. EPIC Velocity Vector Plots to 200 Microseconds.

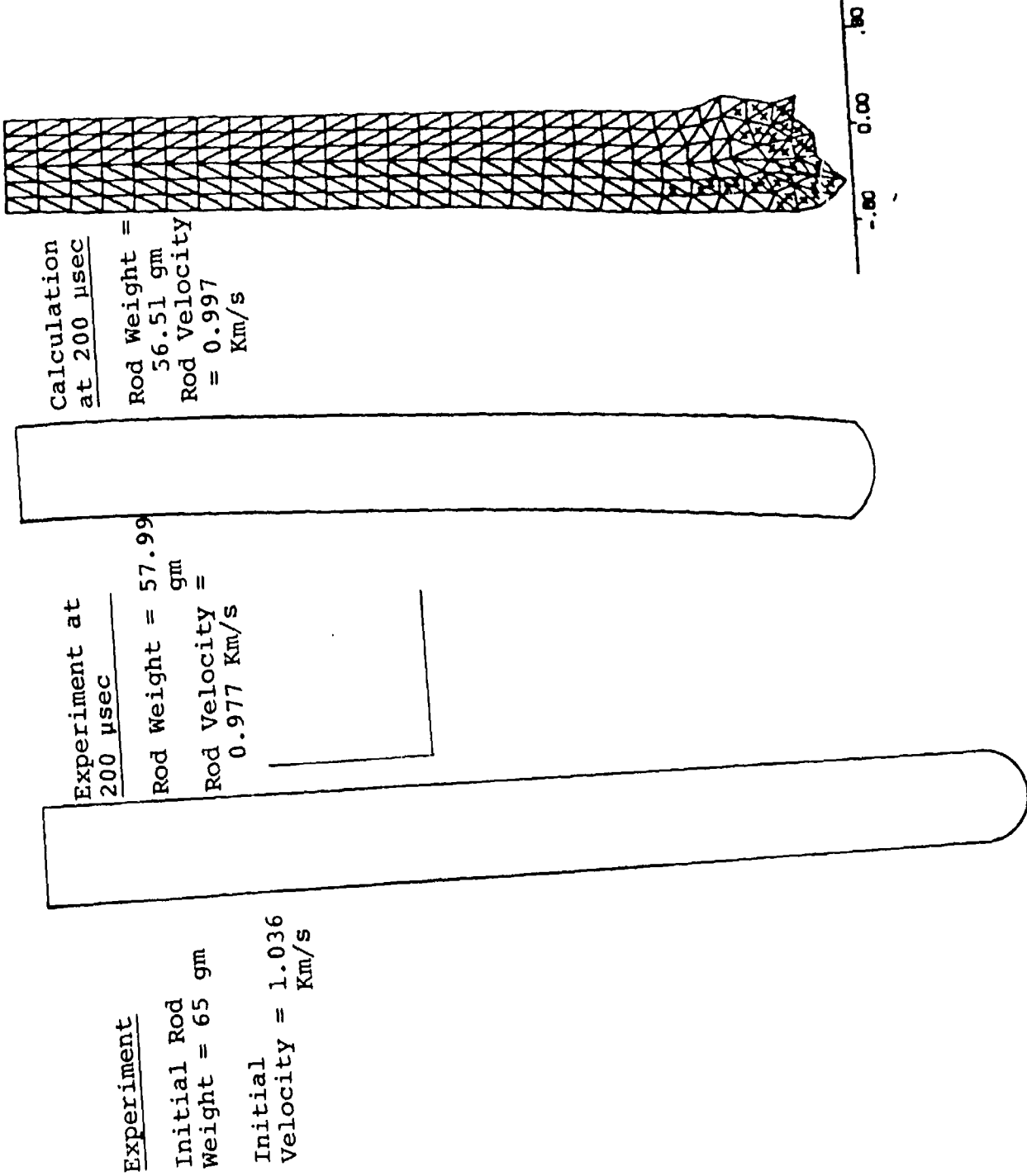


Figure 18. Experimental versus Calculational Results.

zoning would have provided better replication. Completely dropping an element plane because a few elements in the plane are too distorted is a somewhat severe action and can be expected to produce at least some locally non-realistic effects.

During the EPIC run, stresses and strains were monitored and an element was marked as failed if these quantities exceeded the experimentally determined failure curve discussed in Section III. The only elements which exceeded this failure criterion are in the nose of the rod. They are marked with an X in Figure 18. There are no means for determining the accuracy of these failure estimates short of recovering the rod at this time and cross-sectioning it.

Overall, the comparison is considered very good and demonstrates the accuracy and usefulness of the linked technique.

The EPIC run required 840 nodes and 3132 elements. The entire EPIC run took less than 1 CP hour on the BRL CDC 7600 computer. Nodes were run in Large Core memory (LCM) with elements being buffered in and out from intermediate disk storage. There were 64 elements in central memory at any given time. Since unused subroutines are now deleted by the EPIC executive (SAIL), the run required 43,771 words of central memory and 17,024 words of LCM. The run took 1,530 cycles at a CP time per element per cycle of approximately 0.5 milliseconds.

## SECTION VI CONCLUSIONS

The linked Eulerian/Lagrangian methodology demonstrated in this work appears capable of performing fully three-dimensional calculations of the oblique penetration of spaced armor arrays. The calculation reported here was run to 200  $\mu$ sec after initial impact. This corresponded to the time of impact on the next plate in the array. A module in the HULL generator code was then used to transfer the EPIC3 Lagrangian description of the deformed penetrator back into a three-dimensional mesh which included the second plate. This calculation was continued by BRL personnel.

If the calculation had been run entirely with the HULL Eulerian code to 200  $\mu$ sec, a total of about 35 CDC 7600 central processor (cp) hours would have been required. The linked calculation required about 9 cp hours. It is doubtful that the Lagrangian code could have completed the calculation alone because of the severe distortions encountered.

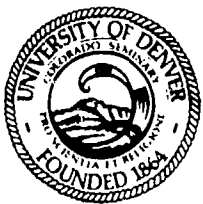
Although this methodology attempts to use Eulerian and Lagrangian techniques in those regimes where each is functioning at its respective advantage, the present link is not without difficulties. The setup and running of two large computer codes requires considerable intervention. Neither HULL nor EPIC3 have been sufficiently exercised in three spatial dimensions to have had their own respective quirks ironed out. The large computer files involved in running a calculation such as this, severely tax the capabilities of current machinery.

The next step in this evolutionary process would be the interactive linking of the two codes. This would require a rework of the total code architecture, but should result in run times of about 2 cp hours for the calculation presented in this report. Such a development would receive the benefit of the experience gained in developing the current linked system.

#### REFERENCES

1. D. A. Matuska and R. E. Durrett, The HULL Code, Finite Difference Solution to-the Equations of Continuum Mechanics, AFATL-TR-78-125, November 1978.
2. G. R. Johnson, D. D. Colby, and D. J. Vavrick, Further Development of the EPIC3 Computer Program For Three-Dimensional Analysis of Intense Impulsive Loading, AFATL-TR-78-81, May 1978.
3. J. J. Osborn, Improvements in EPIC 3, - Link to HULL, - Improved Equation of State, - Improved Fracture Modelling, - SAIL Update System, - Other Improvements, AFATL-TR-81-60, Joint BRL/AFATL Technical Report, June 1981.
4. J. W. Swegle, TOODYIV-A Computer Program for Two-Dimensional Wave Propagation, Sandia Report SAND-78-0552, September 1978.
5. R. F. Benck, Quasi-Static Tensile Stress Strain CurvesII, Rolled Homogeneous Armor, BRL MR 2703, November 1976.

**APPENDIX A**  
**TAYLOR-ANVIL EXPERIMENTS**



## UNIVERSITY OF DENVER

An Independent University

University Park, Denver, Colorado 80208

Denver Research Institute

Laboratories for Applied Mechanics 303•753•2616

21 February 1980

Mr. John Osborne  
Orlando Technology, Inc.  
P. O. Box 855  
Shalimar, FL 32579

Dear Sir:

Twenty Taylor Anvil specimens were fired as per our agreement of 7 November 1979. The experimental conditions are described below.

### 1. The Anvil

The anvil used in the DRI tests was a piece of 4340 steel, 9 inches in diameter weighing about 80 pounds. This anvil was hardened to  $R_c$  40 and both faces were surface ground.

Alignment of the anvil was accomplished by placing a mirror on the surface and rotating the anvil until the reflection of the gun barrel muzzle was visible in the mirror and centered in the bore.

### 2. Gun barrel

Initially the Taylor Anvil specimens were launched in a .30 caliber smoothbore using a lexan sabot. This method produced highly variable velocities due to the large cartridge case. To solve this problem and to improve on the percentage of good axial hits a smoothbore barrel with a .256 inch bore diameter and chambered for a .22 Hornet cartridge case was purchased. This eliminated the need for a sabot and, because of the small size of the Hornet case, better velocity control was also achieved.

### 3. Velocity Measurement

Velocity measurement was accomplished in the last foot of the gun barrel. Powder gases were vented prior to the cylinder passing by a small

hole in the gun barrel which had a light beam passing through it. After traveling one foot the cylinder passed another hole with a light beam passing through it. At the first hole, passage of the cylinder through the light beam triggered a chronograph (accurate to the nearest 0.1  $\mu$ sec) starting the count. Passage of the cylinder through the second light beam stopped the chronograph yielding the elapsed time for the cylinder to travel one foot. This information was then used to compute the velocity.

#### 4. Data

TABLE 1  
D.U. - .75 Ti Alloy Cylinders

Cylinder No.	Weight (grains)	Dia.-Length (inches)	Impact Orientation	Impact Velocity (fps)
1	237.8	.254-1.002	$\pm 1^\circ$	510-B <sup>1</sup>
2	237.8	.254-1.002	$\pm 1^\circ$	484-B
3	238.9	.255-1.002	$\pm 1^\circ$	213-L
4	237.9	.254-1.002	$\pm 1^\circ$	353-M
5	237.7	.254-1.004	$\pm 1^\circ$	365-B
6 <sup>2</sup>	Not Fired - Diameter too large			
7	237.3	.253-1.004	$\pm 4^\circ$	341-M
8	237.0	.254-1.005	$\pm 1^\circ$	399-B
9	237.8	.254-1.002	$\pm 1^\circ$	360-B
10	237.9	.254-1.005	$\pm 1^\circ$	315-M

<sup>1</sup>Letters refer to deformation. L = light, M = medium, H = heavy, B = broke end of cylinder, NG = no good.

<sup>2</sup>This cylinder was too large in diameter for the gun barrel and was returned to Nuclear metals for remachining.

TABLE 2  
RHA Cylinders

<u>Cylinder No.</u>	<u>Weight (grains)</u>	<u>Dia.-Length (inches)</u>	<u>Impact Orientation</u>	<u>Impact Velocity (fps)</u>
1	95.2	.250-.988	+ 1°	518-L
2	95.2	.251-1.005	-	509-NG
3	96.7	.251-1.001	-	929-NG
4	97.5	.251-1.010	+ 1°	1459-H
5	96.2	.250-1.008	+ 1°	1083-H
6	96.7	.251-1.005	-	722-NG
7	96.8	.251-1.007	+ 1°	855-H
8	94.6	.250-.985	+ 5°	786-M
9	96.2	.250-1.000	-	950-NG

TABLE 3  
Length of Unfractured Taylor Anvil Specimens  
Before and After Impact

D.U. - .75 Ti Cylinders

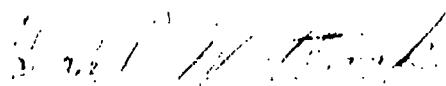
<u>Cylinder No.</u>	<u>Original Length</u>	<u>Final Length (inches)</u>	<u>Condition After Impact</u>	<u>Impact Velocity (fps)</u>
1	1.002	-	Fractured	510
2	1.002	-	Fractured	484
3	1.002	.9843	Intact	213
4	1.002	.9483	Intact	353
5	1.004	-	Fractured	365
6	Not Fired (Dia. too large)			
7	1.004	.956	Intact	341
8	1.005	-	Fractured	399
9	1.002	-	Sheared	360
10	1.005	.9628	Intact	315

RHA Cylinders

1	.988	.933	Intact	518
2	1.005	-	-	509-NG
3	1.001	-	Intact	929-NG
4	1.010	.805	Fracture Lines	1459
5	1.008	.825	Intact	1083
6	1.005	-	Intact	722-NG
7	1.007	.870	Intact	855
8	.985	.870	Intact	786
9	1.000	-	-	950-NG

Please note that when the values given for the impact angle are  $\pm 1^\circ$  the distance traveled by the cylinder after leaving the gun muzzle was only 6 to 8 inches. This short distance virtually guaranteed good axial hits estimated in most cases to be within  $\pm 1^\circ$ . When the angle is given a value other than  $1^\circ$  it was measured with a protractor to within  $1^\circ$ . The plus or minus associated with these angles has no real meaning except to indicate that the exact orientation at impact is unknown.

Very truly yours,



Edward P. Wittrock  
Research Engineer

EPW:jw

**APPENDIX B**  
**NOTCHED TENSILE EXPERIMENTS**

# SOUTHWEST RESEARCH INSTITUTE

POST OFFICE DRAWER 28610 • 8220 CULEBRA ROAD • SAN ANTONIO, TEXAS 78284 • (512) 684-6111

Department of Materials Sciences  
July 22, 1980

Mr. John J. Osborn  
Orlando Technology, Inc.  
P. O. Box 855  
Shalimar, Florida 32579

Reference: P.O. No. 420-914-204

Subject: SwRI Project No. 02-5845-107  
"Tensile Tests"  
FINAL REPORT

Dear John:

This letter constitutes our final report on the referenced project. Procedures used and the test results are summarized in the following paragraphs.

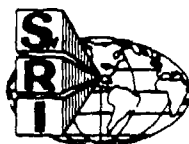
Both smooth and notched round tensile specimens were tested in order to determine the relation between  $P/Y$  and  $\bar{\epsilon}^P$  at failure for staballoy specimens. All specimens were prepared by Nuclear Metals, Inc. in accordance with the attached SwRI drawing, Figure 1.

The critical parameters and the notch geometry are given in Figure 2. Three notch radii were selected to yield nominal values for  $P/Y$  of 0.333, 0.682 and 0.939. The initial values  $D_0$ ,  $d_0$  and  $R_0$  are given in Figure 2. The following definitions are used in the data reduction and presentation:

$$\frac{P}{Y} = \frac{1}{3} + \ln\left(\frac{d}{2R_0} + 1\right)$$

$$\bar{\epsilon}^P = \ln(d_0/d)$$

The tensile tests were performed at a constant axial strain rate of 0.0025 in/sec. Diametral strain was measured with a strain-gage type flexural extensometer positioned such that the contact points were at the notch root minimum radius. For smooth specimens or large root radii, this positioning is difficult because a priori location of the tensile neck is not possible. For this reason, the extensometer was used for transient recording of the load-deformation history but the minimum diameter of the failure cross section was measured directly from the broken specimen. Load was measured in the standard way by an in-series load cell. Maximum crosshead velocity used was limited by the dynamic response of the extensometer.



SAN ANTONIO, HOUSTON, TEXAS, AND WASHINGTON, D.C.

Mr. John J. Osborn

-2-

July 22, 1980

Five specimens of each notch radius were tested. The failure data for these specimens are given in Table I. The failure data are computed based on the minimum diameter at fracture ( $d = d_f$ ) and the initial notch radius ( $R = R_0$ ). The notch radius at failure is not easily defined and was not measured. Appended to this report are plots of the axial true net section stress ( $\sigma = \text{Load}/\text{Actual net cross-sectional area}$ ) vs. the logarithmic strain ( $\epsilon_P = 2 \ln d_0/d$ ). For the standard smooth 0.505 inch round tensile specimens, the average ultimate true tensile stress was 228.3 ksi (15.53 kbar).

The failure data from Table I are plotted in Figure 3. A curve is drawn through the crosses which designate the average effective failure strains for each value of P/Y. The larger scatter in failure strain for the smooth specimens ( $P/Y = 0.33$ ) may be expected because a larger volume of material reaches the maximum stress condition. The probability of a critical flaw experiencing this stress is therefore greater. The notch concentrates the zone of maximum stress in a much smaller volume.

The failure strains determined from the diameter of the broken specimen (Table I) are plotted as crosses on the axial stress-diametral strain curves. This strain is larger than the maximum measured extensometer strain when the extensometer arms fail to follow the minimum diameter in the notch or neck. This is particularly a problem with the smooth specimens where the location of the neck is indeterminate.

If you have any questions regarding these tests, please do not hesitate to contact us. Unless otherwise instructed, we will dispose of all specimens. It has been a pleasure working with you and I hope we can do more in the future. It would be interesting to explore the temperature and strain-rate sensitivity of this data.

Respectfully submitted,

*llue*  
J. S. Lindholm, Director  
Department of Materials Sciences

USL/mb  
Attachments

cc: S. H. Birgel

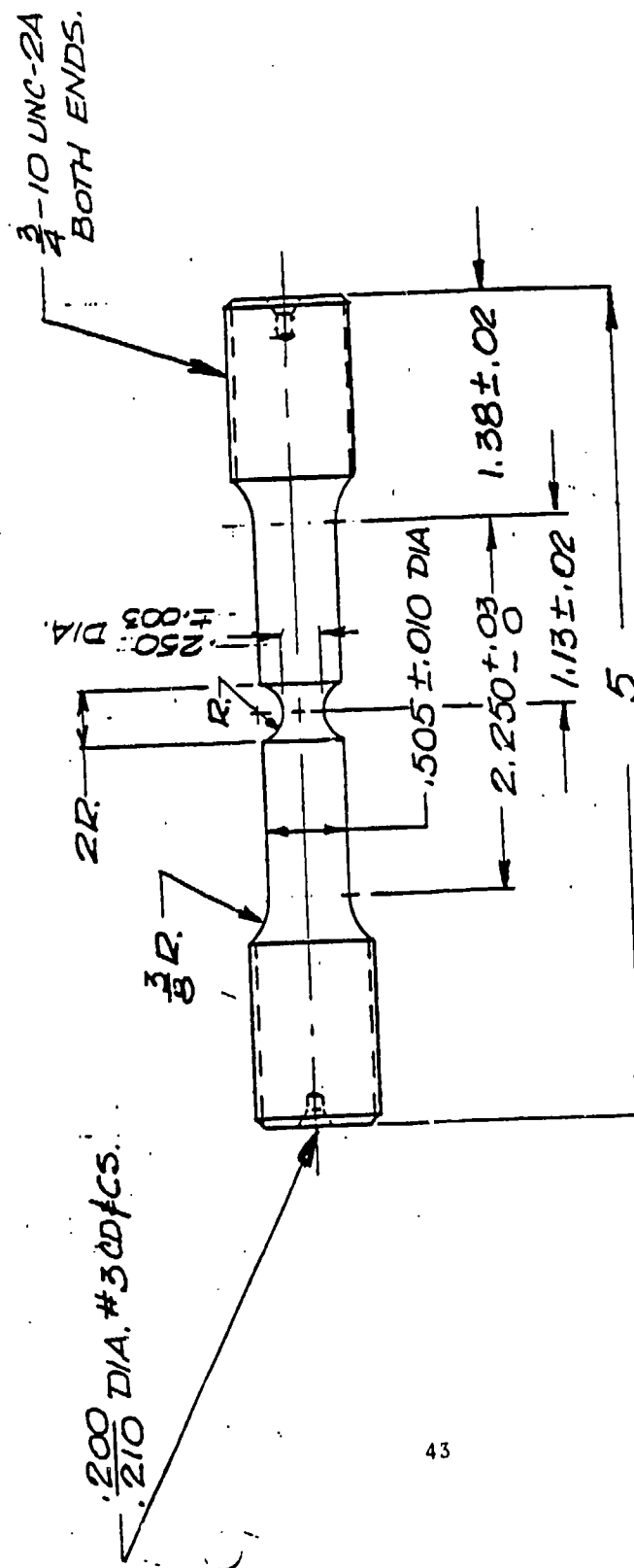
TABLE I  
FAILURE DATA

<u>Specimen Number</u>	<u>R<sub>o</sub></u> (in)	<u>d<sub>o</sub></u> (in)	<u>d<sub>f</sub></u> (in)	<u>(P/Y)<sub>f</sub></u>	<u><math>\bar{\epsilon}^p_f</math></u>	<u><math>\bar{\epsilon}^p_f</math></u> (ave)
1	∞	.5055	.4396	.3333	.2794	
2	∞	.5045	.4171	.3333	.3805	
3	∞	.5063	.4031	.3333	.4559	.3610
4	∞	.5066	.4738	.3333	.1339*	
5	∞	.5042	.4279	.3333	.3282	
6	.183	.2469	.2254	.6018	.1822	
7	.180	.2508	.2207	.6007	.2557	
8	.185	.2516	.2400	.6142	.0944*	.2134
9	.180	.2522	.223	.6031	.2461	
10	.185	.2471	.227	.6009	.1697	
11	.075	.2450	.2329	.9079	.1013	
12	.075	.2477	.230	.9024	.1483	
13	.073	.2504	.2295	.9133	.1743	.1273
14	.075	.2500	.2380	.9174	.0984	
15	.075	.2482	.2344	.9107	.1144	

\* Failed prematurely. Not included in average.

DRAWING NUMBER	REVISIONS	DESCRIPTION	DATE	APPROVE!
LTR				

FIGURE 1.



43

Q ± .001 REQ'D
NO NOTCH

- NOTE: 1. MACHINE BETWEEN CENTERS  
2. DO NOT UNDERCUT 3/8 RAD/1

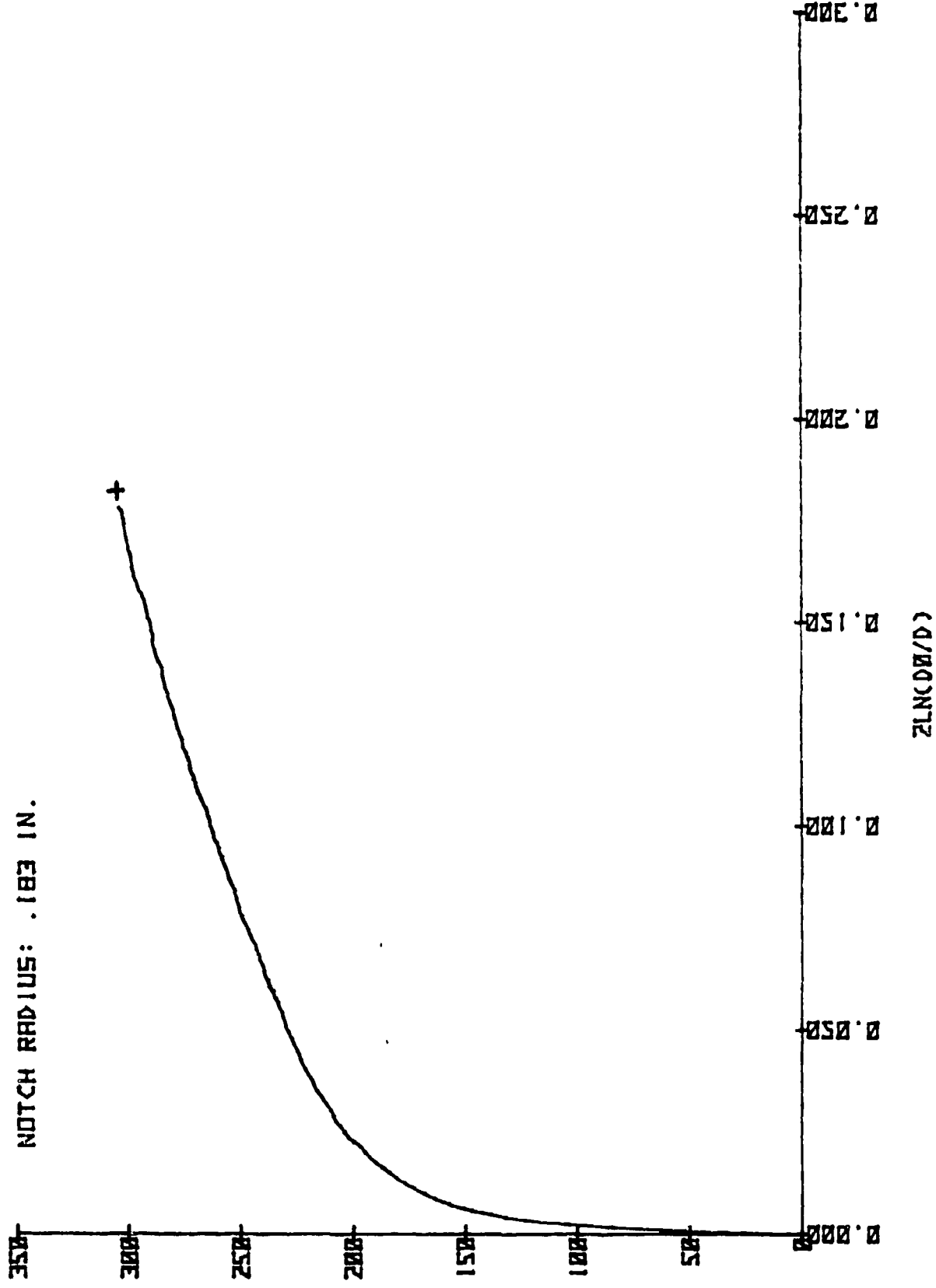
SOUTHWEST RESEARCH INSTITUTE  
SAN ANTONIO, TEXAS

NOTCHED TENSILE SPECIMEN

UNLESS OTHERWISE SPECIFIED DIMENSIONS ARE IN INCHES AND INCLUDE CHEMICALLY APPLIED OR PLATED FINISHES	CONTRACT	DRAW	CHK	DRAWING NO.
TOLERANCES				26401
BASIC DIMENSION	DECIMALS	FRACTIONS	MECH	
UNDER .6	.± .02	.± .005	.± 1/32	ELEC
6-24 INCL	.± .03	.± .010	.± 1/16	
OVER 24	.± .04	.± .015	.± 1/8	
				PROJ.
				ANGLES .± 1° 30'

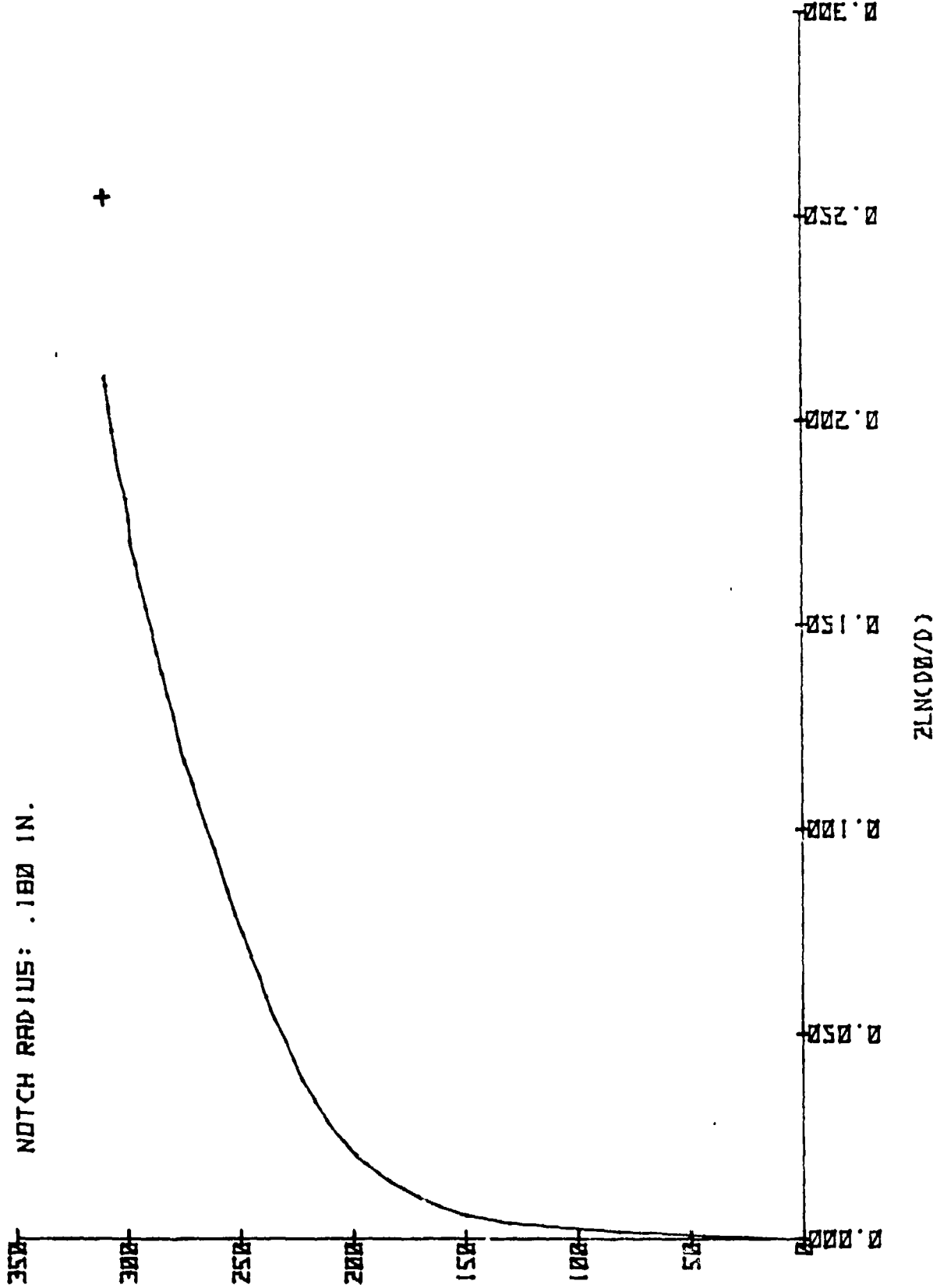
EXCEPT AS MAY BE OTHERWISE PROVIDED BY CONTRACT,  
THESE DRAWINGS AND SPECIFICATIONS ARE THE PROPERTY  
OF SOUTHWEST RESEARCH INSTITUTE. ARE ISSUED IN  
STANDARD CHARTERED FORM AND SHALL NOT BE REPRODUCED, OR

SPECIMEN #: 6  
NOTCH RADIUS: .183 IN.



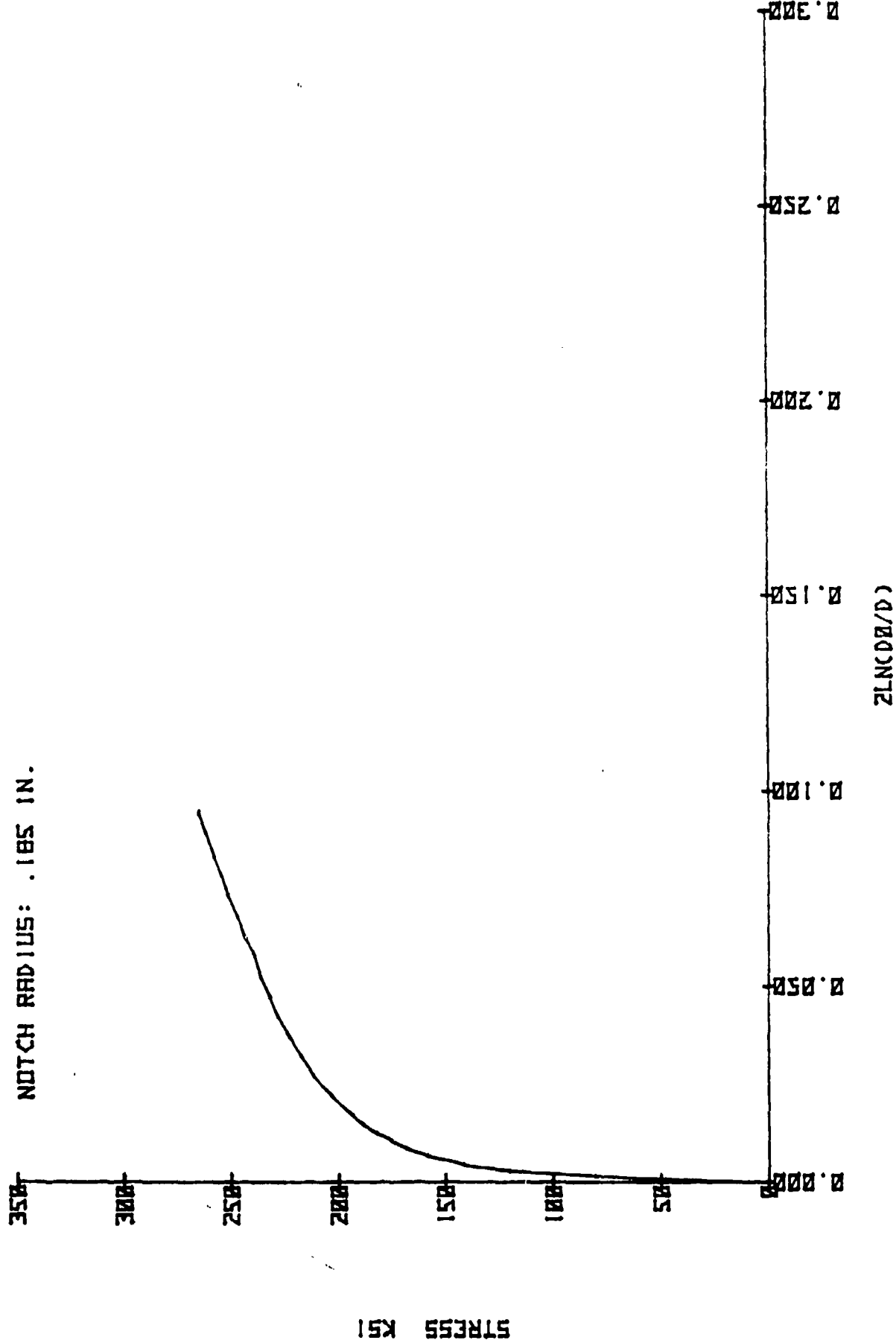
STRESS KSI

SPECIMEN #: 7  
NOTCH RADIUS: .188 IN.

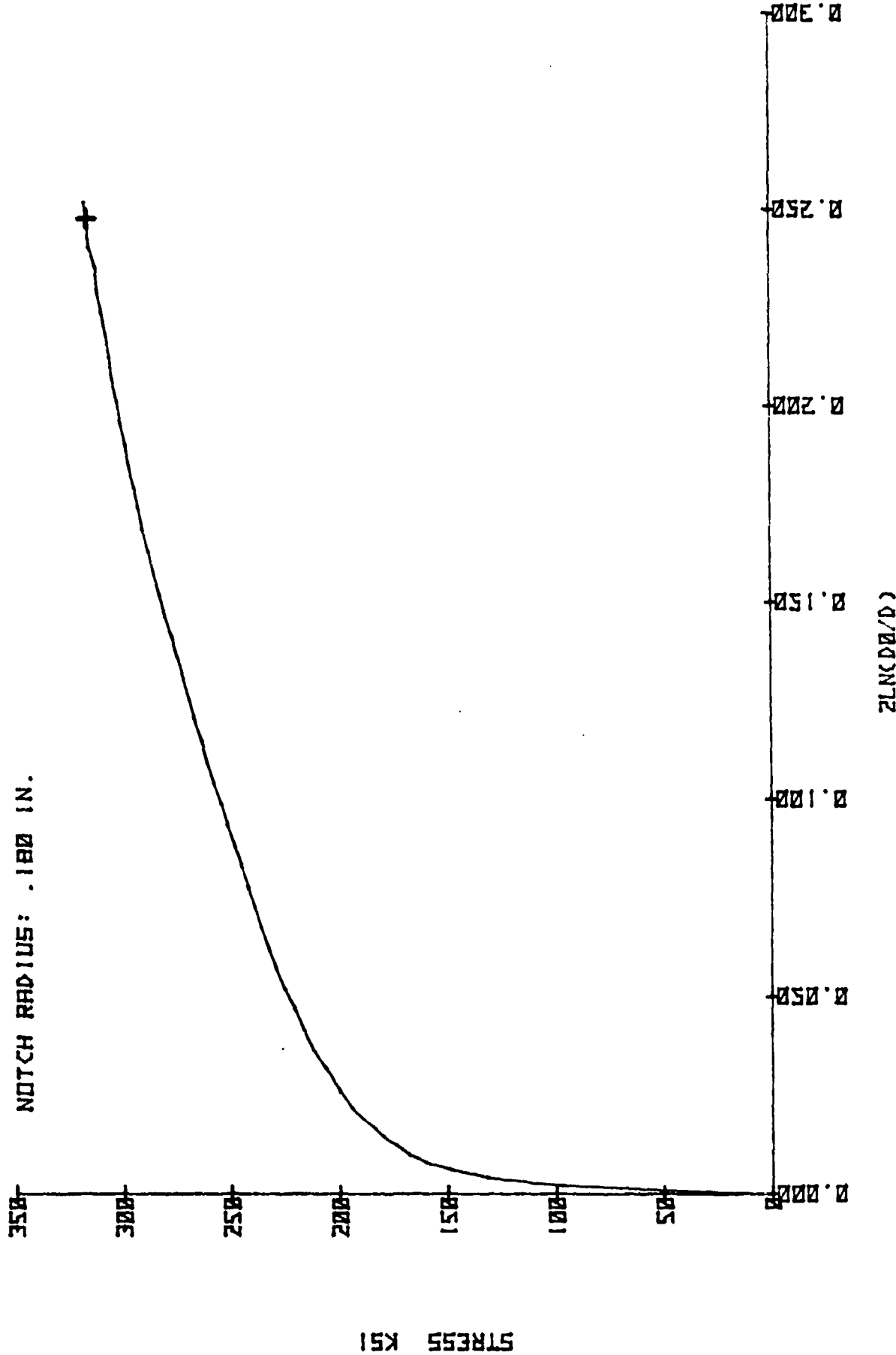


STRESS KSI

SPECIMEN #: 8  
NOTCH RADIUS: .185 IN.

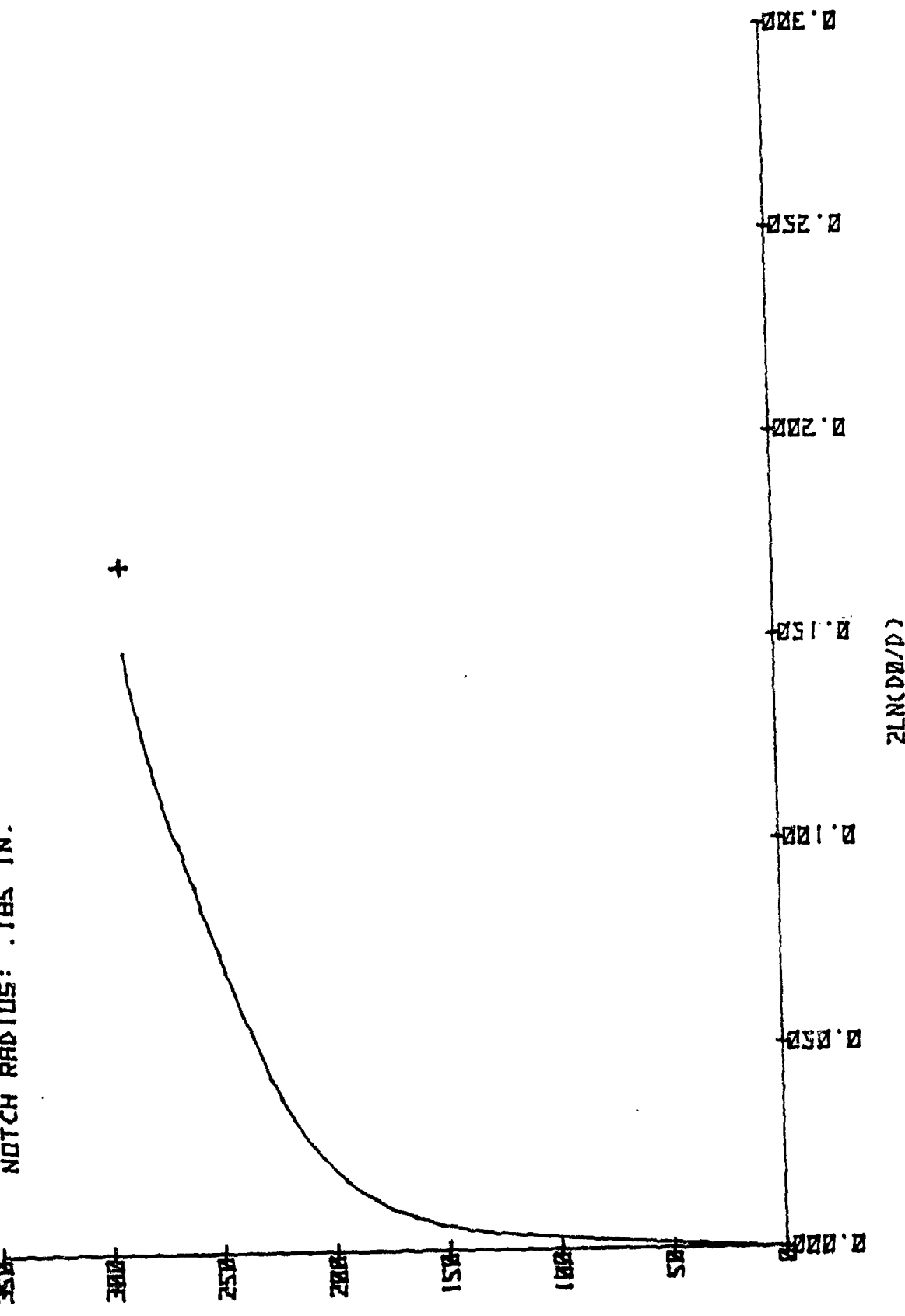


SPECIMEN #: E  
NOTCH RADIUS: .180 IN.



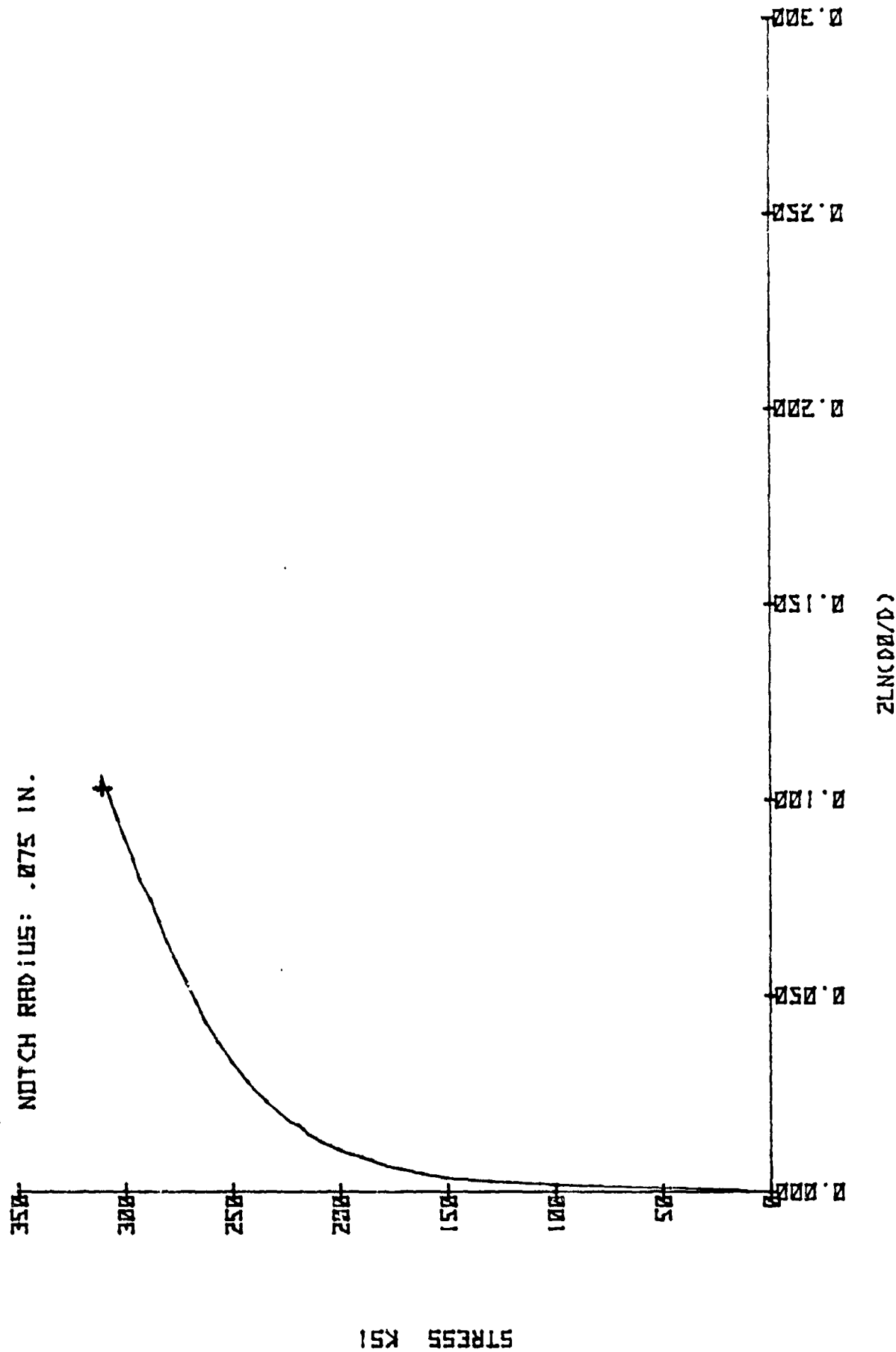
STRESS KSI

SPECIMEN #: 16  
NOTE: CH RADIUS: .185 IN.

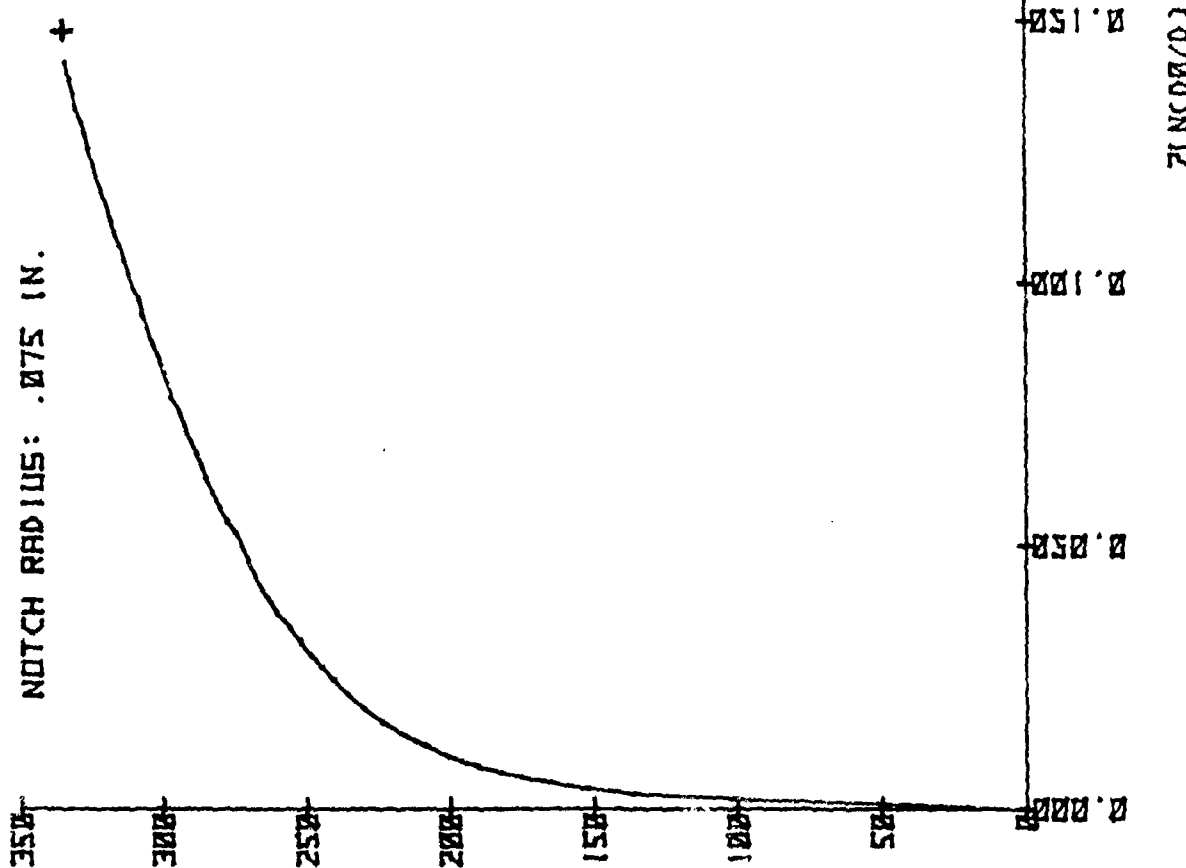


STRESS KSI

SPECIMEN #: 11  
NOTCH RADIUS: .075 IN.



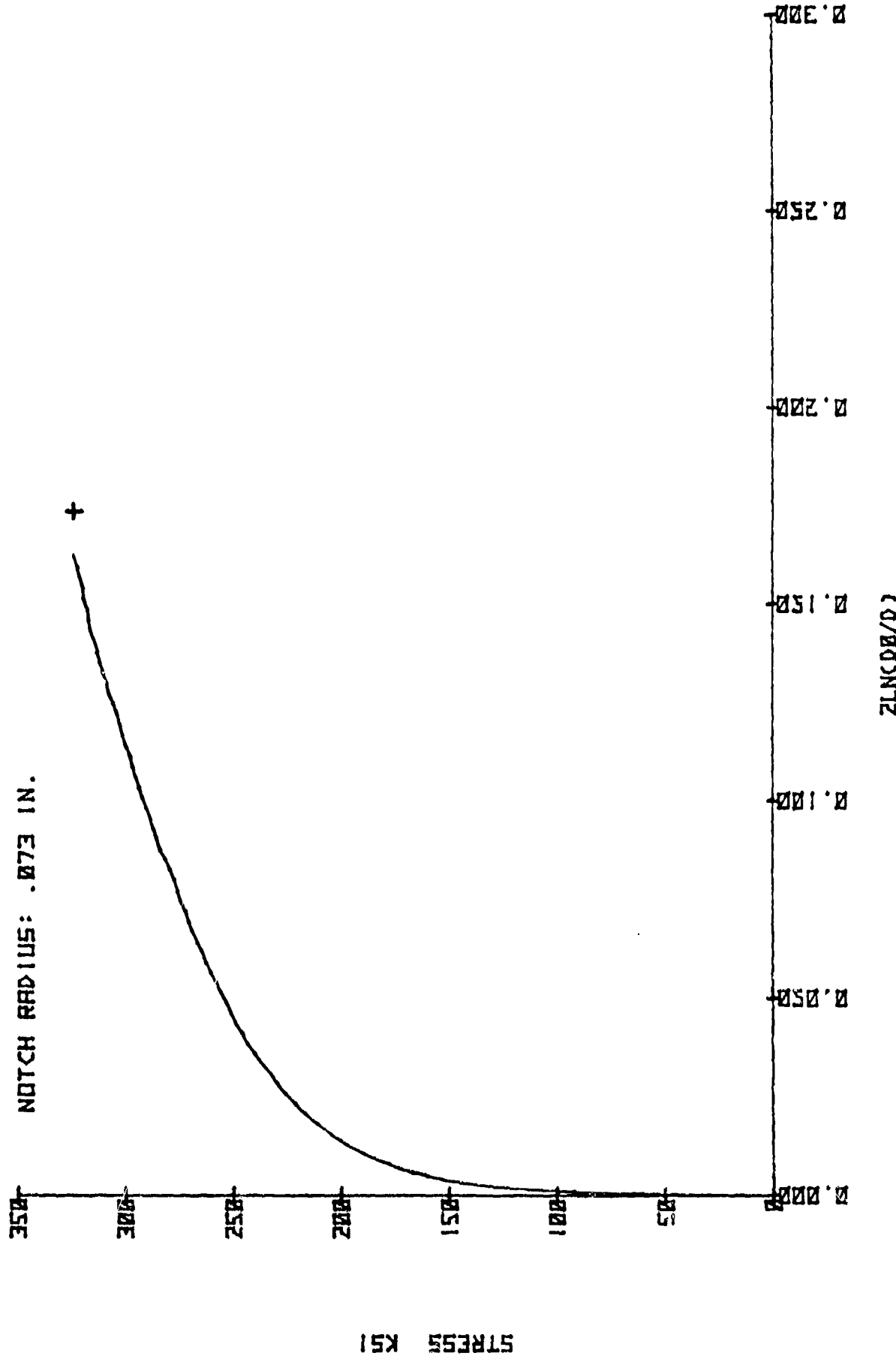
SPECIMEN #: 12  
NOTCH RADIUS: .075 IN.



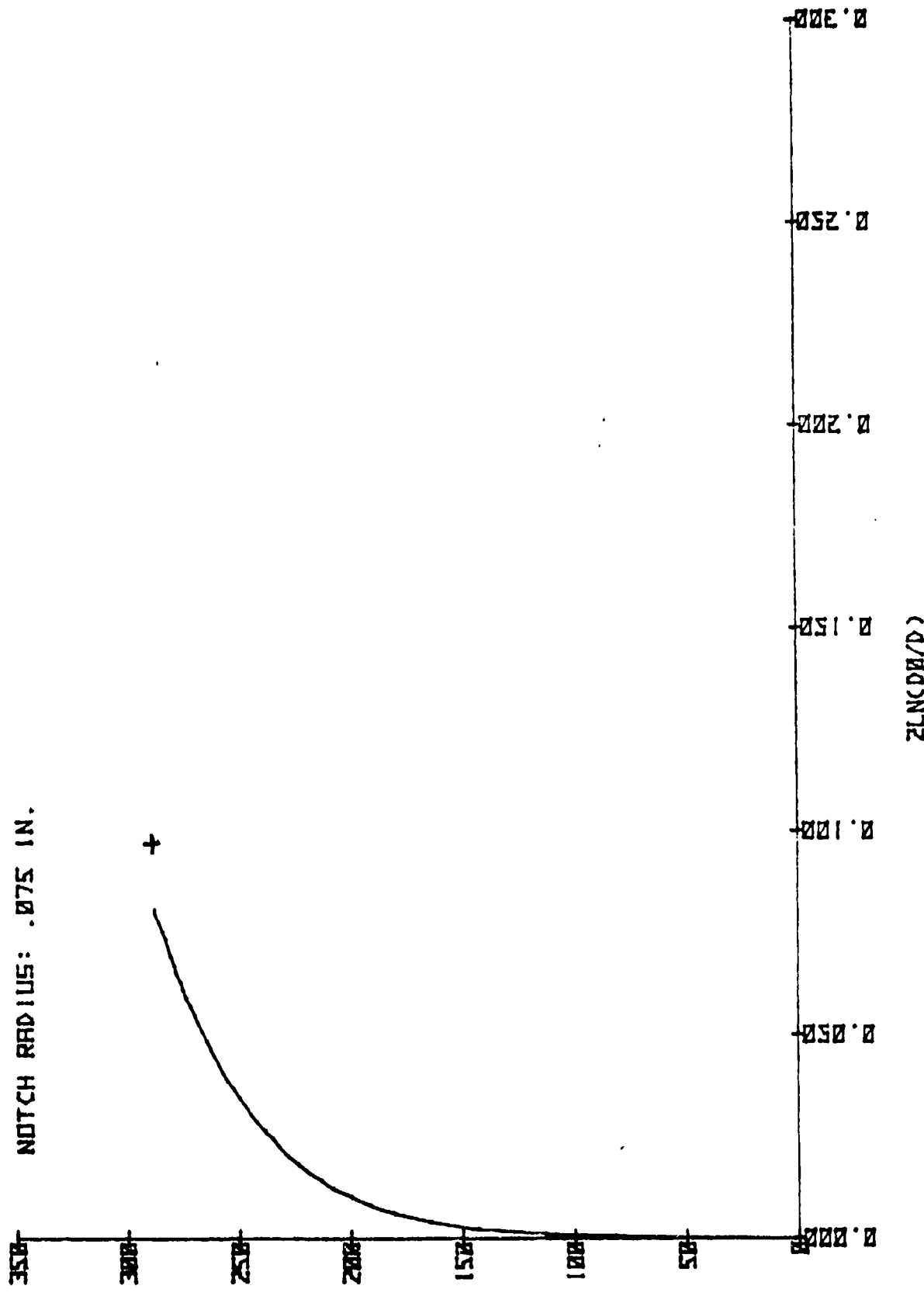
STRESS KSI

0

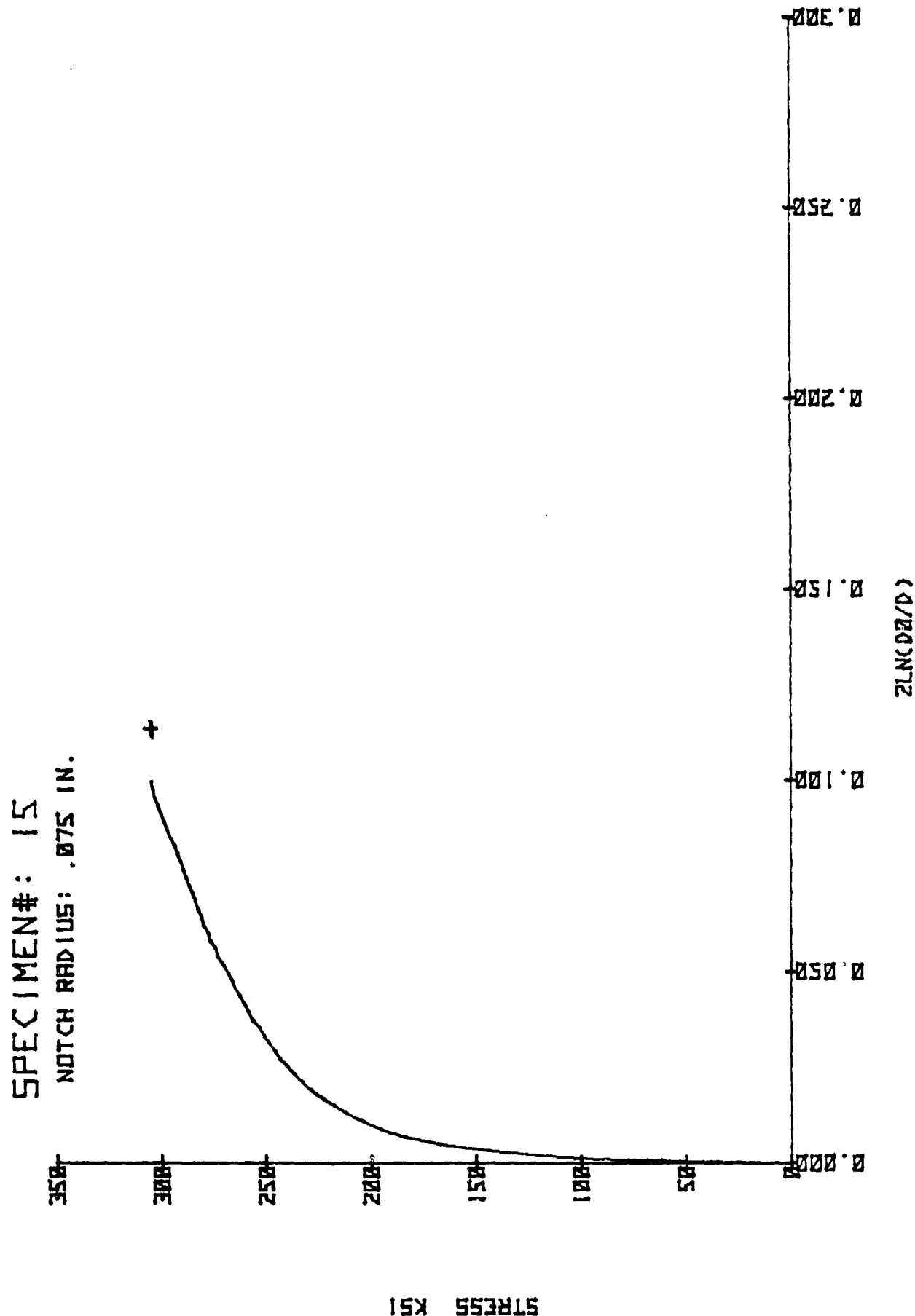
SPECIMEN #: 13  
NOTCH RADIUS: .873 IN.



SPECIMEN# : 14  
NOTCH RADIUS : .075 IN.

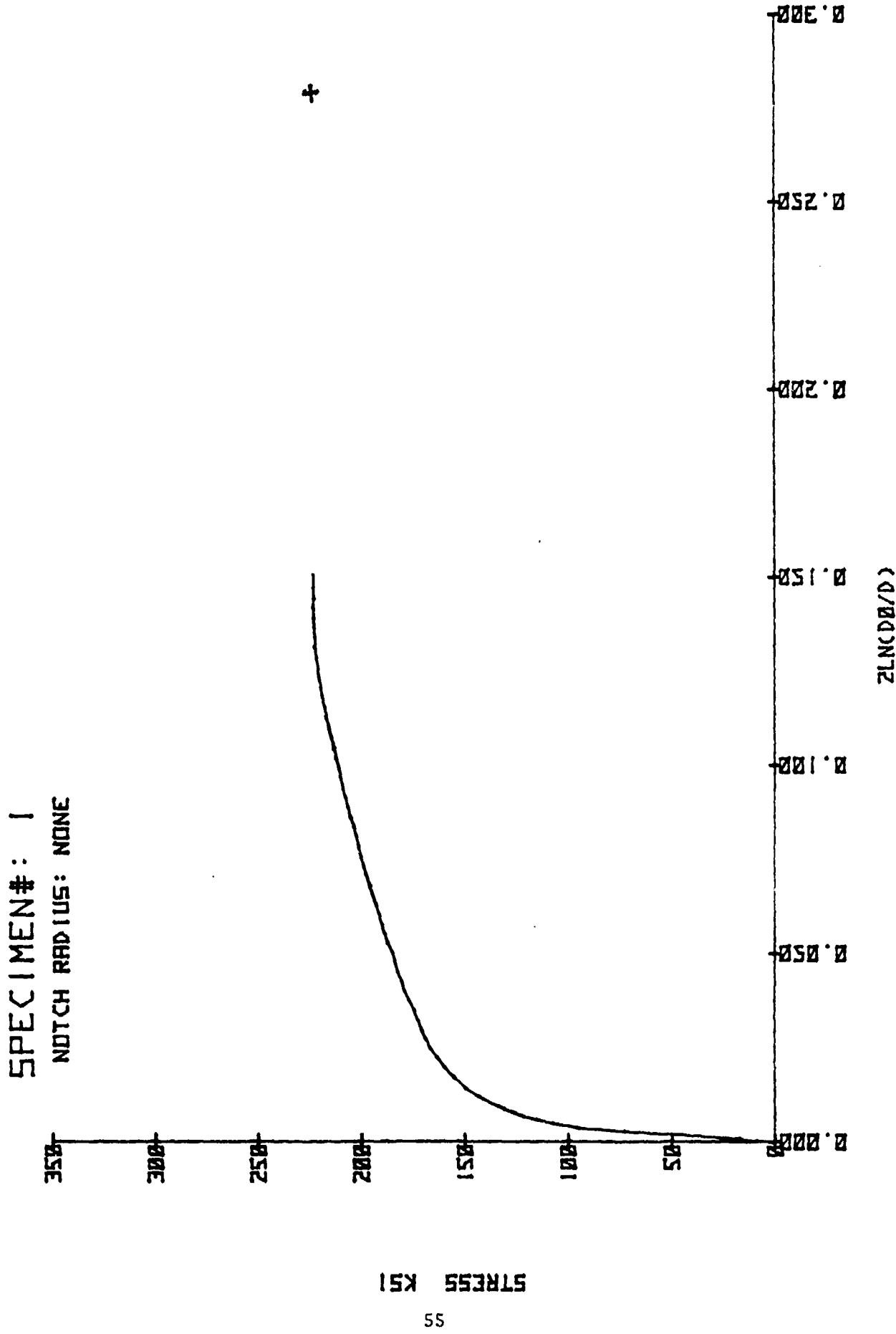


STRESS KSI

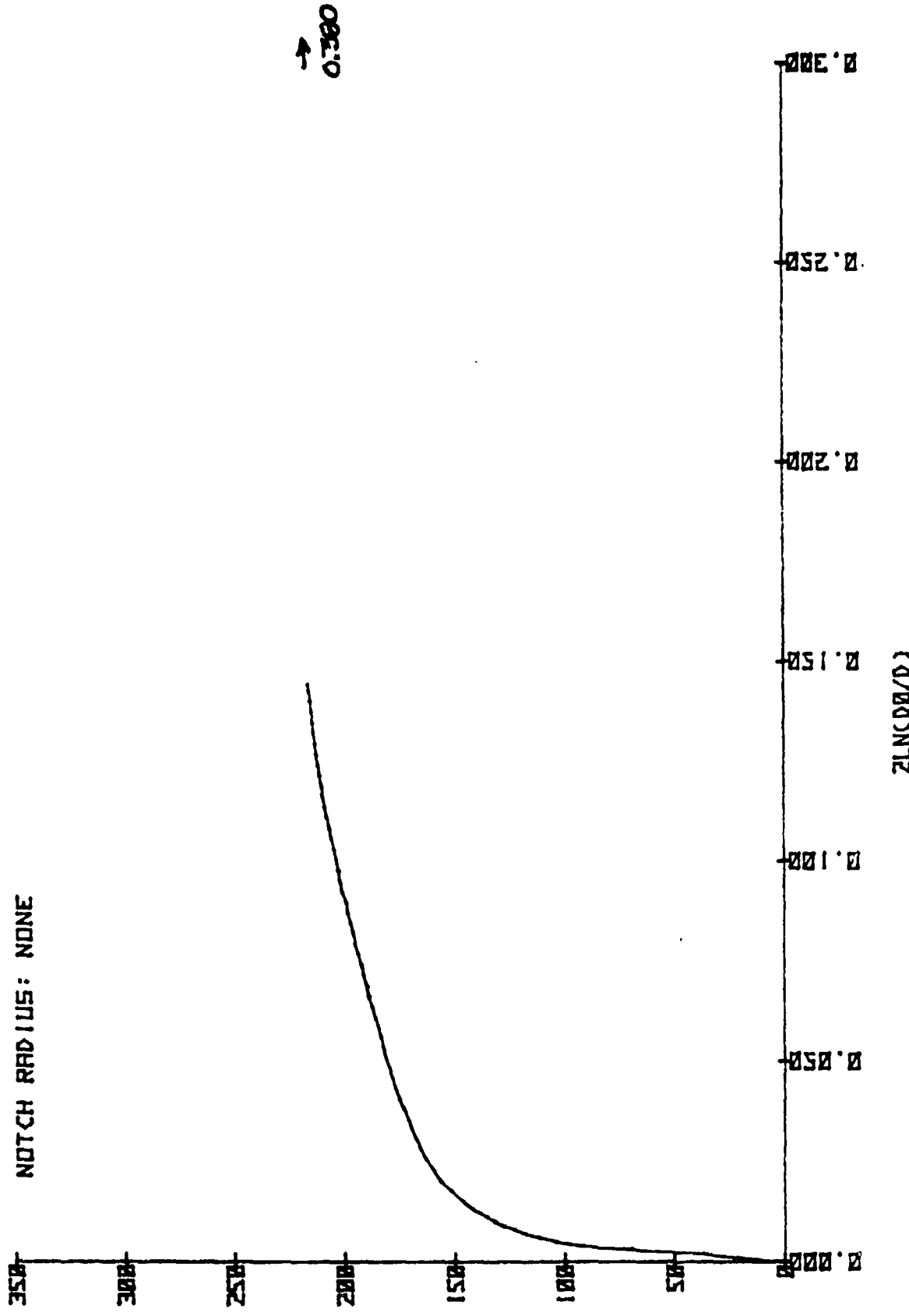


**APPENDIX**

**AXIAL STRESS - DIAMETRAL STRAIN CURVES**



SPECIMEN# : 2  
NOTCH RADIUS: NONE



STRESS KSI

**APPENDIX C**  
**HULL CALCULATION SETUP AND SAMPLE OUTPUT**

This appendix contains the control cards, the HULL generation input deck (KEEL), and the HULL input run deck for the demonstration calculation. Sample outputs from KEEL and HULL are also included.

**KEEL CONTROL CARDS**

KEELR,T500,PO,STMFZ.  
ACCOUNT  
SWITCH,6.  
ATTACH,HULLIB, ID=KIMSEY.  
LIBRARY,HULLIB.  
COPYS(,A)  
ATTACH,CH113, ID=KIMSEY.  
COPYSP(CH113,A)  
RETURN,CH113.  
REWIND,A.  
COPYSP(A,OUTPUT)  
REWIND, INPUT.  
COPYSP(INPUT,OUTPUT)  
PLANK.  
DYTHUL(I=A)  
FTN,I=SAIL,B=KEEL,PL=40000.  
LDSET(PRESET=NGINF)  
KEEL.

HULL CONTROL CARDS

HULLR, T24000, PO, MS220000, STMFZ.  
ACCOUNT  
SWITCH, 6.  
ATTACH, HULLIB, ID=KIMSEY.  
LIBRARY, HULLIB.  
COPYSP(,A)  
ATTACH, CH113, ID=KIMSEY.  
COPYSP(CH113,A)  
RETURN, CH113.  
REWIND, A.  
COPYSP(A,OUTPUT)  
REWIND, INPUT.  
COPYSP(INPUT,OUTPUT)  
PLANK.  
DYTHUL(I=A)  
FTN(I=SAIL, B=HULL, PL=40000, R=2, L=SAVE.  
LDSET(PRESET=NGINF)  
HULL.  
EXIT.  
DISPOSE, SAVE, PR.

## KEEL INPUT DECK

```
KEEL PROB 3212.0002
NM 3 AIR 1 RHA 2 UTI 3
DIMEN=3 VISC=1 EOS=6 FLUXER=3 STRESS=1
IMAX=50 JMAX=25 KMAX=100
REZONE=7
NSTN=100 NOP=100
AREF=.FALSE. TREF=.FALSE.
LREF=.FALSE. RREF=.FALSE.
HEADER
OTI/BRL HULL CALCULATION OF RHA IMPACTED BY DU AT 1 KM/SEC, 65 DEGREES
MESH
CONSTANT SURGRID
  NX=30 X0= -1.155 XMAX= 1.155
  NY=15 Y0= 0 YMAX= 1.155
  NZ=60 Z0= -1.386 ZMAX= 3.234
    RXNEG=1.5 XOLIM= -4 RXPOS=1.5 XMLIM= 4
    RYNEG=1.5 YOLIM= 0 RYPOS=1.5 YMLIM= 4
    RZNEG=1.5 ZOLIM= -7 RZPOS=1.5 ZMLIM= 10
GENERATE
PACKAGE AIR BOX           XL=-1.E5 XR=1.E5 ZT= .629 ZB=-1.E5
                           ZCC=.385 ANGLB=-65
PACKAGE RHA W=1.036E5 BOX   XL=-1.E5 XR=1.E5 ZT=-.39 ZB=-.629
                           ZCC=.385 ANGLB=-65
PACKAGE AIR BOX=          XL=-1.E5 XR=1.E5 ZT=1.E5 ZB=-.39
                           ZCC=.385 ANGLB=-65
SPHERE                      XC= 0 YC= 0 ZC= .385 RADIUS=.385
RECTAROT                     XL= 0 XR=.385 ZT=7.7 ZB=.385
PACKAGE UTI SPHERE           XC= 0 YC= 0 ZC= .385 RADIUS=.385
BOX                          ZB=.385
PACKAGE UTI RECTAROT         XL= 0 XR=.385 ZT=7.7 ZB=.385
STATIONS XS=.01 YS=.01 ZL=.01
STATIONS XS=-.424 -.347 -.269 -.193 0 .193 .269 .347 .424
                           YS= 0 .193 .269 .347 .424
                           ZL=.039 .193 .347 .424 .501 .809 .963 1.117 1.27 1.425 1.579
                           1.733
END
```

## HULL INPUT DECK

```
HULL PROB 3212.0002
INPUT
TIMES=3 DMPINT=15.E-6
PTSTOP=50.E-6
MATPROP
MAT=2 YLDMAX=15.E9
MAT=3 YLDMAX=16.E9
END PROP
```

KEEL OUTPUT  
 MATERIAL 2 RHOZ= 7.866L CC= 4.61000E+05 S= 1.7300E+06 AMBII= 7.5559E+08 EMELO= 8.7700E+09  
 EBVO= 2.2440E+09  
 MATERIAL 3 RHOZ= 18.9000 CC= 2.48000E+05 S= 1.5300E+00 AMBII= 2.2693E+08 EMELO= 1.6450E+09  
 EBVO= 5.5000E+09

OTI/BRL HULL CALCULATION OF RHA IMPACTED BY DU AT 1 KM/SEC, 65 DEGREES

ZBLK

PP08	3.2120L020L0001E+03	17336214000064333430
ARLF	0.	77777777777777777776
ATMOS	5.6000L00000000000000	17225000000000000000
BREF	0.	00L00000000000000000
CODE	1.0000060030000000E+00	172J+00000000000000
COLD	0.	77777777777777777776
CYCLE	0.	00000000000000000000
DIMEN	3.60000000000000000000	17216000000000000000
DT	1.00000000000000000000	16655274616704302142
ELC	0.	00000000000000000000
EOS	6.00000000000000000000	17226000000000000000
ETH	0.	00C00000000000000000
EXPAND	5.6000000000000000E-02	17136314631463146315
FAIL	0.	00000000000000000000
FLUXER	3.0000000000000000E+00	17216000000000000000
FREF	0.	00000000000000000000
INAX	5.6000000000000000E+01	17236200000000000000
IQ	4.9000L0000000000E+01	17256100000000000000
ISLAND	0.	00000000000000000000
JMAX	2.5000000000000000E+01	17246200000000000000
J9	2.4400000000000000E+01	17246000000000000000
KMAX	1.0000000000000000E+02	17266200000000000000
KO	9.9000000000000000E+01	17266140000000000000
HOB	0.	00L00000000000000000
LREF	0.	00000000000000000000
METHOD	2.0000000000000000E+00	1721+00000000000000
MLC	0.	00000000000000000000
MTH	0.	00000000000000000000
NH	2.0000000000000000E+01	17245000000000000000
NHIC	1.0000000000000000E+03	17406665000000000000
NHIST	5.1000L0000000000E+00	17225000000000000000
NH	3.6000000000000000E+00	17216000000000000000
NJP	0.	00000000000000000000
NPLP8	4.6000000000000000E+00	17224300000000000000
NPP	3.0000000000000000E+00	17216000000000000000
NSTN	0.	00000000000000000000
NVARST	2.2000000000000000E+01	17245400000000000000
PTSTOP	6.0000L0000000000E+02	17314240000000000000
RADLOS	0.	00000000000000000000
REZONE	7.0000000000000000E+00	17227000000000000000
RREF	0.	00000000000000000000
STABF	7.5000000000000000E-01	17176000000000000000
STRESS	0.0000000000000000E+00	17204000000000000000
SUNE	0.	00000000000000000000
T	0.	00000000000000000000
TERAD	0.	00000000000000000000
TLC	0.	(00000000000000000000
TREF	0.	00000000000000000000
TTIME	0.	00000000000000000000
TTSTOP	1.0000000000000000E+02	17266200000000000000
UPEZ	0.	00000000000000000000
VISC	0.0000000000000000E+00	17204300000000000000
VREZ	0.	00000000000000000000
VOIDS	0.	00000000000000000000
WORK	0.	00000000000000000000
WREZ	0.	00000000000000000000
X1	-1.0000000000000000E+00	6.573777777777777777
X2	-1.0000000000000000E+00	6.573777777777777777
X0B	0.	(00000000000000000000
Y1	-1.0000000000000000E+00	6.573777777777777777
Y2	-1.0000000000000000E+00	6.573777777777777777
Y0B	0.	00000000000000000000
YGND	-1.0000000000000000E+20	57942450342416451635
YIELD	0.	00000000000000000000
Z1	0.	00000000000000000000
Z2	0.	00000000000000000000
AIR	-0.0000000000000000E+00	17204300000000000000
RHA	1.0000000000000000E+00	17214000000000000000
UTI	3.0000000000000000E+00	17216000000000000000

MESH INCREMENTS AND COORDINATES

I	DX	X	I	DX	X	I	DX	X	I	DX	X	
J	DY	Y	J	DY	Y	J	DY	Y	J	DY	Y	
K	DZ	Z	K	DZ	Z	K	DZ	Z	K	DZ	Z	
1	-3.9987692E+00		2	4.9436478E-01	-2.89658792E+00	3	4.02086035E-01	-2.49449688E+00				
4	3.27032155E-01	-2.16766473E+00	5	3.65987926E-01	-1.9014768E+00	6	2.16338289E-01	-1.68913851E+00				
7	-1.75956315E-01	-1.50918220E+00	8	2.4312490E-01	-1.36607011E+00	9	1.16398639E-01	-1.24967150E+00				
10	9.46715000E-02	-1.05300000E+00	11	7.70000000E-02	-1.07800000E+00	12	7.70000000E-02	-1.00100000E+00				
13	7.70000000E-02	-9.24000000E-01	14	7.70000000E-02	-8.47000000E-01	15	7.70000000E-02	-7.70000000E-01				
16	7.70000000E-02	-6.93000000E-01	17	7.70000000E-02	-6.16000000E-01	18	7.70000000E-02	-5.39000000E-01				
19	7.70000000E-02	-4.62000000E-01	20	7.70000000E-02	-3.85000000E-01	21	7.70000000E-02	-3.08000000E-01				
22	7.70000000E-02	-2.31000000E-01	23	7.70000000E-02	-1.54000000E-01	24	7.70000000E-02	-7.70000000E-02				
25	7.70000000E-02	3.55271368E-15	26	7.70000000E-02	7.70000000E-02	27	7.70000000E-02	1.54610000E-01				
28	7.70000000E-02	2.31000000E-01	29	7.70000000E-02	3.08000000E-01	30	7.70000000E-02	3.85000000E-01				
31	7.70000000E-02	4.62000000E-01	32	7.70000000E-02	5.39000000E-01	33	7.70000000E-02	6.16000000E-01				
34	7.70000000E-02	6.93000000E-01	35	7.70000000E-02	7.70000000E-01	36	7.70000000E-02	8.47000000E-01				
37	7.70000000E-02	8.24000000E-01	38	7.70000000E-02	1.02100000E+00	39	7.70000000E-02	1.07800000E+00				
40	7.70000000E-02	1.15500000E+00	41	9.4671500E-02	1.24967150E+00	42	1.16398639E-01	1.36607011E+00				
43	1.43112090E-01	1.05918220E+00	44	1.75956315E-01	1.68513d51E+00	45	2.16338289E-01	1.90147680E+00				
46	2.05987926E-01	2.16746473E+00	47	3.27032155E-01	2.49449688E+00	48	4.02086035E-01	2.89658292E+00				
49	4.9436478E-01	3.39619477E+00	50	5.7811497E-01	3.99876920E+00							
J	DY	Y	J	DY	Y	J	DY	Y	J	DY	Y	
Y	1	7.70000000E-02	7.70000000E-02	2	7.70000000E-02	1.54000000E-01	3	7.70000000E-02	2.31000000E-01			
4	7.70000000E-02	3.08000000E-01	5	7.70000000E-02	3.85000000E-01	6	7.70000000E-02	4.62000000E-01				
7	7.70000000E-02	5.39000000E-01	8	7.70000000E-02	6.16000000E-01	9	7.70000000E-02	6.93000000E-01				
10	7.70000000E-02	7.70000000E-01	11	7.70000000E-02	8.47000000E-01	12	7.70000000E-02	9.24000000E-01				
13	7.70000000E-02	1.02100000E+00	14	7.70000000E-02	1.07800000E+00	15	7.70000000E-02	1.15500000E+00				
16	7.70000000E-02	1.24967150E+00	17	7.70000000E-02	1.36607011E+00	18	7.70000000E-02	1.43112090E+00				
19	7.70000000E-02	1.68513d51E+00	20	7.70000000E-02	1.90147680E+00	21	7.70000000E-02	2.16746473E+00				
22	7.70000000E-02	2.49449688E+00	23	7.70000000E-02	2.89658292E+00	24	7.70000000E-02	3.39094770E+00				
K	DZ	Z	K	DZ	Z	K	DZ	Z	K	DZ	Z	
ZU	-6.09716441E+01											
1	6.41243180E-01	-6.35571501E+00	2	5.76763576E-01	-5.77915274E+00	3	5.18765134E-01	-5.26038760E+00				
4	4.66549329E-01	-4.79370828E+00	5	4.19679195E-01	-4.37410908E+00	6	3.77477240E-01	-3.99663184E+00				
7	3.05916440E-01	-3.65712032E+00	8	3.03377770E-01	-3.35173505E+00	9	2.74669745E-01	-3.07706534E+00				
10	2.47649504E-01	-2.13001578E+00	11	2.22206839E-01	-2.60780894E+00	12	1.99862241E-01	-2.40794670E+00				
13	1.97649563E-01	-2.22810214E+00	14	1.61687860E-01	-2.06649428E+00	15	1.45428908E-01	-1.92106537E+00				
16	1.30049492E-01	-1.79020045E+00	17	1.17651482E-01	-1.67260897E+00	18	1.05820725E-01	-1.56678824E+00				
19	9.51796415E-02	-1.14716060E+00	20	8.56066909E-02	-1.38600000E+00	21	7.70000000E-02	-1.30900000E+00				
22	7.70000000E-02	-1.23200000E+00	23	7.70000000E-02	-1.15500000E+00	24	7.70000000E-02	-1.07800000E+00				
25	7.70000000E-02	-1.00000000E+00	26	7.70000000E-02	-9.24000000E-01	27	7.70000000E-02	-8.47000000E-01				
28	7.70000000E-02	-7.70000000E-01	29	7.70000000E-02	-6.93000000E-01	30	7.70000000E-02	-6.16000000E-01				
31	7.70000000E-02	-5.39000000E-01	32	7.70000000E-02	-4.02000000E-01	33	7.70000000E-02	-3.85000000E-01				
34	7.70000000E-02	-3.61800000E-01	35	7.70000000E-02	-2.31600000E-01	36	7.70000000E-02	-1.54000000E-01				
37	7.70000000E-02	-7.70000000E-02	38	7.70000000E-02	-1.82076576E-14	39	7.70000000E-02	-7.70000000E-02				
40	7.70000000E-02	1.05918220E+00	41	7.70000000E-02	2.31030000E-01	42	7.70000000E-02	3.08000000E-01				
43	7.70000000E-02	3.85000000E-01	44	7.70000000E-02	4.62000000E-01	45	7.70000000E-02	5.39000000E-01				
46	7.70000000E-02	6.16000000E-01	47	7.70000000E-02	6.93000000E-01	48	7.70000000E-02	7.70000000E-01				
49	7.70000000E-02	8.47000000E-01	50	7.70000000E-02	9.24000000E-01	51	7.70000000E-02	1.00100000E+00				
52	7.70000000E-02	1.07800000E+00	53	7.70000000E-02	1.13500000E+00	54	7.70000000E-02	1.23200000E+00				
55	7.70000000E-02	1.30900000E+00	56	7.70000000E-02	1.38600000E+00	57	7.70000000E-02	1.46300000E+00				
58	7.70000000E-02	1.34100000E+00	59	7.70000000E-02	1.61700000E+00	60	7.70000000E-02	1.69400000E+00				
61	7.70000000E-02	1.77100000E+00	62	7.70000000E-02	1.84000000E+00	63	7.70000000E-02	1.92500000E+00				
64	7.70000000E-02	2.02021000E+00	65	7.70000000E-02	2.07900000E+00	66	7.70000000E-02	2.15600000E+00				
67	7.70000000E-02	2.23300000E+00	68	7.70000000E-02	2.31000000E+00	69	7.70000000E-02	2.38700000E+00				
70	7.70000000E-02	2.46400000E+00	71	7.70000000E-02	2.54100000E+00	72	7.70000000E-02	2.61860000E+00				
73	7.70000000E-02	2.69500000E+00	74	7.70000000E-02	2.77200000E+00	75	7.70000000E-02	2.84900000E+00				
76	7.70000000E-02	2.92600000E+00	77	7.70000000E-02	3.00300000E+00	78	7.70000000E-02	3.08000000E+00				
79	7.70000000E-02	3.15790000E+00	80	7.70000000E-02	3.23400000E+00	81	8.67636000E-02	3.32076360E+00				
82	9.77652244E-02	3.41852882E+00	83	1.10161855E-01	3.52869068E+00	84	1.24130378E-01	3.655282106E+00				
85	1.39870110E-01	3.79269117E+00	86	1.57605640E-01	3.95029681E+00	87	1.77590035E-01	4.12780664E+00				
88	2.00010845E-01	4.32790529E+00	89	2.25482213E-01	4.55347751E+00	90	2.54073347E-01	4.80755908E+00				
91	2.86289847E-01	5.09384069E+00	92	3.2259140E-01	5.41643209E+00	93	3.63495989E-01	5.77992808E+00				
94	4.69587281E-01	6.18951536E+00	95	4.61522948E-01	6.65143831E+00	96	5.20044058E-01	7.17108237E+00				
97	5.85985644E-01	7.75766001E+00	98	6.6J286624E-01	8.41735663E+00	99	7.64013221E-01	9.16136986E+00				

THIS PRINTOUT WAS GENERATED ON JULY 11, 2013  
FROM JULY 11, 2013 TO JULY 11, 2013

GENERATION OF MACH 3222...12

DEFAULT WILL BE 1

PACKAGE MATERIAL 1 INSIDE A SPHERE  
XC = 0.000000E+00 YC = 0.000000E+00 ZC = 0.000000E+00 RADIUS = 0.000000E+00

AIR = 1

PACKAGE MATERIAL 2 INSIDE A BOX  
XL = -1.000000E+05 XR = 1.000000E+05 YB = -1.000000E+06 YF = 1.000000E+06  
ZB = -6.2903000E-01 ZT = -3.900000E-01  
GEOMETRIC FRAME OF REFERENCE SHIFTED BY  
XCC = 0.  
YCC = 0.  
ZCC = 3.850000E-01  
ORIENTATION ALTERED BY  
ANGLA = 0.  
ANGLEB = -6.500000E+01  
ANGLC = 0.

2.392233E-01 GMS 4.144986E+01 ERGS INSERT AS MATERIAL 1

RHA = 2

PACKAGE MATERIAL 2 INSIDE A BOX  
XL = -1.000000E+05 XR = 1.000000E+05 YB = -1.000000E+06 YF = 1.000000E+06  
ZB = -6.2903000E-01 ZT = -3.900000E-01  
GEOMETRIC FRAME OF REFERENCE SHIFTED BY  
XCC = 0.  
YCC = 0.  
ZCC = 3.850000E-01  
ORIENTATION ALTERED BY  
ANGLA = 0.  
ANGLEB = -6.500000E+01  
ANGLC = 0.

1.206110E+02 GMS 7.383000E+01 ERGS INSERT AS MATERIAL 2

AIR = 1

PACKAGE MATERIAL 1 INSIDE A BOX  
XL = -1.000000E+05 XR = 1.000000E+05 YB = -1.000000E+06 YF = 1.000000E+06  
ZB = -3.900000E-01 ZT = 3.000000E+05  
GEOMETRIC FRAME OF REFERENCE SHIFTED BY  
XCC = 0.  
YCC = 0.  
ZCC = 3.850000E-01  
ORIENTATION ALTERED BY  
ANGLA = 0.  
ANGLEB = -6.500000E+01  
ANGLC = 0.  
DELETE MATERIAL 1 INSIDE A SPHERE  
XC = 0.000000E+00 YC = 0.000000E+00 ZC = 3.850000E-01 RADIUS = 3.850000E-01  
DELETE MATERIAL INSIDE A RECTARDT  
XL = 0.000000E+00 XR = 3.850000E-01 ZB = 3.850000E-01 ZT = 7.700000E+00

4.056437E-01 GMS 4.395647E+08 ERGS INSERT AS MATERIAL 1

UTI = 3

PACKAGE MATERIAL 3 INSIDE A SPHERE  
XC = 0.000000E+00 YC = 0.000000E+00 ZC = 3.850000E-01 RADIUS = 3.850000E-01  
DELETE MATERIAL INSIDE A BOX  
XL = -1.000000E+06 XR = 1.000000E+06 YB = -1.000000E+06 YF = 1.000000E+06  
ZB = -3.750000E-01 ZT = 3.000000E+06

1.144711E+00 GMS 2.597710E+08 ERGS INSERT AS MATERIAL 3

UTI = 3

PACKAGE MATERIAL 3 INSIDE A RECTARDT  
XL = 0.000000E+00 XR = 3.850000E-01 ZB = 3.850000E-01 ZT = 7.700000E+00  
3.286042E+01 GMS 7.457073E+00 ERGS INSERT AS MATERIAL 3

STATION 1 XP = 1.000000E-02 YP = 1.000000E-02 ZP = 1.000000E-02

L PARTICLES AND - STATIONS GENERATED

LOCATIONS OF STATIONS GENERATED ARE ...

THIS PAGE IS PART OF THE ORIGINAL

PLANE 9 Z = -3.077E-02 METERS STATIONS/DUST/PARTICLES  
( 1- 50)

	1	2	3	4	5	Y METERS
1	1234567890	1234567890	1234567890	1234567890	1234567890	7.700E-04
2						1.540E-03
3						2.310E-03
4						3.080E-03
5						3.850E-03
6						4.620E-03
7						5.390E-03
8						6.160E-03
9						6.930E-03
10						7.700E-03
11						8.470E-03
12						9.240E-03
13						1.001E-02
14						1.078E-02
15						1.155E-02
16						1.250E-02
17						1.366E-02
18						1.509E-02
19						1.685E-02
20						1.901E-02
21						2.167E-02
22						2.494E-02
23						2.897E-02
24						3.391E-02
25						3.999E-02

1234567890 1234567890 1234567890 1234567890 1234567890

	1	2	3	4	5
--	---	---	---	---	---

PLANE 9

Z = -3.077E-02 METERS

MATERIAL MAP  
( 1- 50 )

	1	2	3	4	5	Y
	1234567890	1234567890	1234567890	1234567890	1234567890	METERS
1	+++++	+++++	+++++	+++++	+++++	7.700E-04
2	+++++	+++++	+++++	+++++	+++++	1.540E-03
3	+++++	+++++	+++++	+++++	+++++	2.310E-03
4	+++++	+++++	+++++	+++++	+++++	3.080E-03
5	+++++	+++++	+++++	+++++	+++++	3.850E-03
6	+++++	+++++	+++++	+++++	+++++	4.620E-03
7	+++++	+++++	+++++	+++++	+++++	5.390E-03
8	+++++	+++++	+++++	+++++	+++++	6.160E-03
9	+++++	+++++	+++++	+++++	+++++	6.930E-03
10	+++++	+++++	+++++	+++++	+++++	7.700E-03
11	+++++	+++++	+++++	+++++	+++++	8.470E-03
12	+++++	+++++	+++++	+++++	+++++	9.240E-03
13	+++++	+++++	+++++	+++++	+++++	1.010E-02
14	+++++	+++++	+++++	+++++	+++++	1.078E-02
15	+++++	+++++	+++++	+++++	+++++	1.155E-02
16	+++++	+++++	+++++	+++++	+++++	1.250E-02
17	+++++	+++++	+++++	+++++	+++++	1.366E-02
18	+++++	+++++	+++++	+++++	+++++	1.509E-02
19	+++++	+++++	+++++	+++++	+++++	1.685E-02
20	+++++	+++++	+++++	+++++	+++++	1.901E-02
21	+++++	+++++	+++++	+++++	+++++	2.167E-02
22	+++++	+++++	+++++	+++++	+++++	2.494E-02
23	+++++	+++++	+++++	+++++	+++++	2.897E-02
24	+++++	+++++	+++++	+++++	+++++	3.391E-02
25	+++++	+++++	+++++	+++++	+++++	3.999E-02
	1234567890	1234567890	1234567890	1234567890	1234567890	
	1	2	3	4	5	

PLANE 19

Z = -1.472E-02 METERS

STATIONS/DUST/PARTICLES  
( 1- 50)

	1	2	3	4	5	Y
	1234567890	1234567890	1234567890	1234567890	1234567890	METERS
1						7.700E-04
2						1.540E-03
3						2.310E-03
4						3.080E-03
5						3.850E-03
6						4.620E-03
7						5.390E-03
8						6.160E-03
9						6.930E-03
10						7.700E-03
11						8.470E-03
12						9.240E-03
13						1.001E-02
14						1.078E-02
15						1.155E-02
16						1.250E-02
17						1.366E-02
18						1.509E-02
19						1.685E-02
20						1.901E-02
21						2.167E-02
22						2.494E-02
23						2.897E-02
24						3.391E-02
25						3.999E-02

PLANE .9

Z = -1.472E-02 METERS

MATERIAL MAP  
( 1- 50)

	1	2	3	4	5	Y
	123456789012345678901234567890123456789012345678901234567890					METERS
1	+++++	+++++	+++++	+++++	+++++	7.700E-04
2	+++++	+++++	+++++	+++++	+++++	1.540E-03
3	+++++	+++++	+++++	+++++	+++++	2.310E-03
4	+++++	+++++	+++++	+++++	+++++	3.080E-03
5	+++++	+++++	+++++	+++++	+++++	3.850E-03
6	+++++	+++++	+++++	+++++	+++++	4.620E-03
7	+++++	+++++	+++++	+++++	+++++	5.390E-03
8	+++++	+++++	+++++	+++++	+++++	6.160E-03
9	+++++	+++++	+++++	+++++	+++++	6.930E-03
10	+++++	+++++	+++++	+++++	+++++	7.700E-03
11	+++	+++	+++	+++	+++	8.470E-03
12	+++	+++	+++	+++	+++	9.240E-03
13	+++	+++	+++	+++	+++	1.001E-02
14	+++	+++	+++	+++	+++	1.078E-02
15	+++	+++	+++	+++	+++	1.155E-02
16	+++	+++	+++	+++	+++	1.250E-02
17	+++	+++	+++	+++	+++	1.366E-02
18	+++	+++	+++	+++	+++	1.509E-02
19	+++	+++	+++	+++	+++	1.685E-02
20	+++	+++	+++	+++	+++	1.901E-02
21	+++	+++	+++	+++	+++	2.167E-02
22	+++	+++	+++	+++	+++	2.494E-02
23	+++	+++	+++	+++	+++	2.897E-02
24	+++	+++	+++	+++	+++	3.391E-02
25	+++	+++	+++	+++	+++	3.999E-02
	123456789012345678901234567890123456789012345678901234567890					
	1	2	3	4	5	

PLANE 29 Z = -6.930E-03 METERS STATIONS/DUST/PARTICLES  
( 1- 50)

	1	2	3	4	5	Y METERS
1	1234567890	1234567890	1234567890	1234567890	1234567890	7.700E-04
2						1.540E-03
3						2.310E-03
4						3.080E-03
5						3.850E-03
6						4.620E-03
7						5.390E-03
8						6.160E-03
9						6.930E-03
10						7.700E-03
11						8.470E-03
12						9.240E-03
13						1.001E-02
14						1.078E-02
15						1.155E-02
16						1.250E-02
17						1.366E-02
18						1.509E-02
19						1.685E-02
20						1.901E-02
21						2.167E-02
22						2.494E-02
23						2.897E-02
24						3.391E-02
25						3.999E-02

12345678901234567890123456789012345678901234567890  
1 2 3 4 5

PLANE 29

Z = -6.930E-03 METERS

MATERIAL MAP  
( 1- 50)

	1	2	3	4	5	Y
	1234567890	1234567890	1234567890	1234567890	1234567890	METERS
1	+++++	+++++	XXXX	+++++	+++++	7.700E-04
2	+++++	+++++	XXXX	+++++	+++++	1.540E-03
3	+++++	+++++	XXXX	+++++	+++++	2.310E-03
4	+++++	+++++	XXXX	+++++	+++++	3.080E-03
5	+++++	+++++	XXXX	+++++	+++++	3.850E-03
6	+++++	+++++	XXXX	+++++	+++++	4.620E-03
7	+++++	+++++	XXXX	+++++	+++++	5.390E-03
8	+++++	+++++	XXXX	+++++	+++++	6.160E-03
9	+++++	+++++	XXXX	+++++	+++++	6.930E-03
10	+++++	+++++	XXXX	+++++	+++++	7.700E-03
11	+++++	+++++	XXXX	+++++	+++++	8.470E-03
12	+++++	+++++	XXXX	+++++	+++++	9.240E-03
13	+++++	+++++	XXXX	+++++	+++++	1.001E-02
14	+++++	+++++	XXXX	+++++	+++++	1.078E-02
15	+++++	+++++	XXXX	+++++	+++++	1.155E-02
16	+++++	+++++	XXXX	+++++	+++++	1.250E-02
17	+++++	+++++	XXXX	+++++	+++++	1.366E-02
18	+++++	+++++	XXXX	+++++	+++++	1.509E-02
19	+++++	+++++	XXXX	+++++	+++++	1.685E-02
20	+++++	+++++	XXXX	+++++	+++++	1.901E-02
21	+++++	+++++	XXXX	+++++	+++++	2.167E-02
22	+++++	+++++	XXXX	+++++	+++++	2.494E-02
23	+++++	+++++	XXXX	+++++	+++++	2.897E-02
24	+++++	+++++	XXXX	+++++	+++++	3.391E-02
25	+++++	+++++	XXXX	+++++	+++++	3.999E-02
	1234567890	1234567890	1234567890	1234567890	1234567890	
	1	2	3	4	5	

PLANE 39 Z = 7.700E-04 METERS STATIONS/DUST/PARTICLES  
( 1- 50)

	1	2	3	4	5	Y
	1234567890	1234567890	1234567890	1234567890	1234567890	METERS
1	LLLL	L	LLLL			7.700E-04
2						1.540E-03
3	LLLL	L	LLLL			2.310E-03
4	LLLL	L	LLLL			3.080E-03
5	LLLL	L	LLLL			3.850E-03
6	LLLL	L	LLLL			4.620E-03
7						5.390E-03
8						6.160E-03
9						6.930E-03
10						7.700E-03
11						8.470E-03
12						9.240E-03
13						1.001E-02
14						1.078E-02
15						1.155E-02
16						1.250E-02
17						1.366E-02
18						1.509E-02
19						1.685E-02
20						1.901E-02
21						2.167E-02
22						2.494E-02
23						2.897E-02
24						3.391E-02
25						3.999E-02
	1234567890	1234567890	1234567890	1234567890	1234567890	
	1	2	3	4	5	

PLANE 39

Z = 7.700E-04 METERS

MATERIAL MAP  
( 1 - 50 )

PLANE 49 Z = 8.470E-03 METERS STATIONS/DUST/PARTICLES  
( 1- 50)

	1	2	3	4	5	Y
1	1234567890	1234567890	1234567890	1234567890	1234567890	METERS
2	LLLL	L LLLL				7.700E-04
3	LLLL	L LLLL				1.540E-03
4	LLLL	L LLLL				2.310E-03
5	LLLL	L LLLL				3.080E-03
6	LLLL	L LLLL				3.850E-03
7						4.620E-03
8						5.390E-03
9						6.160E-03
10						6.930E-03
11						7.700E-03
12						8.470E-03
13						9.240E-03
14						1.001E-02
15						1.078E-02
16						1.155E-02
17						1.250E-02
18						1.366E-02
19						1.509E-02
20						1.685E-02
21						1.901E-02
22						2.167E-02
23						2.494E-02
24						2.897E-02
25						3.391E-02
	1234567890	1234567890	1234567890	1234567890	1234567890	3.999E-02
	1	2	3	4	5	

PLANE 49

Z = 8.4703-03 METERS

**MATERIAL MAP  
( 1- 50 )**

PLANE 59

Z = 1.617E-02 METERS

STATIONS/DUST/PARTICLES  
( 1- 50 )

	1	2	3	4	5	Y METERS
1234567890	1234567890	1234567890	1234567890	1234567890	1234567890	7.700E-04
1	LLLL	L	LLLL			1.540E-03
2						2.310E-03
3	LLLL	L	LLLL			3.080E-03
4	LLLL	L	LLLL			3.850E-03
5	LLLL	L	LLLL			4.620E-03
6	LLLL	L	LLLL			5.390E-03
7						6.160E-03
8						6.930E-03
9						7.700E-03
10						8.470E-03
11						9.240E-03
12						1.001E-02
13						1.078E-02
14						1.155E-02
15						1.250E-02
16						1.366E-02
17						1.509E-02
18						1.685E-02
19						1.901E-02
20						2.167E-02
21						2.494E-02
22						2.897E-02
23						3.391E-02
24						3.999E-02
25						
1234567890	1234567890	1234567890	1234567890	1234567890	1234567890	
1	2	3	4	5		

PLANE 59

Z = 2.027E-02 METERS

MATERIAL MAP  
( 1 - 50 )

	1	2	3	4	5	Y
	12345678901234567890123456789012345678901234567890	12345678901234567890123456789012345678901234567890	12345678901234567890123456789012345678901234567890	12345678901234567890123456789012345678901234567890	12345678901234567890123456789012345678901234567890	METERS
1	++++++ +XXX+	++++++ +XXX+	++++++ +XXX+	++++++ +XXX+	++++++ +XXX+	7.700E-04
2	++++++ +XXX+	++++++ +XXX+	++++++ +XXX+	++++++ +XXX+	++++++ +XXX+	1.540E-03
3	++++++ +XXX+	++++++ +XXX+	++++++ +XXX+	++++++ +XXX+	++++++ +XXX+	2.310E-03
4	++++++ +XXX+	++++++ +XXX+	++++++ +XXX+	++++++ +XXX+	++++++ +XXX+	3.080E-03
5	++++++ +XXX+	++++++ +XXX+	++++++ +XXX+	++++++ +XXX+	++++++ +XXX+	3.850E-03
6	++++++ +XXX+	++++++ +XXX+	++++++ +XXX+	++++++ +XXX+	++++++ +XXX+	4.620E-03
7	++++++ +XXX+	++++++ +XXX+	++++++ +XXX+	++++++ +XXX+	++++++ +XXX+	5.390E-03
8	++++++ +XXX+	++++++ +XXX+	++++++ +XXX+	++++++ +XXX+	++++++ +XXX+	6.160E-03
9	++++++ +XXX+	++++++ +XXX+	++++++ +XXX+	++++++ +XXX+	++++++ +XXX+	6.930E-03
10	++++++ +XXX+	++++++ +XXX+	++++++ +XXX+	++++++ +XXX+	++++++ +XXX+	7.700E-03
11	++++++ +XXX+	++++++ +XXX+	++++++ +XXX+	++++++ +XXX+	++++++ +XXX+	8.470E-03
12	++++++ +XXX+	++++++ +XXX+	++++++ +XXX+	++++++ +XXX+	++++++ +XXX+	9.240E-03
13	++++++ +XXX+	++++++ +XXX+	++++++ +XXX+	++++++ +XXX+	++++++ +XXX+	1.01E-02
14	++++++ +XXX+	++++++ +XXX+	++++++ +XXX+	++++++ +XXX+	++++++ +XXX+	1.078E-02
15	++++++ +XXX+	++++++ +XXX+	++++++ +XXX+	++++++ +XXX+	++++++ +XXX+	1.155E-02
16	++++++ +XXX+	++++++ +XXX+	++++++ +XXX+	++++++ +XXX+	++++++ +XXX+	1.250E-02
17	++++++ +XXX+	++++++ +XXX+	++++++ +XXX+	++++++ +XXX+	++++++ +XXX+	1.366E-02
18	++++++ +XXX+	++++++ +XXX+	++++++ +XXX+	++++++ +XXX+	++++++ +XXX+	1.519E-02
19	++++++ +XXX+	++++++ +XXX+	++++++ +XXX+	++++++ +XXX+	++++++ +XXX+	1.685E-02
20	++++++ +XXX+	++++++ +XXX+	++++++ +XXX+	++++++ +XXX+	++++++ +XXX+	1.901E-02
21	++++++ +XXX+	++++++ +XXX+	++++++ +XXX+	++++++ +XXX+	++++++ +XXX+	2.167E-02
22	++++++ +XXX+	++++++ +XXX+	++++++ +XXX+	++++++ +XXX+	++++++ +XXX+	2.494E-02
23	++++++ +XXX+	++++++ +XXX+	++++++ +XXX+	++++++ +XXX+	++++++ +XXX+	2.897E-02
24	++++++ +XXX+	++++++ +XXX+	++++++ +XXX+	++++++ +XXX+	++++++ +XXX+	3.391E-02
25	++++++ +XXX+	++++++ +XXX+	++++++ +XXX+	++++++ +XXX+	++++++ +XXX+	3.999E-02
	12345678901234567890123456789012345678901234567890	12345678901234567890123456789012345678901234567890	12345678901234567890123456789012345678901234567890	12345678901234567890123456789012345678901234567890	12345678901234567890123456789012345678901234567890	
	1	2	3	4	5	

PLANE 69 Z = 2.387E-02 METERS STATIONS/DUST/PARTICLES  
( 1- 50)

	1	2	3	4	5	Y METERS
1	1234567890	1234567890	1234567890	1234567890	1234567890	7.700E-04
2						1.540E-03
3						2.310E-03
4						3.080E-03
5						3.850E-03
6						4.620E-03
7						5.390E-03
8						6.160E-03
9						6.930E-03
10						7.700E-03
11						8.470E-03
12						9.240E-03
13						1.0010E-02
14						1.070E-02
15						1.155E-02
16						1.250E-02
17						1.366E-02
18						1.509E-02
19						1.685E-02
20						1.911E-02
21						2.167E-02
22						2.494E-02
23						2.897E-02
24						3.391E-02
25						3.999E-02
	1234567890	1234567890	1234567890	1234567890	1234567890	
	1	2	3	4	5	

PLANE 69

$\therefore = 2.387 \times 10^{-3}$  METERS

**MATERIAL MAP**  
**( 1- 50 )**

PLANE 79 Z = 3.157E-02 METERS STATIONS/DUST/PARTICLES  
( 1- 50)

	1	2	3	4	5	Y
	12345678901234567890123456789012345678901234567890					METERS
1						7.700E-04
2						1.540E-03
3						2.310E-03
4						3.080E-03
5						3.850E-03
6						4.620E-03
7						5.390E-03
8						6.160E-03
9						6.930E-03
10						7.700E-03
11						8.470E-03
12						9.240E-03
13						1.001E-02
14						1.078E-02
15						1.155E-02
16						1.230E-02
17						1.306E-02
18						1.389E-02
19						1.485E-02
20						1.581E-02
21						1.677E-02
22						2.494E-02
23						2.897E-02
24						3.391E-02
25						3.999E-02
	12345678901234567890123456789012345678901234567890					
	1	2	3	4	5	

PLAN I 79

Z = 3,157E-02 METERS

MATERIAL MAP  
( 1- 5u)

	1	2	3	4	5	Y
	12345678901234567890123456789012345678901234567890	12345678901234567890123456789012345678901234567890	12345678901234567890123456789012345678901234567890	12345678901234567890123456789012345678901234567890	12345678901234567890123456789012345678901234567890	METERS
1	+++++X++++++	+++++X++++++	000011110000	+++++X++++++	+++++X++++++	7.700E-04
2	+++++X++++++	+++++X++++++	000011100000	+++++X++++++	+++++X++++++	1.540E-03
3	+++++X++++++	+++++X++++++	000011100000	+++++X++++++	+++++X++++++	2.310E-03
4	+++++X++++++	+++++X++++++	000011100000	+++++X++++++	+++++X++++++	3.080E-03
5	+++++X++++++	+++++X++++++	000011100000	+++++X++++++	+++++X++++++	3.850E-03
6	+++++X++++++	+++++X++++++	000011100000	+++++X++++++	+++++X++++++	4.620E-03
7	+++++X++++++	+++++X++++++	000011100000	+++++X++++++	+++++X++++++	5.390E-03
8	+++++X++++++	+++++X++++++	000011100000	+++++X++++++	+++++X++++++	6.160E-03
9	+++++X++++++	+++++X++++++	000011100000	+++++X++++++	+++++X++++++	6.930E-03
10	+++++X++++++	+++++X++++++	000011100000	+++++X++++++	+++++X++++++	7.700E-03
11	+++++X++++++	+++++X++++++	000011100000	+++++X++++++	+++++X++++++	8.470E-03
12	+++++X++++++	+++++X++++++	000011100000	+++++X++++++	+++++X++++++	9.240E-03
13	+++++X++++++	+++++X++++++	000011100000	+++++X++++++	+++++X++++++	1.000E-02
14	+++++X++++++	+++++X++++++	000011100000	+++++X++++++	+++++X++++++	1.078E-02
15	+++++X++++++	+++++X++++++	000011100000	+++++X++++++	+++++X++++++	1.155E-02
16	+++++X++++++	+++++X++++++	000011100000	+++++X++++++	+++++X++++++	1.250E-02
17	+++++X++++++	+++++X++++++	000011100000	+++++X++++++	+++++X++++++	1.366E-02
18	+++++X++++++	+++++X++++++	000011100000	+++++X++++++	+++++X++++++	1.509E-02
19	+++++X++++++	+++++X++++++	000011100000	+++++X++++++	+++++X++++++	1.685E-02
20	+++++X++++++	+++++X++++++	000011100000	+++++X++++++	+++++X++++++	1.901E-02
21	+++++X++++++	+++++X++++++	000011100000	+++++X++++++	+++++X++++++	2.167E-02
22	+++++X++++++	+++++X++++++	000011100000	+++++X++++++	+++++X++++++	2.494E-02
23	+++++X++++++	+++++X++++++	000011100000	+++++X++++++	+++++X++++++	2.897E-02
24	+++++X++++++	+++++X++++++	000011100000	+++++X++++++	+++++X++++++	3.391E-02
25	+++++X++++++	+++++X++++++	000011100000	+++++X++++++	+++++X++++++	3.999E-02
	12345678901234567890123456789012345678901234567890	12345678901234567890123456789012345678901234567890	12345678901234567890123456789012345678901234567890	12345678901234567890123456789012345678901234567890	12345678901234567890123456789012345678901234567890	
	1	2	3	4	5	

PLANE 09 Z = 4.553E-02 METERS STATIONS/DUST/PARTICLES  
( 1- 50)

	1	2	3	4	5	Y
	12345678901234567890123456789012345678901234567890					METERS
1						7.740E-04
2						1.540E-03
3						2.310E-03
4						3.080E-03
5						3.850E-03
6						4.620E-03
7						5.390E-03
8						6.160E-03
9						6.930E-03
10						7.700E-03
11						8.470E-03
12						9.240E-03
13						1.001E-02
14						1.078E-02
15						1.155E-02
16						1.250E-02
17						1.366E-02
18						1.509E-02
19						1.685E-02
20						1.901E-02
21						2.167E-02
22						2.494E-02
23						2.897E-02
24						3.391E-02
25						3.999E-02
	12345678901234567890123456789012345678901234567890					
	1	2	3	4	5	

PLANE 39

Z = 4.553E-2 METERS

MATERIAL MAP  
( 1 - 50 )

	1	2	3	4	5	Y METERS
	12345678901234567890123456789012345678901234567890					
1	++**++++++	++**++++++	++**++++++	++**++++++	++**++++++	7.700E-04
2	++**++++++	++**++++++	++**++++++	++**++++++	++**++++++	1.540E-03
3	++**++++++	++**++++++	++**++++++	++**++++++	++**++++++	2.310E-03
4	++**++++++	++**++++++	++**++++++	++**++++++	++**++++++	3.080E-03
5	++**++++++	++**++++++	++**++++++	++**++++++	++**++++++	3.850E-03
6	++**++++++	++**++++++	++**++++++	++**++++++	++**++++++	4.620E-03
7	++**++++++	++**++++++	++**++++++	++**++++++	++**++++++	5.390E-03
8	++**++++++	++**++++++	++**++++++	++**++++++	++**++++++	6.160E-03
9	++**++++++	++**++++++	++**++++++	++**++++++	++**++++++	6.930E-03
10	++**++++++	++**++++++	++**++++++	++**++++++	++**++++++	7.700E-03
11	++**++++++	++**++++++	++**++++++	++**++++++	++**++++++	8.470E-03
12	++**++++++	++**++++++	++**++++++	++**++++++	++**++++++	9.240E-03
13	++**++++++	++**++++++	++**++++++	++**++++++	++**++++++	1.001E-02
14	++**++++++	++**++++++	++**++++++	++**++++++	++**++++++	1.078E-02
15	++**++++++	++**++++++	++**++++++	++**++++++	++**++++++	1.155E-02
16	++**++++++	++**++++++	++**++++++	++**++++++	++**++++++	1.230E-02
17	++**++++++	++**++++++	++**++++++	++**++++++	++**++++++	1.306E-02
18	++**++++++	++**++++++	++**++++++	++**++++++	++**++++++	1.389E-02
19	++**++++++	++**++++++	++**++++++	++**++++++	++**++++++	1.465E-02
20	++**++++++	++**++++++	++**++++++	++**++++++	++**++++++	1.541E-02
21	++**++++++	++**++++++	++**++++++	++**++++++	++**++++++	2.167E-02
22	++**++++++	++**++++++	++**++++++	++**++++++	++**++++++	2.494E-02
23	++**++++++	++**++++++	++**++++++	++**++++++	++**++++++	2.897E-02
24	++**++++++	++**++++++	++**++++++	++**++++++	++**++++++	3.391E-02
25	++**++++++	++**++++++	++**++++++	++**++++++	++**++++++	3.999E-02
	12345678901234567890123456789012345678901234567890					
	1	2	3	4	5	

PLANE 29 Z = 9.16E-02 METERS STATIONS/DUST/PARTICLES  
( 1- 50)

	1	2	3	4	5	Y
1	1234567890	1234567890	1234567890	1234567890	1234567890	METERS
2						7.700E-04
3						1.540E-03
4						2.310E-03
5						3.080E-03
6						3.850E-03
7						4.620E-03
8						5.390E-03
9						6.160E-03
10						6.930E-03
11						7.700E-03
12						8.470E-03
13						9.240E-03
14						1.001E-02
15						1.078E-02
16						1.155E-02
17						1.250E-02
18						1.366E-02
19						1.509E-02
20						1.685E-02
21						1.901E-02
22						2.167E-02
23						2.494E-02
24						2.897E-02
25						3.391E-02
	1234567890	1234567890	1234567890	1234567890	1234567890	3.999E-02
	1	2	3	4	5	

PLANE 99  $\bar{z} = 9.1644 - 0.2$  METERS

**MATERIAL MAP  
( 1- 50)**

# HULL OUTPUT

FROB 3212.6002 CYCLE 373 TIME 3.602430E-05 DT 1.007492E-07

INTERNAL ENERGY	KINETIC ENERGY	TOTAL ENERGY	ETH	PFL, PFLP
1.29022638812345E+11	7.1617255661803E+11	6.4119519088742E+11	0.6119519088742E+11	2.15027475207950E-03
		TOTAL MASS	RTH	PFLRHO
		1.70585498039267E+02	1.70585498039267E+02	2.29792244091542E-12

HAR VEL = 1.91146E+05 AT I 25 J 0 K 92

HAR CS = 4.76507E+05 AT I 32 J 1 K 41

HAR T = 1.39366E+05 AT I 29 J 1 K 40

CELL SETTING DT: I 16 J 1 K 40

TOTAL TIME FOR THIS PROBLEM 5 HOURS, 56 MIN, 59 SEC

TIME FOR THIS RUN 1 HOURS, 0 MIN, 36 SEC

UMIZ FACTOR TOTAL PROBLEM = 4.57E-04 SEC/CELL/CYCLE

UMIZ FACTOR SINCE LAST DUMP = 4.863E-04 SEC/CELL/CYCLE

I= 1 J= 1 X(I,J)= -3.391 Y(J)= .077	K	P	U	V	W	XI	RHO	SXX	SYY	SXY	SXZ	SYZ	Z	VOL
1	1.01295E+06	0.	0.	0.	0.	2.0675E+09	1.225E-03	0.	0.	0.	0.	0.	-2.6919E+00	900
2	1.01296E+06	0.	0.	0.	0.	2.0675E+09	1.225E-03	0.	0.	0.	0.	0.	-5.1111E+00	900
3	1.01296E+06	0.	0.	0.	0.	2.0675E+09	1.225E-03	0.	0.	0.	0.	0.	-4.1111E+00	900
4	1.01296E+06	0.	0.	0.	0.	2.0675E+09	1.225E-03	0.	0.	0.	0.	0.	-6.1227E+00	900
5	1.01296E+06	0.	0.	0.	0.	2.0675E+09	1.225E-03	0.	0.	0.	0.	0.	-3.7101E+00	900
6	1.01296E+06	0.	0.	0.	0.	2.0675E+09	1.225E-03	0.	0.	0.	0.	0.	-3.3326E+00	900
7	1.01296E+06	0.	0.	0.	0.	2.0675E+09	1.225E-03	0.	0.	0.	0.	0.	-2.9931E+00	900
8	1.01296E+06	0.	0.	0.	0.	2.0675E+09	1.225E-03	0.	0.	0.	0.	0.	-2.4077E+00	900
9	1.01296E+06	0.	0.	0.	0.	2.0675E+09	1.225E-03	0.	0.	0.	0.	0.	-2.1301E+00	900
10	1.01296E+06	0.	0.	0.	0.	2.0675E+09	1.225E-03	0.	0.	0.	0.	0.	-1.9438E+00	900
11	1.01296E+06	0.	0.	0.	0.	2.0675E+09	1.225E-03	0.	0.	0.	0.	0.	-1.7439E+00	900
12	1.01296E+06	0.	0.	0.	0.	2.0675E+09	1.225E-03	0.	0.	0.	0.	0.	-1.5641E+00	900
13	1.01296E+06	0.	0.	0.	0.	2.0675E+09	1.225E-03	0.	0.	0.	0.	0.	-1.4025E+00	900
14	1.01296E+06	0.	0.	0.	0.	2.0675E+09	1.225E-03	0.	0.	0.	0.	0.	-1.2970E+00	900
15	1.01296E+06	0.	0.	0.	0.	2.0675E+09	1.225E-03	0.	0.	0.	0.	0.	-1.1894E+00	900
16	1.01296E+06	0.	0.	0.	0.	2.0675E+09	1.225E-03	0.	0.	0.	0.	0.	-1.0084E+00	900
17	1.01296E+06	0.	0.	0.	0.	2.0675E+09	1.225E-03	0.	0.	0.	0.	0.	-8.0275E-01	900
18	1.01296E+06	0.	0.	0.	0.	2.0675E+09	1.225E-03	0.	0.	0.	0.	0.	-6.0737E-01	900
19	1.01296E+06	0.	0.	0.	0.	2.0675E+09	1.225E-03	0.	0.	0.	0.	0.	-4.0737E-01	900
20	1.01296E+06	0.	0.	0.	0.	2.0675E+09	1.225E-03	0.	0.	0.	0.	0.	-2.1546E-01	900
21	1.01296E+06	0.	0.	0.	0.	2.0675E+09	1.225E-03	0.	0.	0.	0.	0.	-6.4496E-01	900
22	1.01296E+06	0.	0.	0.	0.	2.0675E+09	1.225E-03	0.	0.	0.	0.	0.	-5.6798E-01	900
23	1.01296E+06	0.	0.	0.	0.	2.0675E+09	1.225E-03	0.	0.	0.	0.	0.	-4.0946E-01	900
24	1.01296E+06	0.	0.	0.	0.	2.0675E+09	1.225E-03	0.	0.	0.	0.	0.	-3.1694E-01	900
25	1.01296E+06	0.	0.	0.	0.	2.0675E+09	1.225E-03	0.	0.	0.	0.	0.	-2.3999E-01	900
26	1.01296E+06	0.	0.	0.	0.	2.0675E+09	1.225E-03	0.	0.	0.	0.	0.	-1.4296E-01	900
27	1.01296E+06	0.	0.	0.	0.	2.0675E+09	1.225E-03	0.	0.	0.	0.	0.	-7.2154E-01	900
28	1.01296E+06	0.	0.	0.	0.	2.0675E+09	1.225E-03	0.	0.	0.	0.	0.	-2.0961E-02	900
29	1.01296E+06	0.	0.	0.	0.	2.0675E+09	1.225E-03	0.	0.	0.	0.	0.	4.1039E-02	900
30	1.01296E+06	0.	0.	0.	0.	2.0675E+09	1.225E-03	0.	0.	0.	0.	0.	1.2042E-01	900
31	1.01296E+06	0.	0.	0.	0.	2.0675E+09	1.225E-03	0.	0.	0.	0.	0.	2.0240E-01	900
32	1.01296E+06	0.	0.	0.	0.	2.0675E+09	1.225E-03	0.	0.	0.	0.	0.	7.1904E-01	900
33	1.01296E+06	1.311E-05	0.	0.	0.	2.0675E+09	1.225E-03	0.	0.	0.	0.	0.	3.5604E-01	900
34	1.01296E+06	1.111E-03	0.	0.	0.	2.0675E+09	1.225E-03	0.	0.	0.	0.	0.	5.1004E-01	900
35	1.01296E+06	1.645E-02	0.	0.	0.	2.0675E+09	1.225E-03	0.	0.	0.	0.	0.	5.1004E-01	900
36	1.01296E+06	3.937E-02	0.	0.	0.	2.0675E+09	1.225E-03	0.	0.	0.	0.	0.	5.1004E-01	900
37	1.01296E+06	6.189E-02	0.	0.	0.	2.0675E+09	1.225E-03	0.	0.	0.	0.	0.	5.1004E-01	900
38	1.01296E+06	1.111E-01	0.	0.	0.	2.0675E+09	1.225E-03	0.	0.	0.	0.	0.	5.1004E-01	900
39	1.01296E+06	1.811E-01	0.	0.	0.	2.0675E+09	1.225E-03	0.	0.	0.	0.	0.	5.1004E-01	900
40	1.01296E+06	2.781E-01	0.	0.	0.	2.0675E+09	1.225E-03	0.	0.	0.	0.	0.	7.1104E-01	900
41	1.01296E+06	4.142E-01	0.	0.	0.	2.0675E+09	1.225E-03	0.	0.	0.	0.	0.	8.1804E-01	900
42	1.01296E+06	6.043E-01	0.	0.	0.	2.0675E+09	1.225E-03	0.	0.	0.	0.	0.	9.7804E-01	900
43	1.01295E+06	9.488E-01	0.	0.	0.	2.0675E+09	1.225E-03	0.	0.	0.	0.	0.	1.0490E+00	900
44	1.01288E+06	1.222E+00	0.	0.	0.	2.0675E+09	1.225E-03	0.	0.	0.	0.	0.	1.1240E+00	900
45	1.01288E+06	1.493E+00	0.	0.	0.	2.0675E+09	1.225E-03	0.	0.	0.	0.	0.	1.1830E+00	900
46	1.01288E+06	1.533E+00	0.	0.	0.	2.0675E+09	1.225E-03	0.	0.	0.	0.	0.	1.1830E+00	900
47	1.01288E+06	1.541E+00	0.	0.	0.	2.0675E+09	1.225E-03	0.	0.	0.	0.	0.	1.1570E+00	900
48	1.01278E+06	4.210E+00	0.	0.	0.	2.0675E+09	1.225E-03	0.	0.	0.	0.	0.	1.4340E+00	900
49	1.01278E+06	5.553E+00	0.	0.	0.	2.0675E+09	1.225E-03	0.	0.	0.	0.	0.	1.5110E+01	900
50	1.01278E+06	7.252E+00	0.	0.	0.	2.0675E+09	1.225E-03	0.	0.	0.	0.	0.	1.5804E+00	900
51	1.01286E+06	9.303E+00	0.	0.	0.	2.0675E+09	1.225E-03	0.	0.	0.	0.	0.	1.6620E+00	900
52	1.01286E+06	1.120E+01	0.	0.	0.	2.0675E+09	1.225E-03	0.	0.	0.	0.	0.	1.7420E+00	900
53	1.01286E+06	1.205E+01	0.	0.	0.	2.0675E+09	1.225E-03	0.	0.	0.	0.	0.	1.8130E+00	900
54	1.01286E+06	1.247E+01	0.	0.	0.	2.0675E+09	1.225E-03	0.	0.	0.	0.	0.	1.8840E+00	900
55	1.01286E+06	1.251E+01	0.	0.	0.	2.0675E+09	1.225E-03	0.	0.	0.	0.	0.	1.9560E+00	900
56	1.01286E+06	1.261E+01	0.	0.	0.	2.0675E+09	1.225E-03	0.	0.	0.	0.	0.	2.0270E+00	900
57	1.01186E+06	4.211E+01	0.	0.	0.	2.0666E+09	1.2231E-03	0.	0.	0.	0.	0.	2.1270E+00	900
58	1.01156E+06	5.202E+01	0.	0.	0.	2.0666E+09	1.2231E-03	0.	0.	0.	0.	0.	2.1010E+00	900
59	1.01156E+06	6.152E+01	0.	0.	0.	2.0666E+09	1.2231E-03	0.	0.	0.	0.	0.	2.0810E+00	900
60	1.01020E+06	7.254E+01	0.	0.	0.	2.0666E+09	1.2231E-03	0.	0.	0.	0.	0.	2.0520E+00	900
61	1.01031E+06	8.403E+01	0.	0.	0.	2.0666E+09	1.2231E-03	0.	0.	0.	0.	0.	1.9130E+00	900
62	1.00966E+06	1.046E+02	0.	0.	0.	2.0666E+09	1.2231E-03	0.	0.	0.	0.	0.	1.7120E+00	900
63	1.00989E+06	1.671E+02	0.	0.	0.	2.0666E+09	1.2231E-03	0.	0.	0.	0.	0.	1.7930E+00	900
64	1.00989E+06	1.411E+02	0.	0.	0.	2.0666E+09	1.2231E-03	0.	0.	0.	0.	0.	1.6601E+00	900
65	1.00970E+06	1.466E+02	0.	0.	0.	2.0666E+09	1.2231E-03	0.	0.	0.	0.	0.	1.5401E+00	900
66	1.00941E+06	1.444E+02	0.	0.	0.	2.0666E+09	1.2231E-03	0.	0.	0.	0.	0.	1.4597E+00	900
67	1.00941E+06	1.412E+02	0.	0.	0.	2.0666E+09	1.2231E-03	0.	0.	0.	0.	0.	1.4211E+00	900
68	1.00941E+06	1.352E+02	0.	0.	0.	2.0666E+09	1.2231E-03	0.	0.	0.	0.	0.	1.3921E+00	900
69	1.00941E+06	1.312E+02	0.	0.	0.	2.0666E+09	1.2231E-03	0.	0.	0.	0.	0.	1.3631E+00	900
70	1.00923E+06	1.312E+02	0.	0.	0.	2.0662E+09	1.2231E-03	0.	0.	0.	0.	0.	1.3205E+00	900
71	9.97998E+05	9.26F+02	0.	0.	0.	2.0598E+09	1.2195E-03	0.	0.	0.	0.	0.	1.2840E+00	900

ENERGY MAP

## MATERIALS AND

DISTRIBUTION LIST

<u>No. of Copies</u>	<u>Organization</u>	<u>No. of Copies</u>	<u>Organization</u>
12	Commander Defense Technical Info Center ATTN: DDC-DDA Cameron Station Alexandria, VA 22314	1	Commander US Army Materiel Development and Readiness Command ATTN: DRCDMD-ST 5001 Eisenhower Avenue Alexandria, VA 22353
1	Director Defense Advanced Research Projects Agency ATTN: Tech Info 1400 Wilson Boulevard Arlington, VA 22209	10	Commander US Army Armament Research and Development Command ATTN: DRDAR-TD, Dr. R. Weigle DRDAR-LC, Dr. J. Frasier DRDAR-SC, Dr. D. Gyorog DRDAR-LCF, G. Demitack DRDAR-LCA, G. Randers-Pehrson DRDAR-SCS-M, R. Kwatnoski DRDAR-LCU, E. Barrières DRDAR-SCM, Dr. E. Bloore DRDAR-TSS (2 cys) Dover, NJ 07801
1	Director Defense Nuclear Agency Washington, DC 20305		
1	Deputy Assistant Secretary of the Army (R&D) Department of the Army Washington, DC 20310		
2	Commander US Army BMD Advanced Technology Center ATTN: BMDATC-M, Mr. P. Boyd Mr. S. Brockway PO Box 1500 Huntsville, AL 35807	2	Director US Army ARRADCOM Benet Weapons Laboratory ATTN: DRDAR-LCB-TL Dr. Joseph E. Flaherty Watervliet, NY 12189
1	HQDA (DAMA-ARP) WASH DC 20310	1	Commander US Army Armament Materiel Readiness Command ATTN: DRSAR-LEP-L, Tech Lib Rock Island, IL 61299
1	HQDA (DAMA-MS) WASH DC 20310		
2	Commander US Army Engineer Waterways Experiment Station ATTN: Dr. P. Hadala Dr. B. Rohani PO Box 631 Vicksburg, MS 39180	1	Commander US Army Aviation Research and Development Command ATTN: DRDAV-E 4300 Goodfellow Blvd. St. Louis, MO 63120

DISTRIBUTION LIST

<u>No. of Copies</u>	<u>Organization</u>	<u>No. of Copies</u>	<u>Organization</u>
1	Director US Army Air Mobility Research and Development Laboratory Ames Research Center Moffett Field, CA 94035	6	Director US Army Materials and Mechanics Research Center ATTN: DRXMR-T, Mr. J. Bluhm Mr. J. Mescall Dr. M. Lenoe R. Shea F. Quigley DRXMR-ATL Watertown, MA 02172
1	Commander US Army Communications Research and Development Command ATTN: DRDCO-PPA-SA Fort Monmouth, NJ 07703	2	Commander US Army Research Office ATTN: Dr. E. Saibel Dr. G. Mayer PO Box 12211 Research Triangle Park NC 27709
1	Commander US Army Electronics Research and Development Command Technical Support Activity ATTN: DELSD-L Fort Monmouth, NJ 07703	1	Director US Army TRADOC Systems Analysis Activity ATTN: ATAA-SL (Tech Lib) White Sands Missile Range NM 88002
3	Commander US Army Missile Research and Development Command ATTN: DRSMI-R DRSMI-RBL DRSMI-YDL Redstone Arsenal, AL 35809	1	Office of Naval Research Department of the Navy ATTN: Code ONR 439, N. Perrone 800 North Quincy Street Arlington, VA 22217
2	Commander US Army Tank-Automotive Research and Development Command ATTN: DRDTA-UL V. H. Pagano Warren, MI 48090	3	Commander Naval Air Systems Command ATTN: AIR-604 Washington, DC 20360
1	Commander TARADCCM Tank-Automotive Systems Laboratory ATTN: T. Dean Warren, MI 48090		

DISTRIBUTION LIST

<u>No. of Copies</u>	<u>Organization</u>	<u>No. of Copies</u>	<u>Organization</u>
2	Commander Naval Air Development Center, Johnsville Warminster, PA 18974	6	Commander Naval Weapons Center ATTN: Code 3181, John Morrow Code 3261, Mr. C. Johnson Code 3171, Mr. B. Galloway Code 3831, Mr. M. Backman Mr. R.E. VanDevender,Jr. Dr. O.E.R. Heimdahl China Lake, CA 93555
1	Commander Naval Missile Center Point Mugu, CA 93041	2	Director Naval Research Laboratory ATTN: Dr. C. Sanday Dr. H. Pusey Washington, DC 20375
2	Naval Ship Engineering Center ATTN: J. Schell Tech Lib Washington, DC 20362	2	Superintendent Naval Postgraduate School ATTN: Dir of Lib Dr. R. Ball Monterey, CA 93940
1	Commander & Director David W. Taylor Naval Ship Research & Development Center ATTN: Code 1740.4, R.A. Gramm Bethesda, MD 20084	3	Long Beach Naval Shipyard ATTN: R. Kessler T. Eto R. Fernandez Long Beach, CA 90822
3	Commander Naval Surface Weapons Center ATTN: Dr. W. G. Soper Mr. N. Rupert Code G35, D.C. Peterson Dahlgren, VA 22448	1	HQ USAF/SAMI Washington, DC 20330
10	Commander Naval Surface Weapons Center ATTN: Dr. S. Fishman (2 cys) Code R-13, F.J. Zerilli K. Kim E.T. Toton M.J. Frankel Code U-11, J.R. Renzi R.S. Gross Code K-22, F. Stecher J.M. Etheridge Silver Spring, MD 20084	1	AFIS/INOT Washington, DC 20330
		20	ADTC/DLJW (MAJ G. Spitale) Eglin AFB, FL 32542
		10	ADTC/DLYV (Mr. J. Collins) Eglin AFB, FL 32542
3	Commander Naval Weapons Center ATTN: Code 31804, Mr. M. Smith Code 326, Mr. P. Cordle Code 3261, Mr. T. Zulkoski China Lake, CA 93555	1	AFATL/DLYV Eglin AFB, FL 32542
		1	AFATL/DLODL Eglin AFB, FL 32542

DISTRIBUTION LIST

<u>No. of Copies</u>	<u>Organization</u>	<u>No. of Copies</u>	<u>Organization</u>
1	AFATL/CC Eglin AFB, FL 32542	4	Lawrence Livermore Laboratory PO Box 808 ATTN: Dr. R. Werne Dr. J.O. Hallquist Dr. M. L. Wilkins Dr. G. Goudreau Livermore, CA 94550
1	AFATL/DLODR Eglin AFB, FL 32542		
1	HQ PACAF/DOQQ Hickam AFB, HI 96853	6	Los Alamos Scientific Laboratory PO Box 1663 ATTN: Dr. R. Karpp Dr. J. Dienes Dr. J. Taylor Dr. E. Fugelso Dr. D. E. Upham Dr. R. Keyser Los Alamos, NM 87545
1	HQ PACAF/OA Hickam AFB, HI 96853		
1	OOALC/MMWMC Hill AFB, UT 84406		
1	HQ TAC/DRA Langley AFB, VA 23665		
1	TAC/INAT Langley AFB, VA 23665	6	Sandia Laboratories ATTN: Dr. R. Woodfin Dr. M. Sears Dr. W. Herrmann Dr. L. Bertholf Dr. A. Chabai Dr. C. B. Selleck Albuquerque, NM 87115
1	AUL-LSE 71-249 Maxwell AFB, AL 36112		
1	AFWAL/MLLN (Mr. T. Nicholas) Wright-Patterson AFB, OH 45433	1	Headquarters National Aeronautics and Space Administration Washington, DC 20546
1	ASD/ENESS (S. Johns) Wright-Patterson AFB, OH 45433		
1	ASD/ENFEA Wright-Patterson AFB, OH 45433	1	Jet Propulsion Laboratory 4800 Oak Grove Drive ATTN: Dr. Ralph Chen Pasadena, CA 91102
1	ASD/XRP Wright-Patterson AFB, OH 45433		
1	HQUSA/DOQ APO New York 09012	1	Director National Aeronautics and Space Administration Langley Research Center Langley Station Hampton, VA 23365
1	COMIPAC/I-32 Box 38 Camp H. I. Smith, HI 96861		
10	Battelle Northwest Laboratories PO Box 999 ATTN: G. D. Marr Richland, WA 99352		

DISTRIBUTION LIST

<u>No. of Copies</u>	<u>Organization</u>	<u>No. of Copies</u>	<u>Organization</u>
1	US Geological Survey 2255 N. Gemini Drive ATTN: Dr. D. Roddy Flagstaff, AZ 86001	2	Brunswick Corporation 4300 Industrial Avenue ATTN: P. S. Chang R. Grover Lincoln, NE 68504
1	AAI Corporation PO Box 6767 ATTN: R. L. Kachinski Baltimore, MD 21204	1	Computer Code Consultants, Inc. 1680 Camino Redondo ATTN: Dr. Wally Johnson Los Alamos, NM 87544
1	Aerojet Ordnance Company 9236 East Hall Road Downey, CA 90241	1	Dresser Center PO Box 1407 ATTN: Dr. M.S. Chawla Houston, TX 77001
1	Aeronautical Research Associates of Princeton, Inc. 50 Washington Road Princeton, NJ 08540	1	Effects Technology, Inc. 5383 Hollister Avenue Santa Barbara, CA 93111
1	Aerospace Corporation 2350 E. El Segundo Blvd. ATTN: Mr. L. Rubin El Segundo, CA 90009	1	Electric Power Research Institute PO Box 10412 ATTN: Dr. George Sliter Palo Alto, CA 94303
1	AVCO Systems Division 201 Lowell Street ATTN: Dr. Reinecke Wilmington, MA 01803	2	Firestone Defense Research and Products 1200 Firestone Parkway ATTN: R. L. Woodall L. E. Vescelius Akron, OH 44317
4	Battelle Columbus Laboratories 505 King Avenue ATTN: Dr. M. F. Kanninen Dr. G. T. Hahn Dr. L. E. Hulbert Dr. S. Sampath Columbus, OH 43201	1	FMC Corporation Ordnance Engineering Division San Jose, CA 95114
	Boeing Aerospace Company ATTN: Mr. R. G. Blaisdell (M.S. 40-25) Dr. N. A. Armstrong, C. J. Artura (M.S. 8C-23) Dr. B. J. Henderson (M.S. 43-12) Seattle, WA 98124	1	Ford Aerospace and Communications Corporation Ford Road, PO Box A ATTN: L. K. Goodwin Newport Beach, CA 92660
		1	General Atomic Company PO Box 81608 ATTN: R. M. Sullivan F. H. Ho S. Kwei San Diego, CA 92158

DISTRIBUTION LIST

<u>No. of Copies</u>	<u>Organization</u>	<u>No. of Copies</u>	<u>Organization</u>
1	General Dynamics PO Box 2507 ATTN: J. H. Cuadros Pomona, CA 91745	1	Lockheed Palo Alto Research Laboratory 3251 Hanover Street ATTN: Org 5230, Bldg. 201 Mr. R. Robertson Palo Alto, CA 94394
1	General Electric Company Lakeside Avenue ATTN: D. A. Graham, Room 1311 Burlington, VT 05401	1	Lockheed Missiles and Space Company PO Box 504 ATTN: R. L. Williams Dept. 81-11, Bldg. 154 Sunnyvale, CA 94086
1	President General Research Corporation ATTN: Lib McLean, VA 22101	1	Materials Research Laboratory, Inc. 1 Science Road Glenwood, IL 60427
1	Goodyear Aerospace Corporation 1210 Massillon Road Akron, OH 44315	2	McDonnell-Douglas Astro- nautics Company 5301 Bolsa Avenue ATTN: Dr. L. B. Greszczuk Dr. J. Wall Huntington Beach, CA 92647
5	Honeywell, Inc. Government and Aerospace Products Division ATTN: Mr. J. Blackburn Dr. G. Johnson Mr. R. Simpson Mr. K. H. Doeringsfeld Dr. D. Vavrick 600 Second Street, NE Hopkins, MN 55343	1	New Mexico Institute of Mining and Technology ATTN: TERA Group Socorro, NM 87801
1	Hughes Aircraft Corporation ATTN: Mr. W. Keppel MS M-5, Bldg. 808 Tucson, AZ 85706	1	Northrup Corporation 3901 W. Broadway ATTN: R. L. Ramkumar Hawthorne, CA 90250
2	Kaman Sciences Corporation 1500 Garden of the Gods Road ATTN: Dr. P. Snow Dr. D. Williams Colorado Springs, CO 80933	1	Nuclear Assurance Corporation 24 Executive Park West ATTN: T. C. Thompson Atlanta, GA 30245
		2	Orlando Technology, Inc. PO Box 855 ATTN: Mr. J. Osborn Mr. D. Matuska Shalimar, FL 32579

DISTRIBUTION LIST

<u>No. of Copies</u>	<u>Organization</u>	<u>No. of Copies</u>	<u>Organization</u>
1	Pacific Technical Corporation 460 Ward Drive ATTN: Dr. F. K. Feldmann Santa Barbara, CA 93105	1	US Steel Corporation Research Center 125 Jamison Lane Monroeville, PA 15146
1	Rockwell International Missile Systems Division ATTN: A. R. Glaser 4300 E. Fifth Avenue Columbus, OH 43216	1	VPI & SU 106C Norris Hall ATTN: Dr. M. P. Kamat Blacksburg, VA 24061
3	Schumberger Well Services Perforating Center ATTN: J. E. Brooks J. Brookman Dr. C. Aseltine PO Box A Rosharon, TX 77543	2	Vought Corporation PO Box 225907 ATTN: Dr. G. Hough Dr. Paul M. Kenner Dallas, TX 75265
1	Science Applications, Inc. 101 Continental Boulevard Suite 310 El Segundo, CA 90245	1	Westinghouse, Inc. PO Box 79 ATTN: J. Y. Pan W. Mifflin, PA 15122
1	Ship Systems, Inc. 11750 Sorrento Valley Road ATTN: Dr. G. G. Erickson San Diego, CA 92121	1	Drexel University Department of Mechanical Engr. ATTN: Dr. P. C. Chou 32d and Chestnut Streets Philadelphia, PA 19104
1	Systems, Science and Software PO Box 1620 ATTN: Dr. R. Sedgwick La Jolla, CA 92038	3	Southwest Research Institute Dept. of Mechanical Sciences ATTN: Dr. U. Lindholm Dr. W. Baker Dr. R. White 8500 Culebra Road San Antonio, TX 78228
2	TRW One Space Park, R1/2120 ATTN: D. Ausherman M. Bronstein Redondo Beach, CA 90277	4	SRI International 333 Ravenswood Avenue ATTN: Dr. L. Seaman Dr. L. Curran Dr. D. Shockey Dr. A. L. Florence Menlo Park, CA 94025
1	United Technologies Research Center 438 Weir Street ATTN: P. R. Fitzpatrick Glastonbury, CT 06033	2	University of Arizona Civil Engineering Department ATTN: Dr. D. A. DaDeppo Dr. R. Richard Tucson, AZ 85721

DISTRIBUTION LIST

<u>No. of Copies</u>	<u>Organization</u>	<u>No. of Copies</u>	<u>Organization</u>
1	University of Arizona School of Engineering ATTN: Dean R. Gallagher Tucson, AZ 85721	1	University of Oklahoma School of Aerospace, Mechanical and Nuclear Engineering ATTN: Dr. C. W. Bert Norman, OK 73019
1	University of California Los Angeles ATTN: Dr. M. Ziv Los Angeles, CA 90024	<u>Aberdeen Proving Ground</u>	
1	University of California Department of Physics ATTN: Dr. Harold Lewis Santa Barbara, CA 93106	Dir, USAMSAA ATTN: DRXSY-D DRXSY-MP, H. Cohen	
2	University of California College of Engineering ATTN: Prof. W. Goldsmith Dr. A. G. Evans Berkeley, CA 94720	Cdr, USATECOM ATTN: DRSTE-TO-F Dir, USA MTD ATTN: Mr. S. Keithley	
2	University of Delaware Department of Mechanical Engineering ATTN: Prof. J. Vinson Prof. B. Pipes Newark, DE 19711	Dir, USACSL, EA ATTN: DRDAR-CLB-PA Bldg. E3516	
1	University of Denver Denver Research Institute ATTN: Mr. R. F. Recht 2390 S. University Blvd. Denver, CO 80210		
2	University of Florida Department of Engineering Sciences ATTN: Dr. R. L. Sierakowski Dr. L. E. Malvern Gainesville, FL 32601		

### USER EVALUATION OF REPORT

Please take a few minutes to answer the questions below; tear out this sheet, fold as indicated, staple or tape closed, and place in the mail. Your comments will provide us with information for improving future reports.

1. BRL Report Number \_\_\_\_\_

2. Does this report satisfy a need? (Comment on purpose, related project, or other area of interest for which report will be used.)  
\_\_\_\_\_  
\_\_\_\_\_  
\_\_\_\_\_

3. How, specifically, is the report being used? (Information source, design data or procedure, management procedure, source of ideas, etc.)  
\_\_\_\_\_  
\_\_\_\_\_  
\_\_\_\_\_

4. Has the information in this report led to any quantitative savings as far as man-hours/contract dollars saved, operating costs avoided, efficiencies achieved, etc.? If so, please elaborate.  
\_\_\_\_\_  
\_\_\_\_\_  
\_\_\_\_\_

5. General Comments (Indicate what you think should be changed to make this report and future reports of this type more responsive to your needs, more usable, improve readability, etc.)  
\_\_\_\_\_  
\_\_\_\_\_  
\_\_\_\_\_

6. If you would like to be contacted by the personnel who prepared this report to raise specific questions or discuss the topic, please fill in the following information.

Name: \_\_\_\_\_

Telephone Number: \_\_\_\_\_

Organization Address:  
\_\_\_\_\_  
\_\_\_\_\_  
\_\_\_\_\_